The Effect of Brackish Water Extraction on the Brackish Upconing Below the Horstermeer Polder

Creating a 3D Regional Variable-Density Groundwater Model using MODFLOW 6 and FloPy

S.J.S. de Smet

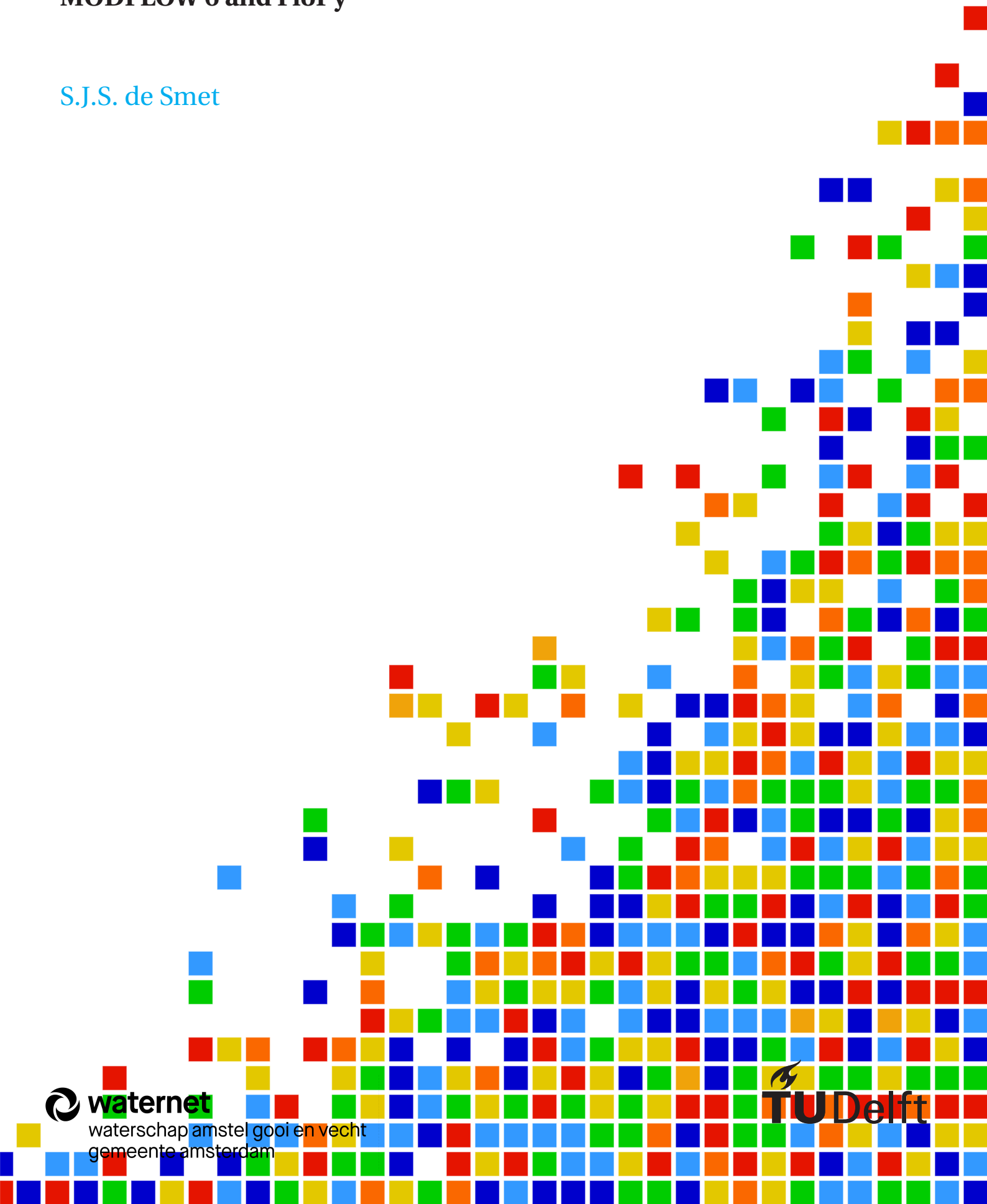

waternet
waterschap amstel gooi en vecht
gemeente amsterdam

TU Delft

The Effect of Brackish Water Extraction on the Brackish Upconing Below the Horstermeer Polder

Creating a 3D Regional Variable-Density Groundwater Model using MODFLOW 6 and FloPy

by

S.J.S. de Smet

to obtain the degree of Master of Science

in Civil Engineering

at the Delft University of Technology

Student number:	4351983	
Project duration:	October 1, 2020 – July 16, 2021	
Thesis committee:	Prof. dr. ir. M. Bakker,	TU Delft
	dr. ir. J. M. Bloemendal,	TU Delft
	dr. ir. G. H. W. Schoups,	TU Delft
	F. J. C. Smits, MSc.,	Waternet & TU Delft

TU Delft Delft University of Technology

waternet waterschap amstel gooi en vecht gemeente amsterdam

ARTESIA Water Research Unlimited

Preface

During my gap year in between my bachelor's and master's degree, I travelled to Guajira in Colombia. Guajira is a desert in the north of the country that is almost entirely enclosed by the sea, and that is characterised by its shortage of freshwater. From that moment on, I wanted to understand the movement of the seawater into the drinkable fresh aquifers and eventually maybe be able to protect these valuable drinking water sources. The master's course Principles of Geohydrology given by professor Mark Bakker introduces the processes behind the salinisation of the coastal aquifers. Afterwards, the course Groundwater Modelling taught me how to visualise these processes with the help of models. After these courses, I was confident that I wanted to proceed in this research direction for the final part of my master's. Hence, I am very thankful that Mark Bakker introduced me to Frank Smits, who works as a geohydrologist at Waternet and, among many other things, is very passionate about the taming of brackish seepage below the Horstermeer Polder near the city of Amsterdam. This illustrates that the salinisation of aquifers is not just a problem abroad. This thesis is the result of nine months of research dedicated to the understanding and modelling of brackish seepage below the Horstermeer Polder with the help of the newly-released MODFLOW 6 software in a Python environment. I am very thankful for the knowledge that I obtained during these past months. However, without the supervisors, friends, and family around me, the outcome of this research would not have been the same. Therefore, I would like to thank some people in particular.

First of all, I would like to thank Frank Smits, who was always willing to take the time, although his schedule was always full, to discuss my work, provide me with new insights and infect me with his endless enthusiasm for the topic. Furthermore, I would like to thank two other employees of Waternet. To start, Iris van Wielink for her time and involvement in my thesis and her regular check-ups on how I was doing since working from home was not always easy. Second, Liesanne Verwij, who spent considerable time collecting additional measurements out of the Waternet database and making sure the format of those data files was easily analysable. Besides supervision from Waternet, I also received a lot of guidance and help from Artesia Water, especially on the modelling with MODFLOW 6. Therefore, I would like to thank Davíd Brakenhoff and Onno Ebbens They provided me with their MODFLOW 6 Python package, which is currently still under development and taught me a lot about (variable-density) groundwater modelling in general. Finally, my appreciation goes to the chair of the thesis committee: Mark Bakker. I want to thank him for the discussions and guidance of my work. Also, a big thanks to all other thesis committee members for taking the time to evaluate my work. Last but not least, I am very grateful for my family, roommates, and friends, who always supported me and who made sure I have many lovely and fun memories of my student days at the TU Delft.

S.J.S. de Smet
Delft, July 2021

Abstract

Extensive usage of vital freshwater is highly undesirable in the current era of climate change and population growth. However, the 6 million m^3/y of brackish seepage that occurs in the deep Horstermeer Polder, located in between the cities of Amsterdam and Hilversum in the Netherlands, is mitigated by using up to 207 million m^3/y of freshwater. This is very unsustainable, especially since the pressure on the freshwater reserves in the Netherlands is rising. Therefore, this research focuses on evaluating a new mitigation measure of the brackish upconing below the polder: the extraction of brackish water. In March 2021 AD, a pilot well has been installed in the polder, and its effects were assessed in this research. To enable the evaluation, an extensive analysis of all available measurements of the geology, hydraulic head, and chloride distribution in the area was performed, and a 3D regional variable-density groundwater model using MODFLOW 6 was built. The model result has a reasonable good agreement with these measurements, since at 70% of the measurement locations, the simulated hydraulic head deviates less than 30 cm, and at 80% of them, the simulated chloride concentration deviates less than 200 mg/l. Moreover, compared to previous research, the representation of the brackish upconing was significantly improved. The effects of the pilot well were calculated using five different operational settings. The results indicated that a shallow well, starting below -50 m NAP, reduces the chloride load in the polder more than a deep well (-100 m NAP). However, even in the best scenario, i.e. an active shallow well with a constant pumping rate of 100 m^3/h, the reduction of the chloride load is limited to 5.5%. In perspective, these results suggested that at least 24 of these wells are needed to lower the chloride concentration in the discharge water out of the polder to 250 mg/l. On the contrary, the shallow wells cause a considerable average drawdown of 4 cm at surface level in a radius of 50 meters around the well, which might result in damage to wooden pile foundations in the northeast of the polder.

Summary

The deep Horstermeer Polder, located between the cities of Amsterdam and Hilversum in the Netherlands, is characterised by a brackish seepage flux of 14 mm/day, which results in a discharge with an average chloride concentration of approximately 550 mg/l at the main pumping station of the polder. To prevent this water from flowing into valuable a freshwater basin, 207 million m^3/y of freshwater is pumped into the river Vecht to flush the brackish water into the Amsterdam-Rhine Canal (ARC) and eventually in the North Sea. However, this solution is far from sustainable, especially since the effects of climate change and population growth require an increasing amount of freshwater. Therefore a new mitigation strategy is explored: taming the brackish seepage by extracting the brackish groundwater before it reaches the surface with the help of wells. In March 2021, the first pilot well was installed within the polder to test this strategy. Before a complete well field can be built, the effects of these wells need to be estimated with the help of a model. This study contributes to the research by providing a numerical model using MODFLOW 6 that simulates the variable-density groundwater flow. In total this research has three objectives. The first objective is to analyse all available data on geology, hydraulic head, and salinity in and around the Horstermeer Polder, to gain a general understanding of the system and test the model performance. The second objective is to build a model that simulates the characteristics of the regional aquifer system close to field conditions in terms of flow regime, salinity distribution, and fluxes into and out of the polders. The last objective is to evaluate the effects of the newly installed pilot well.

The available data on the geology showed that the area is characterised by a thick aquifer till a depth of ± -150 m NAP at which a thick clay layer is located that dips towards the north. However, the aquifer is split by a thin clay layer at a depth of ± -55 m NAP in some parts of the area. The clay layers highly influence the flow regime in the area since the flow velocity is low in those layer. On the other hand, a very coarse layer at a depth of -25 till -35 m NAP is characterised by a very high specific discharge. Moreover, a hill ridge created during the last ice age is located in the east, which consists mainly of sandy deposits. In the remainder of the area, the confining top layer consists either of clay resulting from the sedimentation of the Vecht or peat. However, since the peat was mined at many locations in the past, sand forms the top layer.

Besides the influence on the current top layer, mankind also changed the flow regime in the area due to land reclamation. The Horstermeer Polder was a lake before it was reclaimed in 1882 AD, resulting in a phreatic surface that is more than two meters lower than in the surroundings. The deeper groundwater in the thick aquifer is brackish in the west and north of the area, as it was a tidal area a few million years ago, and only since 1932 AD, the large lake located north of the area has become fresh. Hence, brackish upconing occurs into the surface waters of the polder. The cone is located at the centre-northern half of the polder since there are many fresh surface waters in the southern part of the area, and no brackish groundwater is present. However, the system is not in equilibrium and changes with time. It appeared that the flux originating for the ARC fluctuates since its bottom resistance is time-variant. Moreover, the seasonal variability of the controlled surface level in the polders influences the system. As a result, the hydraulic heads in the area have an average standard deviation of 10 centimetres. These conclusions were drawn after analysing 2606 measurement points with time series of the hydraulic head, 772 points of the chloride concentration in the surroundings and within the Horstermeer Polder, and an additional 182 shallow measurements of Electrical Conductivity (EC) or Electrical Resistivity (ER) within the polder.

The created low-resolution (100 x 100 m) model describes the steady characteristics of the regional aquifer system. The geological structure was schematised with a high level of detail in the MOD-

FLOW 6 model. As a result, the influences of the water-bearing layers are visualised, and it appeared that the thin clay layer in the middle of the aquifer influences the pathway to the surface of the brackish seepage. Furthermore, the deep layer almost completely disconnects the aquifer above and below this clay layer. The race layer, on the other hand, enhances the transport of fresh infiltration water towards the polder. After calibrating the vertical hydraulic conductivity of the top confining layer by hand, the simulated heads deviated in 70% of the 149 locations, at which an average point-water head could be calculated over the period 2000 to 2020 AD, only 30 cm from the measured average head and the Root Mean Square Error (RMSE) has a value of 0.29. Although the model output differs from the mean, it is located within the 95%-confidence interval of many measurement points due to the observed fluctuation of the head. In general, the heads fluctuate between 0.53 m NAP in the east till -3.43 in the Horstermeer Polder. Moreover, the simulated chloride concentration deviates from the observed chloride in some of these locations. Nonetheless, in 78% of the measurement locations, the deviation is less than 200 mg Cl^-/l. However, the simulated upconing below the Horstermeer Polder was simulated a few hundred meters further to the west than observed. The simulated chloride concentration of the discharge out of the polder, on the other hand, is 603 mg/l and thus has the same order of magnitude as the measured chloride concentration of 552 mg/l. Also, the discharge itself has the same order of magnitude. Nevertheless, some improvement could be made by extending the calibration procedure and using automated calibration programs, like PEST. Moreover, the vertical hydraulic conductivity of the confining layer should be simulated in more detail to achieve the observed shape of the upconing.

Since the general outcome of the model is close to the field conditions despite local deviations, the effects of the pilot well in the Horstermeer Polder could still be estimated. The installed pilot well has two well screens, both located in the thick aquifer between the thin clay layer and the thick deeper clay layer, one in the upper part with a length of 37 meters and one in the bottom part with a length of 52 meters. In total, six scenarios were run: four where one of the well screens was active with either a constant pumping rate of 55 m^3/h or 100 m^3/h, one in which both screens pumped with a constant rate of 50 m^3/h and one in which the well was inactive (baseline). From the results can be concluded that the shallow screen has the biggest reducing effect on the chloride concentration reaching the polder's surface waters with a positive correlation with the rate. Nonetheless, the reduction in chloride load in all scenarios is limited between 3 and 5.5%. Therefore, up to 24 shallow wells with a constant pumping rate of 100 m^3/h might be needed to achieve a chloride concentration of 250 mg/l in the discharged water, which would be the drinking water standard of the World Health Organisation. On the other hand, the reduction of the flux is even lower and is only 0.8 to 1.7%. Moreover, the shallow well results in a more significant drawdown at the surface level up to 4 cm. This is the average drawdown in an area of 0.01 km^2 around the well. To estimate the drawdown more precisely, the grid-cell size of the model has to be reduced locally, nevertheless, 4 cm is considerable and could damage the wooden pile foundations in the built-up area in the polder.

To conclude, this research resulted in (1) a better understanding of the aquifer system in and around the Horstermeer Polder, (2) an improved 3D regional variable-density model of this system using MODFLOW 6, (3) a first estimation of the effect of the pilot wells in the polder. Besides local grid refinement and determination of the vertical hydraulic conductivity of the top layer in the polder, the model could still be improved. It is recommended to determine a better estimation of the hydraulic head at the boundaries of the model by creating a low-resolution variable-density model that is larger than the model in this research. Furthermore, airborne electromagnetic measurements are recommended to establish a more realistic initial distribution of chloride. Lastly, the model will always be a simplified version of the field conditions, and therefore, it is recommended to determine the effects of the pilot wells during pumping tests. Nonetheless, the model does demonstrate the beneficial effects of a well on the chloride load. However, more wells with a higher pumping rate will be needed to achieve the desired effect. Therefore, further research is needed to determine the feasibility of the measure.

Contents

Acronyms

ADV Advection Package within MODFLOW 6 that simulates the advection of solutes in the model.

AHN Actueel Hoogtebestand Nederland (Up-to-date Height Model of the Netherlands).

ARC Amsterdam-Rhine Canal.

BiCGSTAB Biconjugate Gradient Stabilized.

BUY Buoyancy Package within MODFLOW 6 needed to represent variable-density flow.

CNC Constant Concentration Package within MODFLOW 6 to put a fixed concentration in certain cells within the model throughout the simulation.

DISV Discretisation by Vertices Package within MODFLOW 6 in which an unstructured grid of the model is defined using a list of (x,y) vertex pairs.

DRN Drain Package within MODFLOW that can be used to simulate drainage from the aquifer into surface water.

EC Electrical Conductivity.

ER Electrical Resistivity.

GHB General-Head Boundary Package within MODFLOW to simulate flow over the boundary of the model by specifying a head on the boundary cells.

GWF Groundwater Flow.

GWT Groundwater Transport.

HUF Hydrogeologic-Unit Flow Package within MODFLOW-2005 which is used to specify properties of the flow between cells. These units do not have to be equal to the layer boundaries .

IMS Iterative Model Solution Package within MODFLOW 6 that defines the method of solving used in the simulation.

IQR Interquartile Range.

LHM Landelijk Hydrologisch Model (Nation-wide Dutch hydrological model).

MAW Multi-Aquifer Well Package within MODFLOW 6 used to simulate a well-screen over multiple layers within the model grid.

MCM Million Cubic Meters.

MST Mobile Storage and Transfer Package within MODFLOW 6 in which the porosity as well as decay and sorbtion parameters can be defined.

MWT Multi-Aquifer Well Transport Package within MODFLOW 6 used to simulate transport occurring in a well of which the well-screen stretches over multiple layers within the model grid.

NAP Normaal Amsterdams Peil. The standard reference height used in the Netherlands. 0 m NAP is almost equal to the mean sea level in the North Sea.

NHI Nederlands Hydrologisch Instrumentarium (Dutch Hydrological Instrumentarium).

NPF Node Property Flow Package within MODFLOW 6 that calculates intercell conductance values, manages cell wetting and drying, and adds Newton-Raphson terms for intercell flow expressions.

RD New New Rijksdriehoeks coordinate system.

RGWM$_{\text{Waternet}}$ Regional Groundwater Model of Waternet.

RIV River Package within MODFLOW that can be used to simulate head-dependent flux boundaries. Unlike the DRN-Package, the RIV-Package is capable to simulate both drainage as well as infiltration.

RMSE Root Mean Square Error.

STO Storage Package within MODFLOW needed to model transient groundwater flow.

TDIS Temporal-Discretisation Package within MODFLOW 6 in which the time discretisation of the simulation is defined.

1

Introduction

1.1. Motivation

Almost 40% of the world's population lives within 100 km from the shoreline [1], making the coastal zones one of the most densely populated areas of the world [2, 3]. Consequently, there is a high water demand in these areas, increasingly met by groundwater extractions [1, 4]. Simultaneously, fresh groundwater stored in coastal aquifers is particularly susceptible to degradation due to its proximity to saltwater [3]. Marine transgression, seawater intrusion, and sea spray could reduce the available freshwater resources, which are already under stress [5, 6]. Salinisation of the water by 1% of saltwater (250 mg/l) makes a well unfit for drinking-water purposes [3, 7]. Besides being a threat to the drinking-water supply, salt damage also reduces crop yields [8].

There is another salt intrusion hazard in low-lying delta areas that affects the groundwater and surface water system: seepage water [8, 9]. Seepage occurs when the hydraulic head of lower salty aquifers is higher than the phreatic surface or surface water level. In the Netherlands, this process is enhanced by land reclamation of old lakes. Within these deep polders[1], the phreatic surface is lowered, which increases the seepage flux [5]. At the same time, the country's history of marine transgression and regression has led to the salinisation of the deeper aquifers [10]. The resulting brackish seepage decreases the quality of surface waters and root zones and thereby poses a threat to vulnerable ecosystems and agricultural land. One of the deep polders that is characterised by its brackish seepage flux is the Horstermeer Polder, located between the cities of Amsterdam and Hilversum (Figure 1.2). To mitigate the effects of brackish seepage (6 million m^3/yr), about 207 million m^3/yr of freshwater from the Lake Markermeer is used to force the brackish water from the river Vecht into the Amsterdam-Rhine Canal (ARC) and to eventually flush it into the North Sea [11, 12]. A part of this amount (approximately 10 to 30 million m^3/yr) is used for the water-level management in the lakes and surrounding areas of the Horstermeer Polder [13].

This mitigation process is far from sustainable as it uses an extreme amount of freshwater to flush out a relatively limited amount of brackish water. Moreover, extensive use of vital freshwater is highly undesirable in the current era of climate change and population growth, which increase the pressure on the freshwater supply [3, 14]. At the same time, salt loads are expected to increase over the years due to the upconing of deeper and more saline groundwater [8]. Therefore, new strategies are developed to mitigate the saline seepage in the Horstermeer Polder. To create an adequate management strategy, research on the groundwater system and seepage processes in the deep polder of Horstermeer is needed. This is the objective of the PhD of Frank Smits, which this MSc research is part of. The research focuses on the taming of brackish seepage (temmen van brakke kwel) and the feasibility of (1) the extraction of brackish groundwater before it reaches the shallow groundwater

[1] A polder is an area with a completely controlled surface water system, i.e. controlled surface water levels, enclosed by dikes and where pumps are positioned to control the water entering and leaving the system.

system and (2) creating drinking water out of it by using reverse osmosis [13]. The extraction of brackish groundwater and the possible effect are depicted in Figure 1.1.

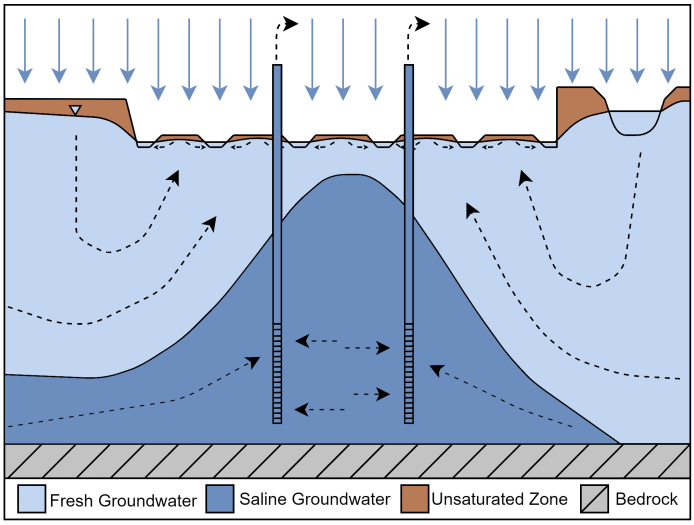

Figure 1.1: Diagram of the taming of brackish seepage by extracting the brackish groundwater with the help of two wells, based on [13].

1.2. Research Gap

The first step of determining the feasibility of the taming of brackish seepage is understanding the chloride distribution in the groundwater system within and around the polder. Prediction of saltwater intrusion and salt distribution can either be done, using analytical solutions or numerical modelling [3]. However, analytical solutions that included variable-density groundwater flow due to the mixing of saline water with freshwater[2], are scarce. Therefore, saltwater intrusion is often simulated using numerical models. So far, two studies have researched the feasibility and effects of brackish water extraction in the Horstermeer Polder with the help of numerical models.

First, Fakhari [12] predicted the chloride distribution in the groundwater system within and around the polder. Moreover, scenarios were run to estimate the effects of different well fields. However, the modelled quantity of salt in the polder was inadequate, and Fakhari [12] hypothesised that there might be saline groundwater coming from below a deep clay layer at a depth of ± -150 m NAP. This hypothesis was refuted by measurements performed in the deep drilling (-231 m NAP[3]) with multiple monitoring wells at the west side of the polder in 2018 AD. Another explanation for the shortage of salt in the model is the negligence of the influence of the former Zuiderzee, located north of the polder (Figure 1.2) on the salinity distribution in the area. The Zuiderzee became highly influenced by the North Sea around 1600 AD, and the water became brackish until it was closed by a dam (Afsluitdijk) and transformed into the freshwater lake IJsselmeer in 1932 AD[4]. This lake was eventually split into lake IJsselmeer and lake Markermeer in 1976 AD [16]. Although both lakes became freshwater lakes, the groundwater below and around the lakes is still brackish.

Second, in a national study by Bos-Burgering *et al.* [17], the effects of the extraction of brackish groundwater on the brackish seepage rates within the Horstermeer Polder could not be determined due to the simulation of a fresh seepage flux within the polder, which does not correspond with the field observations. Nevertheless, the Horstermeer Polder was indicated as a promising location for the extraction of brackish groundwater, although the chance of rotting of the wooden pile foundation systems in the polder should be taken into consideration.

[2] The density of seawater is only 2.5% larger than that of freshwater, but this slight difference has a significant impact [3].
[3] NAP is the reference height used in the Netherlands. 0 m NAP is almost equal to the mean sea level in the North Sea.
[4] 1638 AD is often taken as the starting point of the salinisation of the sediments and 1934 AD as the ending point [15].

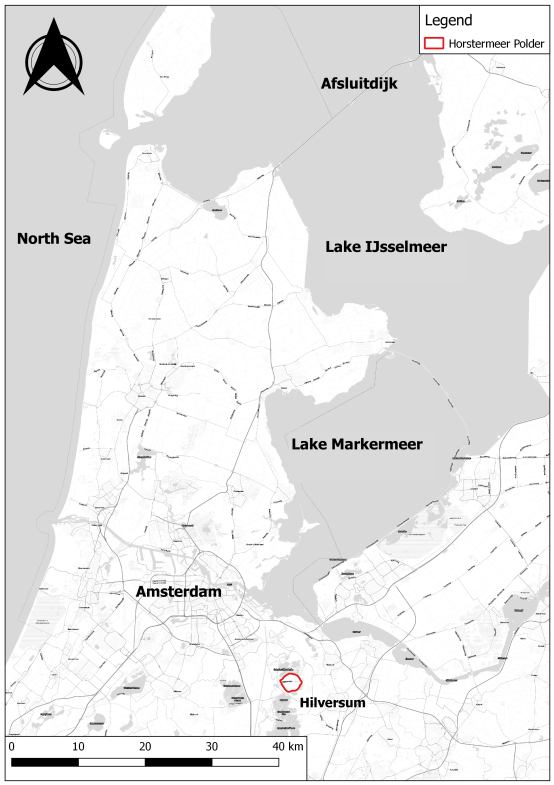

Figure 1.2: Location of the Horstermeer Polder with respect to lake IJsselmeer and lake Markermeer (former Zuiderzee) and North Sea. The delineation of the Horstermeer is depicted in red.

Since the brackish seepage below the Horstermeer Polder is highly underestimated in both studies, none of the models from previous research can be used to evaluate the effects of extraction wells on the chloride distribution below the polder. Nonetheless, in March 2021 AD, a pilot well with two well screens has been placed in the Horstermeer Polder to research its effects in practice. However, the need for a better understanding of the chloride distribution below the Horstermeer Polder to determine the feasibility of a full-scale well field remains.

1.3. Research Objectives

In this research, the existing model of Fakhari [12] is improved by including (1) a more detailed representation of the geology of the area, (2) the recent data of the deep drilling (hydraulic head and salt distribution) in 2018 AD, and (3) a better representation of the salt distribution within the groundwater system outside of the polder. Furthermore, the model evaluation of Fakhari [12] will be changed by using (1) the latest delineation of the 1000 mg Cl^-/l contour surface in the shallow subsurface of the Horstermeer Polder based on both the latest EC-measurements [18] and the measurements of Van Wielink [11], and (2) all available measurement points in the model area.
Hence, this master thesis has three objectives:

1. Analysing all available data on geology, hydraulic head, and salinity in and around the Horstermeer Polder;

2. Creating a numerical model that is as closely as possible to the field conditions, i.e. hydraulic head and chloride concentration measurements in several monitoring wells, and the flux of water and chloride at the pumping stations in the Horstermeer Polder and the surrounding polders, by improving the existing model of Fakhari [12];

3. Evaluating the effects of the brackish groundwater extraction by the pilot wells in the Horstermeer Polder on the spatial distribution of the brackish upconing below the polder, the flux and salt load out of the polder, and the flow regime.

1.4. Thesis Outline

A general understanding of the processes to be modelled is required to create a numerical model of an area. Furthermore, many input data sets need to be inquired, and many steps are necessary. To start, in Chapter 2, a theoretical background of the principles of coastal groundwater flow, seawater intrusion, salinity measurements, and numerical modelling will be given. After this introduction to the topic, the research will be split into two parts: (I) data analysis and (II) variable-density modelling. Hence, this first part will be focused on the first objective, whereas in part II, the second and third objectives will be addressed. Chapter 3, the centre of part I, will zoom in on the specific research area and will discuss its geology, known chloride concentrations, and geohydrology. The second part will start with Chapter 4, in which the methodology of the model will be explained in detail. Moreover, in this chapter, the pilot well will be introduced. In Chapter 5, the model outcome will be presented, and the model performance will be assessed based on the available head measurements, chloride measurements, and the water balance calculations of Waternet. Chapter 6 will contain the visualisations of the effects of the pilot well on the flow regime, chloride distribution, and fluxes in the Horstermeer Polder and its surrounding area. The used methodology and outcomes will be discussed in Chapter 7. The chapter will focus on the discussion of the model results and the limitations of the used methodology. The conclusions of the research will be presented in Chapter 8, and finally, in Chapter 9, the recommendations for the continuation of the research 'Taming of the Brackish Seepage' will be given.

2

Theoretical Background

This chapter provides a comprehensive summary of the scientific literature of the following topics: (1) principles of coastal groundwater flow, (2) principles of solute transport, (3) seawater intrusion, (4) salinity measurements, and (5) numerical modelling of seawater intrusion using MODFLOW 6.

2.1. Principles of Coastal Groundwater Flow

Water flow is driven by an uneven distribution of mechanical energy within the water. A more frequently used parameter is energy per unit weight of water, i.e. hydraulic head [19]. The hydraulic head in groundwater is defined as:

$$h = \frac{P}{\rho g} + z \tag{2.1}$$

where P $\left[ML^{-1}T^{-2}\right]$ is the fluid pore pressure with respect to atmospheric pressure, ρ $\left[ML^{-3}\right]$ is the density of the water, g $\left[LT^{-2}\right]$ is the gravitational constant and z $[L]$ the reference level.

In areas with a constant water density, water flows from a high hydraulic head to a low head according to Darcy's law (Equation 2.2) [19].

$$\vec{q} = -K\vec{\nabla}h \tag{2.2}$$

where $\vec{q}$ $\left[LT^{-1}\right]$ denotes the specific discharge vector (i.e. discharge per unit area in x, y, z-direction), K $\left[LT^{-1}\right]$ is the tensor of hydraulic conductivities, and $\vec{\nabla}h$ $[-]$ is the hydraulic gradient.

However, in a coastal aquifer, the groundwater density changes significantly, and the more general law for groundwater flow should be used (Equation 2.3) [20]. To simplify the governing differential equation, the Oberbeck-Boussinesq approximation is used [21]. This approximation is only valid if the density changes remain small compared to the reference density, and the variation in temperature is negligible [21].

$$\vec{q} = -\frac{\kappa}{\mu}\left(\vec{\nabla}P - \rho\vec{g}\right) \tag{2.3}$$

where κ $\left[L^2\right]$ is the intrinsic permeability tensor, μ $\left[ML^{-1}T^{-1}\right]$ is the dynamic viscosity, and $\vec{g}$ is $\left[LT^{-2}\right]$ the gravity vector in the vertical direction.

By solving Equation 2.1 for the pressure, substituting it in Equation 2.3, and introducing a reference fluid, the above equation can be rewritten to [22]:

$$\vec{q} = -K_0\left[\frac{\rho}{\rho_0}\vec{\nabla}h + (h-z)\vec{\nabla}\frac{\rho}{\rho_0}\right] \tag{2.4}$$

where $K_0 = \frac{k\rho_0 g}{\mu_0}$ $\left[LT^{-1}\right]$ is the hydraulic conductivity for aquifer material saturated with the reference fluid, ρ_0 $\left[ML^{-3}\right]$ and μ_0 $\left[ML^{-1}T^{-1}\right]$ are the density and dynamic viscosity of the reference fluid, and k $\left[L^2\right]$ is the intrinsic permeability scalar.

Equation 2.4 is a function of the hydraulic head corresponding to a specific density, i.e. the point-water head. However, to compare heads at different locations, the hydraulic head has to be reformulated with the help of a reference density. It is common to use the freshwater density and calculate the freshwater head from point-water head measurements using Equation 2.5 [23].

$$h_f = \frac{\rho}{\rho_f} h + \frac{\rho_f - \rho}{\rho_f} z \tag{2.5}$$

where h_f and h $[L]$ are the freshwater head and point-water head respectively, and ρ_f and ρ $\left[ML^{-3}\right]$ are the density belonging to freshwater and the water at specific point in the aquifer, respectively.

With Equation 2.5, Equation 2.4 can be rewritten to a freshwater-head equation [22].

$$\vec{q} = -K_f \left[\vec{\nabla} h_f + \left(\frac{\rho}{\rho_f} - 1 \right) \vec{\nabla} z \right] \tag{2.6}$$

The density, on the other hand, is computed from the chloride concentration as:

$$\rho = \rho_f + DRHODC\left(C - C_f\right) \tag{2.7}$$

where $DRHODC$ $[-]$ is the parameter that describes the relation between the density and concentration, and C_f $\left[ML^{-3}\right]$ is the corresponding reference concentration.

2.2. Principles of Solute Transport

Solutes are transported by advection, molecular diffusion and mechanical dispersion and enter the aquifer via sources and leave via sinks [24]. Hence, the governing differential equation for solute transport in an aquifer is represented by the standard advection-dispersion equation combined with a source/sink term [25]:

$$\frac{\partial C}{\partial t} = D_{ij} \nabla^2 C - \nabla \left(\frac{\overline{q}}{\theta} C \right) - \frac{q_s}{\theta} C_s \tag{2.8}$$

where D_{ij} $\left[L^2T^{-1}\right]$ is the hydrodynamic dispersion coefficient in a combination of the x, y, z-direction corresponding to tensor C, $\overline{q}$ $\left[LT^{-1}\right]$ is the average specific discharge vector, θ $[-]$ is the volumetric water content, q_s is the specific discharge vector out of a source or into a sink, and $\left[LT^{-1}\right]$ C_s $\left[ML^{-3}\right]$ is the solute concentration within a source or sink. The left-hand side of Equation 2.8 is the rate at which the concentration changes over time. The right-hand side describes the processes. The first part entails diffusion and dispersion, the second term is the advection term, and the third term describes the sources and sinks.

2.3. Seawater Intrusion

Fresh groundwater flows from inland areas with a higher head towards coastal zones with a lower head and finally into the ocean[1]. At the same time, since the density of saltwater is higher than that of freshwater, seawater also flows into coastal aquifers. In other words, saltwater intrudes into the coastal aquifer. This saline groundwater with a higher density sinks to the bottom of the aquifer and can stay there for millions of years.

[1] freshwater discharge into the ocean is only possible when the hydraulic head is higher than sea level.

2.3.1. Autonomous Salinisation

The movement of salinity in groundwater as a result of historical events that influenced boundary conditions, e.g. sea-level rise or fall, land reclamation, and subsidence, is called autonomous salinisation [8]. In other words, the current coastal groundwater system can reflect historical events that occurred tens or even hundreds of years ago [8, 10, 26]. Therefore, the process of autonomous salinisation should be taken into account when attempting to model the current salt distribution in a certain area.

2.3.2. Upward Saline Seepage

In the Netherlands, many lakes have been reclaimed for agricultural purposes in the sixteenth and seventeenth centuries. The elevation of these areas is often below mean sea level, and the phreatic surface is controlled below the surface level [27]. Hence, these areas can be susceptible to saline seepage if saline groundwater is present [5, 8]. On the edges of a polder, however, the seepage water is fresh since infiltration water from close-by surface waters, and less deep polder continuously replenishes the local groundwater system (Figure 2.1). In the middle, a cone of saline groundwater is present, which, if the difference between the hydraulic head of the saline groundwater and the phreatic surface is large enough and the resistance of the top layer is low, could reach the surface water. The saline seepage can salinise surface water and fresh shallow groundwater, making it unsuitable for agricultural or drinking water purposes (e.g. [5, 8]). Rainwater lenses counteract the saline seepage. However, De Louw *et al.* [9] determined that the shallow rainwater lenses in seepage areas are controlled by the recharge, seepage flux, and drainage depth, making these lenses very susceptible to climate change.

To summarise, the salt distribution in the subsurface below the polders depends on many factors including (1) its location with respect to (historic) saline surface waters, (2) the surrounding water systems, (3) its elevation, (4) its drainage system, (5) the amount of freshwater recharge [9], (6) the elapsed time since the reclamation [8], and (7) the geological structure of the area [5]. Moreover, the seepage rates differ within the polder as a result of preferential flow paths [5].

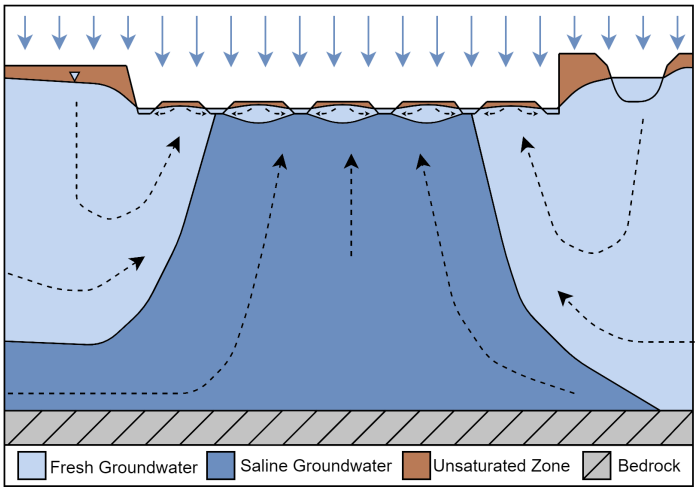

Figure 2.1: Simplified diagram of saline upconing below the centre of a deep polder. The saline seepage has a cone shape, and the borders of the polder experience freshwater seepage. Precipitation replenishes the fresh groundwater and creates rainwater lenses within the polder.

2.4. Salinity Measurements

There are multiple methods to measure salinity, including (1) geophysical measurements using Electrical Resistivity (ER) (2) measurements of the Electrical Conductivity (EC), and (3) measurements of the chloride concentration. The methods are in the order of increasing time requirements. However, the results of the last method can directly be used to compare with the output of saltwater

intrusion models. Measurements of EC should always be combined with temperature measurements, as the EC depends on temperature [28]. EC measurements are fast and inexpensive. The downside of an EC measurement is that the method only results in a point measurement within a groundwater system. Geophysical measurements using electromagnetic methods have the advantage of measuring without being invasive or even the need to be in contact with the surface. In other words, airborne measurement systems can be used [29, 30] and hence large areas can be measured at once. Empirical relations are used to transform the outcome of the first two methods into chloride concentrations. This is possible since the EC of a solution, and hence the ER, primarily depends on the concentration of ionic species, of which chloride is the most important one in seawater [28]. In sediments containing clay particles, this relation cannot be applied, as clay can conduct electricity [11, 31]. If the sediments are not completely saturated, the relation needs to be corrected to Equation 2.9 since the resistivity decreases with increasing saturation [31].

$$\rho_t = F\rho_w S_w^{-n} \tag{2.9}$$

with,

$$F = a\phi^{-m} \tag{2.10}$$

where ρ_t and ρ_w $[\Omega L]$ are the total and groundwater resistivity respectively, S_w $[-]$ is the water saturation, n $[-]$ is an empirical saturation exponent typically around 2, and F $[-]$ is the formation factor. In the formula for the formation factor, a $[-]$ is an empirical constant less than 1, m $[-]$ is an empirical constant related to the cementation of the sediments and ranges between one and three. The value of m increases when the degree in connectivity between the pores decrease. Lastly, ϕ $[-]$ is the porosity.

The next step would be to transform the EC of the groundwater into chloride concentration. This can only be done by using a chloride-EC calibration curve, which depends on the ionic composition of the water, i.e. is area-specific, and needs to be established by measuring both chloride concentrations and EC [32].

2.5. Variable-Density Modelling with MODFLOW 6

Groundwater flow is modelled using MODFLOW-based codes [33]. MODFLOW is a numerical model that uses finite-difference modelling to solve Equation 2.4 and Equation 2.8. Large scale 3D variable-density models have been widely used in studies related to saltwater intrusion. The used grid-cell size depends mainly on the level of detail of the available input data and the purpose of the model. In general, the used grid-cell sizes in saltwater-intrusion models ranges between 20-250 meters [8, 34–42], although smaller cell sizes in the range of 0.5-5 meter [43–48] are applied.

In the latest version of a MODFLOW-based code, MODFLOW 6, variable-density flow can be simulated without the need for another software [49]. In MODFLOW 6, two separate models are created: one for the modelling of flow (GWF Model) and one for the simulation of solute transport (GWT Model), which are coupled using the BUY-Package in which Equation 2.7 is defined [50]. Both have their own initial conditions and discretisation packages, and information between the models is transferred using an exchange package (GWF-GWT). However, to date the discretisation of both models should be equal [51]. Compared to previous options to model variable-density flow, MODFLOW 6 does not require the conversion from point-water head to freshwater heads [22]. Therefore, flow between a pair of neighbouring cells is defined as [49]:

$$\begin{aligned} Q_{nm} &= q_{nm} A_{nm} \\ &= \frac{K_f A_{nm}}{L_{nm} + L_{mn}} \left[(h_m - h_n) + \left(\frac{\rho_{nm}}{\rho_f} - 1 \right) (h_m - h_n) + (h_{nm} - z_{nm}) \frac{\rho_m - \rho_n}{\rho_f} \right] \end{aligned} \tag{2.11}$$

where q_{nm} $\left[LT^{-1}\right]$ is the specific discharge between cell n and m, A_{nm} $\left[L^2\right]$ is the area of flow between cells n and m, K_f $\left[LT^{-1}\right]$ is the hydraulic conductivity of a saturated aquifer with freshwater, L_{nm} and L_{mn} $[L]$ are

the distance from the centre of cell n to its shared face with cell m and the distance from the centre of cell m to the shared face with cell n, respectively. h $[L]$, ρ $\left[ML^{-3}\right]$ with subscript n, m and f are the head and density of cell n, m and freshwater density, respectively. Lastly, the h_{nm} $[L]$, z_{nm} $[L]$ and ρ_{nm} $\left[ML^{-3}\right]$ are the interpolated head, elevation and density at the shared interface between the cell n and m. The $\frac{K_f A_{nm}}{L_{nm} + L_{nm}}$ term is the conductance term.

Moreover, to cope with the changing state (wet to dry) of cells in unconfined aquifers MODFLOW 6 uses the Newton-Raphson Formulation [50], which improves the stability of the model. Lastly, MODFLOW 6 has a more efficient way of dealing with pinch-out layers compared to previous releases of MODFLOW. Thinning of layers, i.e. pinching out of layers, frequently occurs, either as a result of sedimentation and or erosion processes (Figure 2.2) [52] or due to tectonic movement [53].

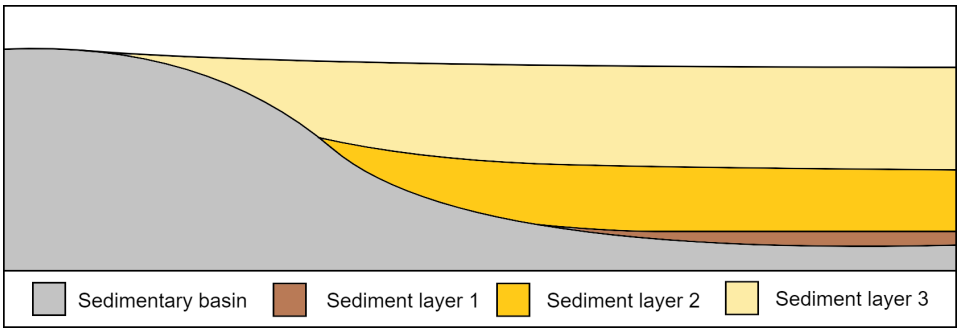

Figure 2.2: Diagram of sediment layers that pinch out in a sedimentary basin of a river. Three different layers are deposited before the sedimentary basin is filled up.

In previous versions of MODFLOW, cells could not become inactive within the model boundary. Only by using the HUF-Package pinch-out layers could be represented. However, this package is not supported anymore, as it requires many additional parameters and is difficult to be used effectively [54]. In MODFLOW 6, on the other hand, a cell can be made inactive within the model boundary by making them a "vertical pass-through cell" [50]. This is done by applying an IDOMAIN value > 0 to the cell, which entails that the cells above and below the vertical pass-through cell are connected.

I

Data Analysis

3

Horstermeer Polder and its Surroundings

To calibrate and build a numerical saltwater-intrusion model close to field conditions, measurements are needed. In the Netherlands, these measurements are collected in the DINOloket [55]. Moreover, Waternet has its own database from which additional data was collected. In total 1569 different measurement locations of the hydraulic head have been used at different depths, with a total of 2602 measurement points within the area. At every measurement point, a time series of the head is available with a varying length and starting date. Based on the chosen period, a selection can be made of the measurement points. Moreover, 772 measurement points of the chloride concentration are used with an additional 182 points located within the polder, measured by Van Wielink [11] and Jain *et al.* [18]. This data was analysed with the help of Python, and those algorithms can be found on Github: `https://github.com/sannedesmet/Saline-Upconing_Horstermeer/Code`.

Before the result of this analysis will be presented in this chapter, the study area will be introduced in more detail. Then a description of the geology will be given, followed by an overview of all salinity measurements. The last section will introduce the hydrogeological characteristics of the geology and give an overview of the expected flow paths based on freshwater heads. These freshwater heads are calculated by combining the measurements of the chloride concentration with the hydraulic-head measurements and applying Equation 2.5. Lastly, some possible explanations of the fluctuation of the hydraulic head are given.

3.1. Background

The Horstermeer Polder is located between the cities of Amsterdam and Hilversum (Figure 1.2 and Figure 3.1). The polder is a former lake, which was successfully reclaimed after several attempts, in 1882 AD [10, 11, 56]. It has a surface area of 616 hectares, which is on average located 2 meters below the surrounding area at a depth of -3.30 m NAP [11, 56]. The drainage level is kept at -3.45 m NAP [27]. The surface water bodies surrounding the Horstermeer Polder result from peat mining in the 16^{th} till the 18^{th} century [57]. Especially, the surface water bodies Spiegelplas and Wijde Blik are of significant depth due to additional sand mining in the mid-1900s AD [57]. Also, part of the surface water body, the Vinkeveense Plassen, located west of the Horstermeer, results from peat and sand mining. Another man-made surface water body is the Amsterdam-Rhine Canal (ARC), flowing west of the Horstermeer next to the river Vecht. The northern part of the canal is located in the study area (Figure 3.1) and already existed in 1892 AD, although with a different name: Merwede Canal. Between 1965 and 1981 AD, the canal was widened to 100 meters and deepened [58, 59].

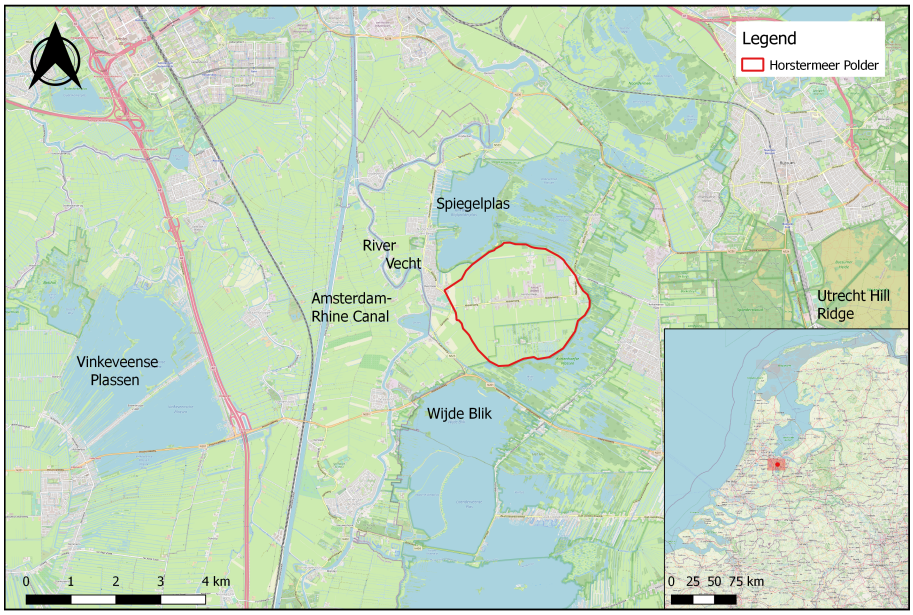

Figure 3.1: Study area from y = 466 971 - 480 170 m and x = 122 180 - 142 518 m (New Rijksdriehoeks coordinate system (RD New)).

3.2. Geology

Groundwater flows only through the pore spaces in between sediment particles, which dimensions depend on the sediment type and particle size distribution of the sediment[19]. Furthermore, sediment characteristics determine the interconnection between pores, and hence the hydraulic conductivity [19]. To understand the groundwater flow, it is therefore essential to understand the geology within the area. The following subsections will describe the evolution of the subsurface within the research area and will zoom in on the top layer, which could explain differences in local seepage rates.

3.2.1. Stratigraphic Evolution

Figure 3.2 shows that the subsurface below the Horstermeer Polder and its surrounding area exists of an alternation between sand layers, clay layers, and complex layers, formed in the period from the Miocene (23 million years ago) till the Holocene (current epoch). During the Miocene and the following Pliocene Epoch, the complete study area was flooded by the sea, and hence the subsurface layers, i.e. the Formation of Breda and the Formation of Oosterhout, are marine depositions [60]. The depositions exist of alternating clay and sand layers and gradually transit from one formation to the other.

In the Early Pleistocene, another layer of marine sediments formed the Formation of Maassluis. The transit from the Formation of Oosterhout to the Formation of Maassluis is gradual. A characteristic of the Maassluis Formation is the two cycles of coarsening upwards [55]. As a result, the two aquifers of a few tens of meters thick are topped off by thick confining layers with very low conductivity. As a result, the Maassluis Formation is often considered as the base layer of the groundwater system. Figure 3.2 shows that the upper clay layer is located at a depth of -150 m NAP in the south of the study area and at a depth of almost -200 m NAP in the northern part. The greater depth is due to tectonic movement. Since the sea regressed, rivers gained influence on the deposits during the Early Pleistocene; the Rhine is responsible for the Formation of Waalre and the Eridanos river system in the north formed the Formation of Peize [60]. These fluvial deposits are formed simultaneously with the upper layers of the Maassluis Formation and therefore grade into the Maassluis Formation in the southwestern and western part of the Netherlands. Unlike the Maassluis Formation, the Formation of Waalre is characterised by cycles of fining-upwards, and the Formation of Peize consists mainly of fine to coarse sand [55].

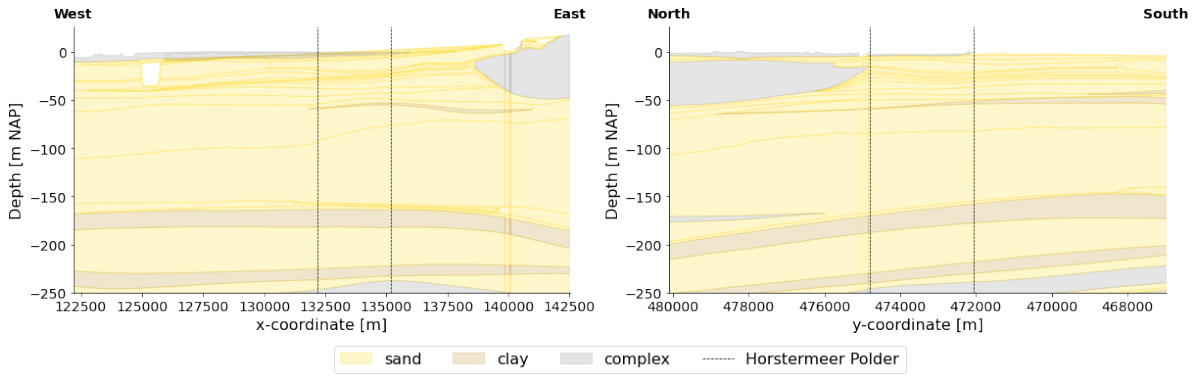

Figure 3.2: Regional geology profile across the study area through the middle of the Horstermeer Polder. The positions of the aquifers (sand layers) and aquitards (clay layers and complexes) are based on REGIS II [61]. The vertical lines within the figure are due to the filling of missing data as a result of an error in the software needed to read REGIS II data. In the left figure, the sand mining area of the Vinkeveense Plassen is visible.

The Middle Pleistocene is characterised by the arrival of Scandinavian glaciers, which occurred twice. After the first time, the Eridanos river lost its influence on the deposition in the Netherlands [60], therefore only fluvial deposits of the river Rhine can be found in the Formation of Urk and the Formation of Sterksel. The latter is not only formed by the river Rhine but also later by the river Meuse. Both formations consist of sand and the Formation of Urk even has high percentages of coarse sand. During the second glacial period the Utrecht Hill Ridge, an important landscape feature that highly influences the hydrogeology of the area, and the complex layer in the Drente Formation was formed by the forces of the glaciers. A complex layer contains all different types of sediment, however the layer is characterised by sandy sediments in this area [55, 62]. This complex layer can only be found in the far east and north of the study area (Figure 3.2). During the Late Pleistocene, the glaciers melted and the river Rhine started to flow again, which led to the sandy Formation of Kreftenheye [60]. After the warmer period, a colder period dawned in which the Netherlands was covered with polar deserts and tundras. Strong polar winds resulted in an aeolian deposit, i.e. a fine sandy layer known as the Boxtel Formation.

The last period, the Holocene, started with a warmer period in which the sea level rose due to the melting of land ice [60]. The rising sea level caused the formation of marshland, which resulted in a peat layer, named the Formation of Nieuwkoop. On the other hand, fluvial deposition was reenabled by the higher temperatures resulting in the Formation of Echteld. This formation consists of clay, silt, peat, and sand. In general, the Holocene layer is categorised as a confining layer with sandy paleochannel belts where the peat layer has been partly eroded by rivers [5].

3.2.2. Top Layer

Both the Holocene semi-confining layer and the Late-Pleistocene sand layers form the current top layer. As shown in Figure 3.3, the layer consists of a large variety of sediment types, e.g. sand, clay and peat. An important feature that determined the consistency of the top layer is the river Vecht. The Vecht is part of the Rhine river system and results from partial avulsion of the Old Rhine in 2600 BC [63]. The river has been flowing through peat and discharged the seepage water from the Utrecht Hill Ridge since peat growth decreased the seepage in the area between the two landscape features. One of the influences of the river Vecht is the levees consisting of fine sand and clay. Furthermore, on top of the peat, there is a small clay layer (< 1 m) present in some areas, as an effect of inundation of the Zuiderzee and the river Vecht [63]. These sediments are often brackish. As a result of the fluvial sediments, the peat settled creating areas with lower elevations. These lower elevated areas filled up via side streams that arose after the inundation, creating so-called 'peat lakes'. Lake Horstermeer was probably one of those lakes, although it is uncertain if lake Horstermeer was already a lake due to local high seepage rates [64] before its connection with the river Vecht [63]. The Horstermeer lake

was probably very shallow since both clay, as well as sand trenches, can be found in the Horstermeer, which is a characteristic of sedimentation in shallow surface waters [63].

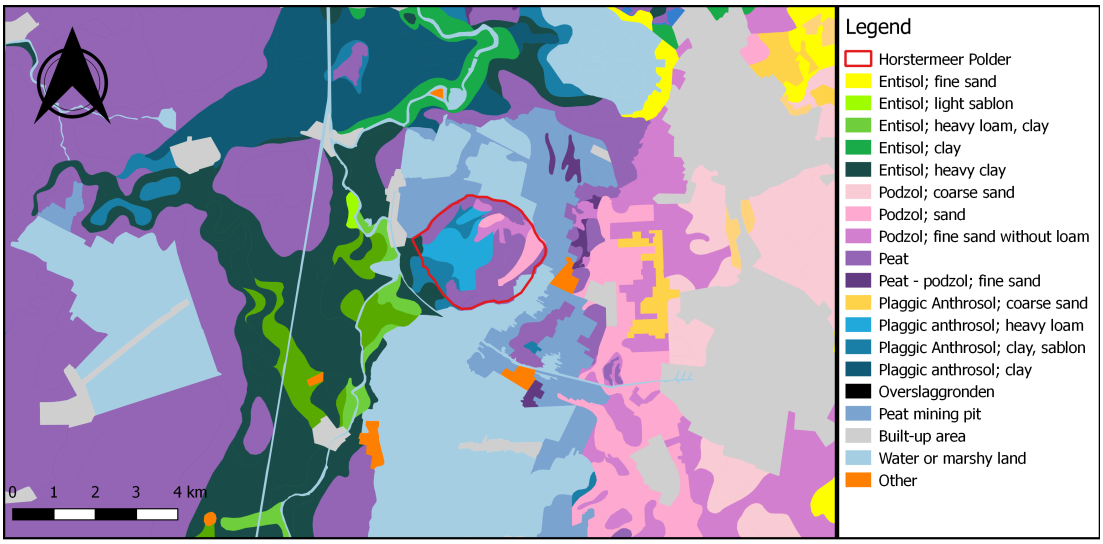

Figure 3.3: Overview of the top layer in the research area, based on the BRO Bodemkaart 2018 [55].

3.3. Chloride Concentration Distribution

In this section, first, the chloride concentration distribution in the whole study area is given after which a detailed overview of the measurements within the Horstermeer Polder is given.

3.3.1. General

The current salinity distribution in the Netherlands is not in equilibrium with the present boundary conditions [10]. Post *et al.* [26] determined that the current distribution results from former transgressions in the Holocene period. As said before, at the beginning of the Holocene period, the sea level started to rise, causing the inundation of saline water on top of the fresh Pleistocene aquifer. Since the Rayleigh number of water flowing through a sandy aquifer is high, salinisation occurred mainly due to free convection [10, 26]. It is therefore expected that the brackish groundwater in the Pleistocene aquifer, i.e. the Peize-Waalre Formation, flows upwards within the Horstermeer Polder, causing salinisation of the surface water. To determine from which sides brackish groundwater reaches the polder, the depth at which brackish groundwater is present in the whole area needs to be evaluated.

Figure 3.4a and Figure 3.4b visualise all available chloride measurements in a specified section of the research area. In the north and west of the research area, high chloride concentrations are found within the Peize-Waalre Formation, whereas, only chloride concentrations corresponding to freshwater are present in the east and south. Furthermore, the brackish groundwater enters the polder in the west at a depth of approximately -100 m NAP. In the north, the depth of entering is lower than -110 m NAP (Figure 3.4a), although an exact depth estimation is impossible. The larger depth is probably due to the surface waters north of the polder that infiltrates large amounts of freshwater into the groundwater system. Seven other cross-sections in the research area can be found in Appendix A.

Moreover, the measurements show that in the deep drilling within the Horstermeer Polder high salinity values can be found close to low salinity values, both at the upper and lower freshwater-saltwater interface. In addition, fresher groundwater was found in the upper clay layer of the Maassluis Formation [13]. Hence, the REGIS II model is not entirely corresponding to the field observation at the location of the deep drilling as the first clay layer of the Formation of Maassluis should be located a few meters upwards [13].

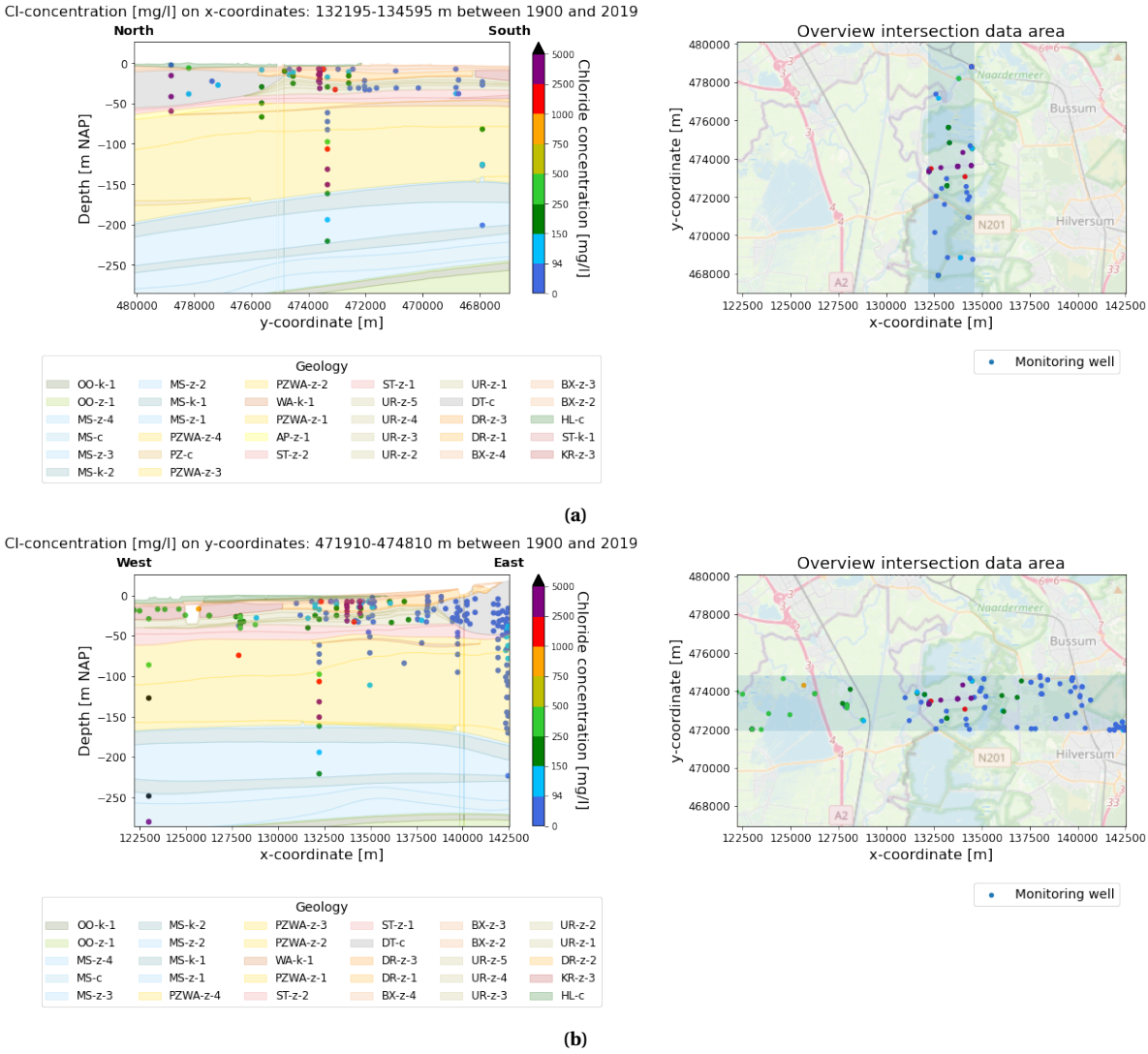

Figure 3.4: Chloride concentration distribution over the depth from (a) from south to north at the x-coordinates of the Horstermeer Polder and (b) west to east at the y-coordinates of the Horstermeer Polder. The chloride concentration is retrieved from DINOloket [55], whereas the geology is based on REGIS II [61]. The names in the legend of the figure are equal to the names used in Table 3.1.

To get a complete overview of the chloride concentration distribution within the Peize-Waalre Formation two horizontal sections were created; one from the top of the Peize-Waalre Formation (-60 m NAP) till -100 m NAP and one from -100 m NAP till approximately the top of the Maassluis Formation (-150 m NAP). Figure 3.5 shows that in the north, till approximately 476500 m in the west and 478000 m in the east, the complete Pleistocene aquifer is brackish, which can be explained by

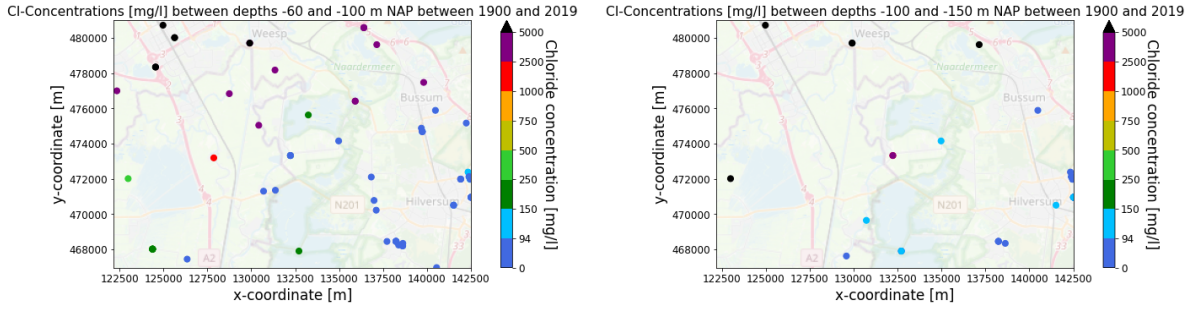

Figure 3.5: Chloride concentrations in top half (left) and bottom half (right) of the Peize-Waalre Formation. If multiple chloride concentrations are available only the lowest one is visualised.

the presence of saline/brackish water in the Zuiderzee till 1934 AD or earlier marine transgressions. In the west, on the other hand, only the bottom half of the aquifer is brackish. The depth at which brackish groundwater is present declines going north. From northeast to southwest, excluding the Horstermeer Polder and y-coordinates higher than 478000 m (RD New), there is only freshwater in the aquifer.

3.3.2. The Horstermeer Polder

Within the Horstermeer Polder, additional measurements in the shallow subsurface (< -5 m NAP) are performed by Van Wielink [11] and Jain *et al.* [18]. Caution is needed when comparing the two data sets since Jain *et al.* [18] measured the salinity in the aquifers directly below the ditches in the polder, whereas Van Wielink [11] performed her measurements mostly in the area between the ditches. De Louw *et al.* [9] showed that the interface between fresh and brackish groundwater is closest to the surface below those ditches and pushed lower by rainwater lenses in the area between the ditches (Figure 2.1). Furthermore, the ditches cut through the semi-confining Holocene layer in almost the whole polder [27], resulting in higher seepage rates. In other words, the interface is at larger depths in between the ditches compared to below the ditches, which was also visualised in Figure 2.1.

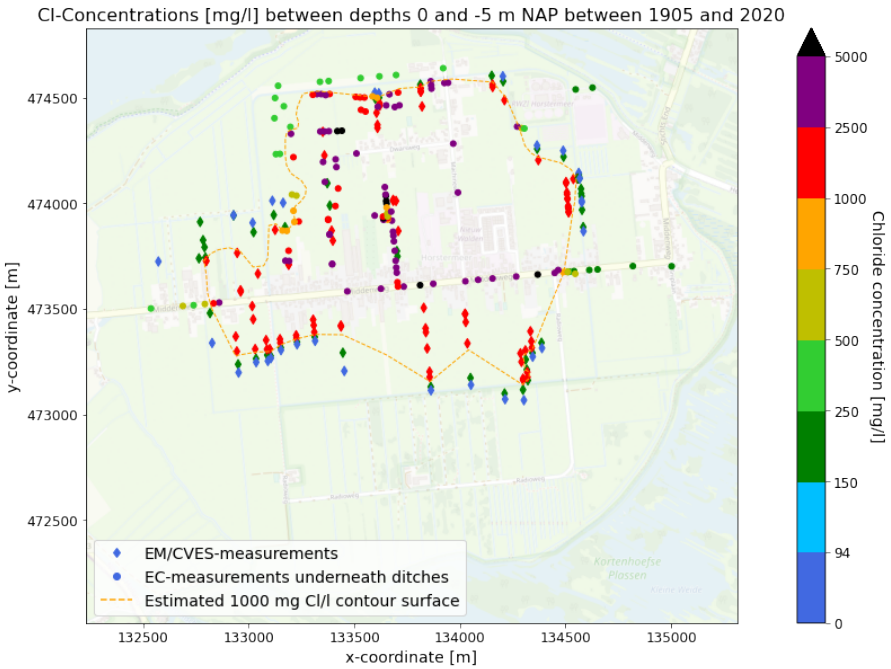

Figure 3.6: All shallow chloride measurements within the Horstermeer Polder and a first estimate of the location of the fresh-brackish interface (1000 mg Cl^-/l) at -1.5 m below surface level. Van Wielink [11] performed the EM/CVES measurements and Jain et al. [18] the EC measurements, afterwards both were translated to chloride concentration. Whenever EC measurements were available, they were used to estimate the interface.

As shown in Figure 3.6, brackish seepage occurs mainly in the centre-northern part of the polder. During the first salinity measurements in 1947 by Hooghoudt [65], the 1000 mg Cl^-/l contour surface was located more southwards, although already during the subsequent measurements in 1988 by Van der Linden and Appello [56] the interface was shifted northwards to approximately the location that is currently observed. Two possible explanations for the northwards shift of the interface are (1) the raising of the phreatic surface in the south of the polder [56] or (2) the filling up of ditches in the south [11]. The latter increases the resistance of the upper layer and decreases the seepage rates of freshwater in the south, thereby pushing the brackish seepage more to the centre of the polder. Therefore, to correctly model the brackish upconing below the polder, it is important to include the ditches.

The notch in the northwest of the polder could be explained by the clay in the top layer (Figure 3.3). Another explanation could be the sand mining pit in the Spiegelplas, which at some locations has a depth of -50 m NAP [66]. This means that the bottom of the Spiegelplas is located in the sand layer of the Urk Formation, which has a low resistance. The low resistance enables infiltration of large quantities of freshwater, possibly pushing the brackish groundwater further to the centre. This effect is enhanced by the presence of a so-called 'race layer' [67], in which the specific discharge is considerably larger (up to a factor 2) than in the layers above and below. The higher specific discharge can be explained by the fact that this layer exists mostly out of very coarse sediments, like gravel. In the Horstermeer Polder, this layer is present at a depth of -25 until -35 m NAP [67].

Moreover, in the middle of the polder, a very local area of fresher (750 mg Cl^-/l) seepage can be identified. This is peculiar since the seepage in the surrounding area has a chloride concentration of approximately 5000 mg/l. There are two possible explanations for the fresher seepage water. The first explanation would be a small preferential flow path connecting the aquifer below the first clay layer of the Maassluis Formation with the surface water. The other reason could be the presence of a rainwater lens. At the specific location of the fresher seepage, the ditch is dammed to contain the freshwater. Hence, the fresh rainwater has more time to mix with the brackish seepage resulting in lower chloride values.

3.4. Hydrogeology

To gain a first insight into the possible flow paths within the research area, freshwater heads are essential. Freshwater heads are, however, only point measurements that can only give an indication. Moreover, they often fluctuate over time, resulting in changing flow paths. The velocity of the groundwater, on the other hand, depends mainly on the hydrogeological characteristics of the local geology, as they determine the ease with which the groundwater can flow through a layer. So, this section will start with the hydrogeological parameters of the different geological layers and will end with an overview of the freshwater equivalents of the observed point-water head and possible explanations for the fluctuation of the point-water heads in the area.

3.4.1. Hydrogeological Parameters

Figure 3.2 visualised the different sediment types within the subsurface in the study area. However, these sediment types can be further classified into lithological classes based on the geochemical and physical properties of the sediment particles [68]. These geochemical and physical properties highly influence the water fluxes within the subsurface. In the Netherlands, information on the geology from deep drillings has been interpolated into nationwide models that estimate the local geology. Lithological classes have been aggregated into hydroclasses, which have then been classified to hydrogeological classes based on the interpretation of experts, [61]. This classification, known as REGIS II, is the basis of most regional and national groundwater models in the Netherlands and estimates all hydrogeological parameters within every hydrogeological class. The latest version of REGIS II, v2.2, [61] has an average coverage depth of -500 m NAP. The downside of this model is the lower level of detail in the upper layers, especially in the Holocene Formations. These formations are represented as one complex layer without differentiation in clay, sand, or peat layers without information on hydrogeological properties. Therefore, in this research REGIS II was combined with GeoTOP v1.3 [69]. GeoTOP is a detailed 3D geological model of the shallow subsurface to a depth of -50 m NAP.

Table 3.1 gives the most critical parameter, the hydraulic conductivity, for all subsurface layers between the base layer and the surface as used in REGIS II and GeoTOP. Since the hydrogeological classes are an aggregation of lithological classes, every layer has a range of occurring hydraulic-conductivity values.

Table 3.1: Summary hydraulic conductivity of the subsurface layers in the study area. The table is ordered from the surface layer of the groundwater system to the base layer. The information is based on REGIS II v2.2 [61], expect the Holocene Formation which is based on GeoTOP v1.3 [69].

Formation	Layer	Sediment Type	Hydraulic Conductivity $[md^{-1}]$
Holocene	Hlc	complex	$K_v = 10^{-4} - 10^{-1}$
Boxtel	BXz2	sand	$K_h = 2.5 - 10$
	BXz3	sand	$K_h = 2.5 - 10$
	BXz4	sand	$K_h = 2.5 - 10$
Kreftenheye	KRz3	sand	$K_h = 25 - 50$
Drente	DRz1	sand	$K_h = 10 - 25$
	DRz2	sand	$K_h = 10 - 25$
	DRz3	sand	$K_h = 10 - 25$
	DTc	complex	-
Urk	URz1	sand	$K_h = 25 - 50$
	URz2	sand	$K_h = 25 - 50$
	URz3	sand	$K_h = 25 - 50$
	URz4	sand	$K_h = 25 - 50$
	URz5	sand	$K_h = 25 - 100$
Sterksel	STz1	sand	$K_h = 10 - 50$
	STz2	sand	$K_h = 10 - 50$
Waalre	WAk1	clay	$K_v = 10^{-2} - 5 \cdot 10^{-2}$
Peize-Waalre	PZWAz1	sand	$K_h = 25 - 50$
	PZWAz2	sand	$K_h = 25 - 50$
	PZWAz3	sand	$K_h = 50 - 100$
	PZWAz4	sand	$K_h = 25 - 50$
Maassluis	MSz1	sand	$K_h = 5 - 10$
	MSk1	clay	$K_v = 10^{-3} - 5 \cdot 10^{-3}$
	MSz2	sand	$K_h = 5 - 10$
	MSk2	clay	$K_v = 10^{-3} - 5 \cdot 10^{-3}$

3.4.2. Hydraulic Head Distribution

As a result of changing chloride concentration within the study area, the measured hydraulic heads (point-water heads) are not directly of use [70]. This is because the hydraulic head decreases as the groundwater density increases, and the pressure remains the same (Equation 2.1). Directly studying point-water heads would therefore lead to anomalies in the estimated groundwater flow path. However, freshwater heads are of use if studied at a horizontal plane (Equation 2.6). Hence, all point-water heads should be transformed into freshwater heads by applying Equation 2.5. However, since the output of a MODFLOW 6 model are in terms of point-water head, an overview of all available average point-water heads in the period 2000 to 2020 AD are given in Appendix B

Although many piezometers are installed in the area, the chloride concentration is known at limited locations. To make a correct distinction between recharge areas and discharge area and hence estimate the groundwater flow paths, the freshwater head distribution is needed [3]. This is because water always flows from high freshwater equivalent head to low freshwater equivalent head at the same depth (Equation 2.6).

To create the freshwater head distribution, the raw data of DINOloket needed to be modified in the following ways:

- The reference level of the point-water heads needed to be changed from surface level to NAP, while taking into account the changing surface level over time as a result of subsidence.
- If the piezometer filter depth was changed over time, a distinction between different periods (before and after the change) needed to be made. A change of filter depth is either a result of subsidence, a previous measurement error of the depth, or the instalment of a new filter at a

different depth.
- Extreme outliers, as a result of measurement errors, needed to be eliminated. This was done by deleting outliers that have a value that is more than five standard deviations from the mean point-water head in that piezometer.

After these modifications, the average freshwater head within a desired period was calculated. A requirement was set on the data, which stated that an observation well should have hydraulic head measurements in at least half of the years within the period in order to be visualised. This ensured that the data set at an observation well contains multiple years within the period, and temporal circumstances do not determine the average. A stricter requirement would have resulted in the non-compliance of many observation wells since DINOloket is not updated frequently enough. The only exception to this requirement was the deep drilling in the Horstermeer Polder, which exists since May 2020 AD and provides valuable data. Before calculating the average head, the point-water heads was transformed into average freshwater heads if the chloride concentration was known at the measurement location. The transformation from a point-water head into a freshwater head was done by applying Equation 2.5 and Equation 2.7. Since the change in chloride concentration of groundwater is a very slow process in deeper aquifers in the Netherlands [8], there was no requirement on the age of the chloride concentration measurement. If, however, multiple chloride measurements existed, the latest measurement was used.

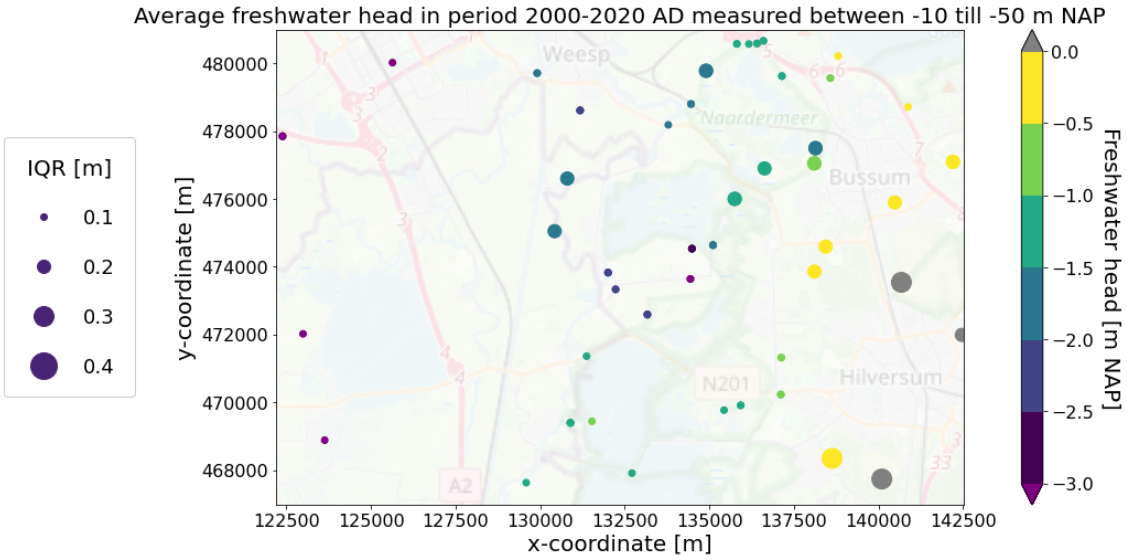

Figure 3.7: Overview of the average freshwater head distribution in the first aquifer of the period 2000 to 2020 AD. Furthermore, the IQR is given, which is a proxy of the fluctuation of the hydraulic head in the period.

Figure 3.7 visualises all average freshwater heads in the study area at one specific depth range, in this specific case, within the first aquifer. It is visible that the Utrecht Hill Ridge in the east has the highest averaged head values, which is expected since it has the highest elevation. Therefore, the ridge is the main infiltration area that recharges the regional groundwater flow [71]. The area between the Horstermeer Polder and the Vinkeveense Plassen is a recharge area that can either cause a flow towards the east or to the west. Moreover, also the Amsterdam-Rhine Canal (ARC) recharges the regional groundwater system. However, before the reclamation of the Horstermeer Polder, the river Vecht attracted regional groundwater flow, and brackish groundwater used to seep upward below the river [10]. After reclamation, the polder became a major discharge area draining the river Vecht and hence the upconed water was transported eastwards and further upwards. A seepage rate of up to 14 mm/day occurred on average between 1976 and 1978 AD, and this rate is still used to date [13, 56]. In the west and south of the polder, there is a semi-confined shallow layer and, in the south, fewer ditches are located, resulting in lower seepage rates. In the northeast, however, seepage rates of up to 30 mm/day exist [56].

3.4.3. Fluctuation of the Hydraulic Heads

Besides the mean freshwater head, Figure 3.7 also gives the Interquartile Range (IQR) of the freshwater heads of the period 2000 to 2020 AD. The IQR is the difference between the 1st and 3rd quartile of the data set. Due to temporal differences between groundwater recharge and natural and human-induced groundwater abstraction, groundwater heads fluctuate over time. Significant fluctuations in the east of the research area can be explained by the reclamation of Flevoland in the 1960s AD, located north of the area, or (a change in) groundwater extraction for drinking water purposes [72]. In the north, the effect is less profound. This could potentially be explained by the fact, during the same period, the Zuiderzee was closed off, probably resulting in a decrease of the chloride concentrations and corresponding rise of the point-water heads. To test these hypotheses, time-series analyses are needed.

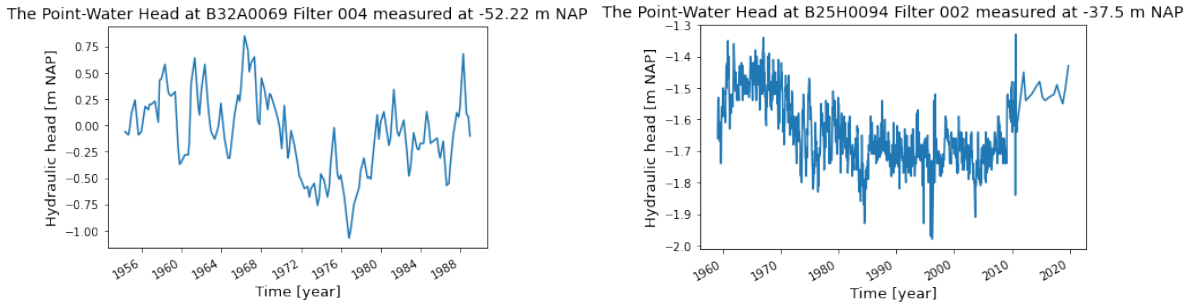

(a) **(b)**

Figure 3.8: The fluctuations of the point-water head in the east (B32A0069) and in the north (B25H0094). The locations of the measurements are given in Figure 3.9d.

Moreover, the ARC induces fluctuations of the hydraulic head in the area [59]. As said before, between 1965 and 1981 AD, the width and depth of the ARC were increased. This decreased the bottom resistance of the river and increased the infiltration rate, inducing an increase of the point-water heads in the surrounding area (Figure 3.9). Afterwards, the bottom resistance slowly increased over time due to sedimentation and corresponding clogging processes. However, from 2000 AD onwards, the bottom resistance decreased due to erosion caused by dredging and the increased speed and draught of industrial shipping in the river [59]. This resulted again in an increase of the point-water heads in the area. Moreover, since the deeper groundwater is brackish in the north of the research area, the increased infiltration of the ARC resulted in freshening of the area and hence a very steep increase of the point-water head (Figure 3.9a and Figure 3.9b). This explains the difference in the increase of the hydraulic head in monitoring well B31E0167, in the southern half of the research area, and the monitoring wells B25G0390 and B25H0238.

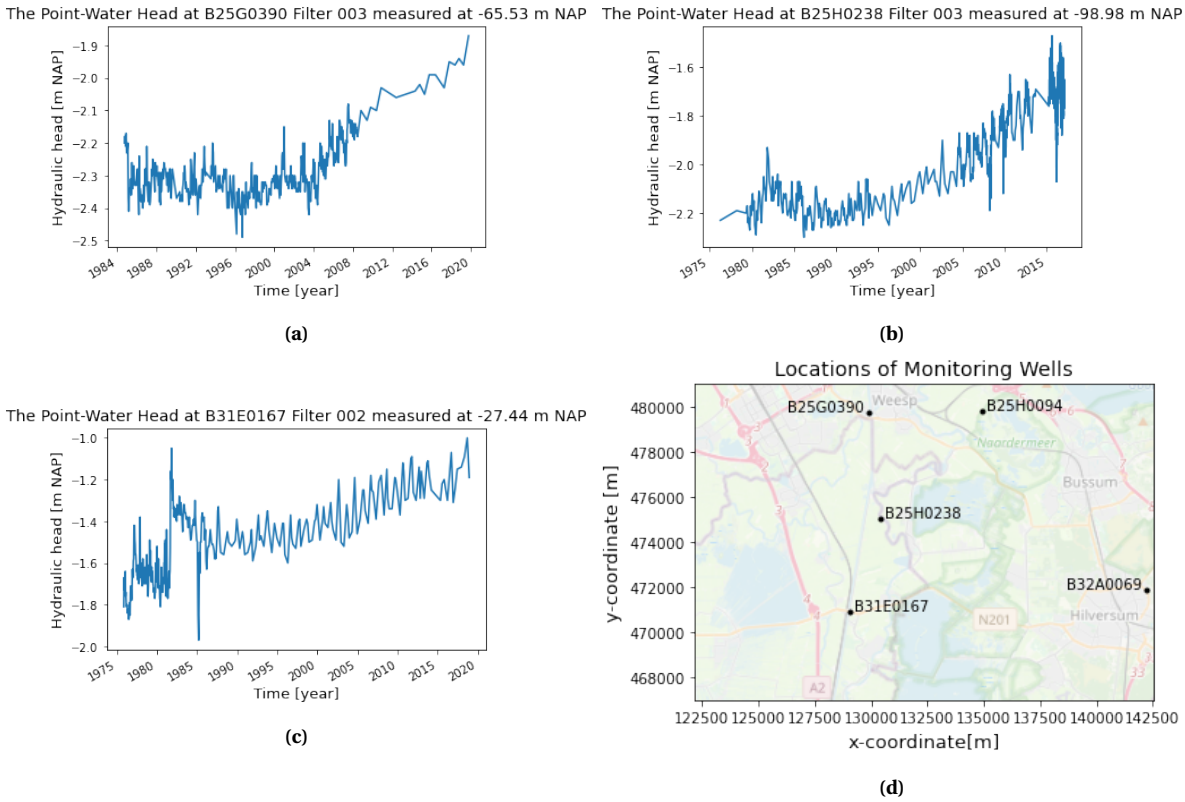

Figure 3.9: The fluctuations of the point-water head in the northern (a) and in middle (b) and in the southern (c) part of the ARC. In (d) an overview of the measurement locations is given.

II

Variable-Density Modelling

4

Methodology

A regional variable-density model was created using MODFLOW 6 in a FloPy environment. With this model, a first estimation could be made of the effects of the extraction of brackish groundwater on the spatial distribution of chloride in the research area. to build this model, several steps were needed, starting with acquiring all needed input data sets and modifying them, e.g. fitting them to the model grid. Next, the model was set up, and all required packages were added in both the groundwater-flow model and the groundwater-transport model. The vertical hydraulic conductivity of the top layer was modified in a calibration process to improve the model performance. Subsequently, the model performance was analysed based on the measurements available, visualised in the previous chapter. The last step was to implement the scenarios of the pilot wells with different operation settings in the Horstermeer Polder.

4.1. Model Description and Tools

The saline upconing below the Horstermeer Polder has been simulated with a 3D variable-density model in MODFLOW 6. It was decided to use MODFLOW 6 rather than other MODFLOW-based codes because of two reasons: (1) there are many pinch-out layers present in the area and only MODFLOW 6 can represent these layers as the HUF-Package is not supported in FloPy and (2) MODFLOW 6 does not require the conversion from point-water heads to freshwater heads before the calculation [22], which makes the model less complex. The model area has a structured grid of 129 by 134 cells with a cell size of 0.01 km^2 (100 x 100 m). In total, 34 layers were defined with spatially varying hydrogeological parameters. The east, south, and north boundaries of the model area are equal to the boundaries of the model area used by Fakhari [12]. However, the west boundary has been placed just east of the Amsterdam-Rhine Canal (ARC) instead of west of the canal. This was chosen since, based on the Regional Groundwater Model of Waternet, the ARC forms a water divide to approximately a depth of -100 m NAP. Therefore, it was more appropriate to place the boundary just east of the canal than west of it[1]. The used model area is shown in Figure 4.1. The used coordinate system was the new Rijksdriehoek coordinate system (EPSG 28992, RD New), which is the standard coordinate system of the Netherlands. The extent of the model stretches from 128100 m in the west to 141400 m in the east and from 468600 m in the south to 481400 m in the north. The used boundary conditions will be explained in Section 4.3.2. All boundaries meet the requirement of being three characteristic lengths (3λ) away from the Horstermeer Polder (Equation 4.1).

$$\lambda = \sqrt{KDc} \tag{4.1}$$

where λ $[L]$ is the characteristic length of a semi-confined aquifer, KD $\left[L^2 T^{-1}\right]$ is the aquifer's transmissivity and c $[T]$ is the vertical resistance of the leaky layer.

[1] When the west boundary was placed west of the ARC, the chloride distribution in the area was inadequate as a result of the water-dividing nature of the ARC.

The calculation was based on a continuous aquifer from the bottom of the Holocene complex to the top of the Maassluis Formation. The used average thickness of this aquifer was 160 m, with an average hydraulic conductivity of 30 m/d, resulting in transmissivity of 4800 m^2/d [12]. To calculate the vertical resistance, an average thickness of 2 m was used for the Holocene complex with an average vertical conductivity of 0.02 m/d [12]. This means that 3λ is equal to approximately 2.1 km. By assuring this requirement is met, the chance that the boundaries have a significant influence on the hydraulic head within the polder is low [73].

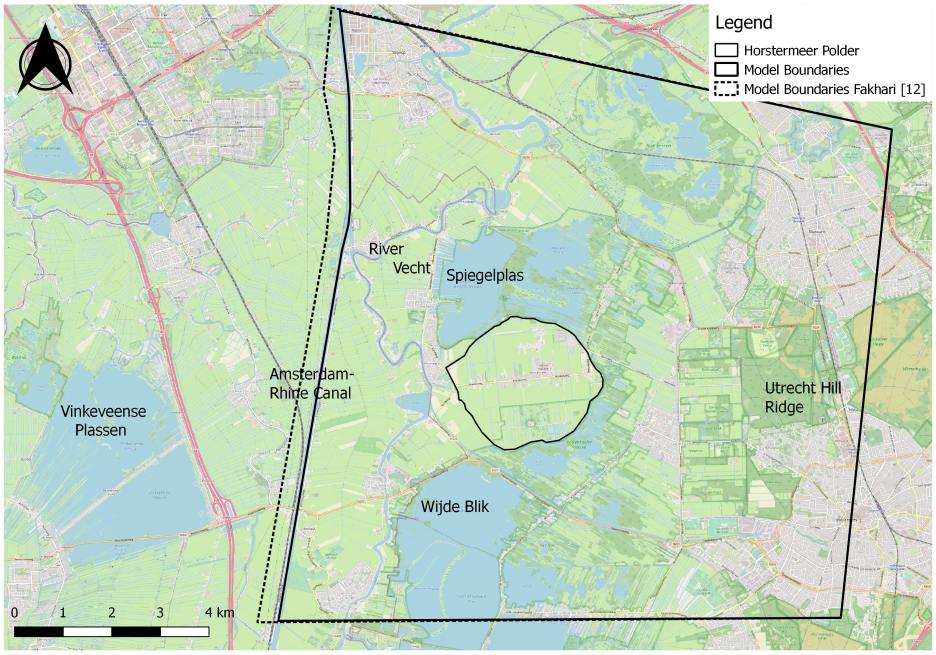

Figure 4.1: Boundaries of the model area (continuous line) and the boundaries of the model of Fakhari [12] (dashed line) in perspective of the study area.

The model was run for 450 years with a steady-state flow with a time step of two years to achieve a fresh-saline distribution and fluxes that are in reasonable agreement with the measurements. The used initial salt distribution will be explained in detail in Section 4.2.2. A larger time step was not suitable, as it resulted in oscillations of the model outcome. After 450 years, the model was run transient for two years with a time step of one month to visualise the effect of installing the pilot wells in the polder to extract the brackish groundwater. The pilot wells will only be running for two years, so a longer time period was not of interest.

The model was built using MODFLOW 6 [49] in a Python 3.7.9 environment (FloPy) [74]. FloPy version 3.3.3 was used in this research, and it was chosen to use the open-source web application of Python, Jupyter Notebook, combined with the Scientific Python Development Environment (SPYDER). The model was partly set up by using Python codes from NLMOD developed by Artesia Water [75]. These codes are part of a Python package that is under development and hence has not yet been released. This package processes, builds, and visualises MODFLOW 6 models in the Netherlands. Since variable-density modelling has not (yet) been implemented in the NLMOD package, the algorithms needed to be slightly modified and were combined with self-made codes to simulate the transport of chloride in the model. Whenever NLMOD was used, it will be stated in this chapter.

Moreover, Python was used to process and visualise all available data on hydraulic head and chloride concentration given in DINOloket and compare these measurements with the simulated values. Besides Python, QGIS 2.18.23 was used to convert external data to the RD-New coordinate system and create some of the maps used in this research. All codes can be found on Github: `https://github.com/sannedesmet/Saline-Upconing_Horstermeer/Modflow`.

4.2. Data Acquisition and Modification

As said before, the geology in the area is based upon REGIS II v2.2 [61] and GeoTOP v1.3 [69]. Besides the geology, more parameters were based upon other available data sets. These data sets were used as input parameter sets for the different MODFLOW packages. An overview of the used data sets is given in Table 4.1. The bottom-resistance and recharge data set were based on a different model, i.e. the Landelijk Hydrologisch Model (Nation-wide Dutch hydrological model) (LHM), and can be freely downloaded at the Nederlands Hydrologisch Instrumentarium (Dutch Hydrological Instrumentarium) (NHI) website. The data set of the geology and initial chloride concentrations were altered before they were used as input parameters, which will be explained below.

Table 4.1: Overview of all used datasets within the model.

Parameter	Name Data set	Data Source
Bottom resistance	NHI Intreeweerstand	`https://data.nhi.nu/`
Geology, K_h, K_v	REGIS II GeoTOP	`http://www.dinodata.nl:80/opendap/REGIS/REGIS.nc` `http://www.dinodata.nl/opendap/GeoTOP/geotop.nc`
Hydraulic head	Regionaal Grondwater Model Triwaco Waternet	-
Initial chloride concentration	NHI zoet-zout (fresh-saline)	`https://data.nhi.nu/`
Recharge	LHM4.1 2011-2018	`https://data.nhi.nu/`
Surface level	AHN3	`https://geodata.nationaalgeoregister.nl/ahn3/wcs?`
Surface waters	Waternet	-
Top layer classification	BRO Bodemkaart 2018	`https://dinoloket.nl/`
Water level polders	Waternet	-

4.2.1. Geology

The local stratigraphic evolution was discussed in detail in Subsection 3.2.1. This estimated geology will be used as the vertical discretisation of the model. The second clay layer from the top of the Maassluis Formation is the impermeable base of the model. Although the upper clay layer of the Maassluis Formation (MSk1) is also a very thick clay layer, and hence very little interaction between the aquifers above and below this clay layer will probably take place, the layer was not chosen to be the lower boundary of the model. This is because Fakhari [12] hypothesised that the aquifer below MSk1 needs to be brackish to have enough salt in the model to achieve the measured concentration of the discharge out of the Horstermeer Polder. Since the new drilling refuted this hypothesis, this model tries to show that even with a (partly) fresh aquifer below MSk1, salinity values close to the measurements can be simulated.

The layer thickness and hydraulic conductivity values were based upon the REGIS II and GeoTOP models for all layers and every cell. As a result, the top and bottom of every layer vary over the model area, and also the horizontal and vertical hydraulic conductivity values vary between cells in the same layer. The only layer that does not have a specified hydraulic conductivity value in neither REGIS II nor GeoTOP is the ice-pushed strata: the Drente Complex (DT-c). In this part of the Netherlands, the ice-pushed deposits are mainly sandy [76]. Based on the MIPWA and HDSR model a horizontal hydraulic conductivity of 19 m/d was chosen for the sandy ice-pushed deposits [76]. Moreover, Des Tombe *et al.* [67] has determined that the specific discharge is significantly larger between -25 and -35 m NAP than just above or below this layer. This "race layer" has not been taken into account in REGIS II yet. Therefore, it was decided to increase the horizontal hydraulic conductivity of URz5 by a factor of 1.5. Lastly, during calibration, the vertical hydraulic conductivity values

of the top layer were changed to achieve a model result that is closer to field measurements. This will be explained in Section 4.4.

The geology of the study area is complex, especially in the upper Holocene complex layer, in which eight small layers with different geohydrological properties are present [69]. These layers vary from anthropogenic to tidal sediments and peat layers [55], influencing the local conductance. Since the estimation of seepage rates is the objective of this research, the Holocene complex should be handled with care. However, the thickness of these individual layers is smaller than one meter at many locations. This fine vertical discretisation affects the computational time negatively. Therefore, it was chosen to combine these layers into one layer, which is justifiable since all layers have a comparable horizontal and vertical hydraulic conductivity. The individual layers were combined into one heterogeneous anisotropic layer with one equivalent value for horizontal and vertical hydraulic conductivity. The equivalent horizontal conductivity (K_{he}) was calculated using Equation 4.2.

$$K_{he} = \frac{\sum_{i=1}^{n} K_{hi} d_i}{\sum_{i=1}^{n} d_i} \tag{4.2}$$

where K_{hi} $\left[LT^{-1}\right]$ is the horizontal hydraulic conductivity of layer i, d_i $[L]$ the thickness of the same layer and n the total number of layers to be combined.

The equivalent vertical conductivity (K_{ve}), on the other hand, is computed as:

$$K_{ve} = \frac{\sum_{i=1}^{n} d_i}{\sum_{i=1}^{n} (d_i / K_{vi})} \tag{4.3}$$

where K_{vi} $\left[LT^{-1}\right]$ is the vertical hydraulic conductivity of layer i.

This modification was implemented in every column that contained at least one layer of the Holocene complex. Moreover, a layer was combined with a layer in the same formation whenever its thickness is smaller than one meter over a large stretch of the layer (Figure 4.2). The other layers that were combined together are all the Boxtel Formation sand layers, all the sand layers of the Drente Formation, URz1 with URz2, and URz3 with URz4. Within the newly formed Holocene top layer specific combinations of layer thickness and hydraulic conductivity resulted in either unrealistic high vertical hydraulic conductivity or very low values for both types of hydraulic conductivity in one cell. Therefore a minimum K_{he} and a minimum K_{ve} were set based on the minimum estimated K_h in the polder, which is 0.05 m/d [77], and an anisotropy factor of 10. In other words, the minimum occurring K_v is 0.005 m/d in the combined layers.

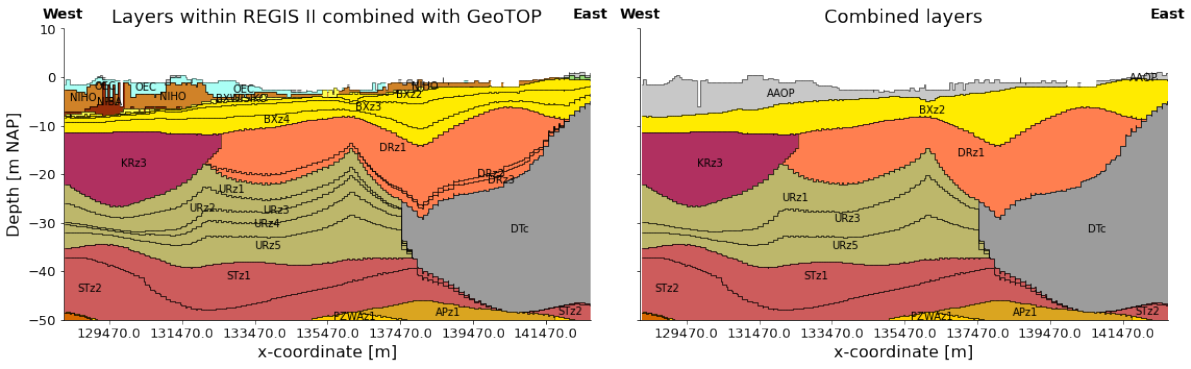

Figure 4.2: Overview of the layers that were combined in the model. The cross-section is made in the middle of the model area. The abbreviations used in the figure correspond with the abbreviations in Table 3.1 and additional abbreviation of layers in the Holocene Complex.

At the same time, the deeper layers are very thick in the REGIS II representation (> 50 meters locally) and resulted in thick cells. In variable-density groundwater models, like in this research, these thick cells are problematic as one cell can only contain one chloride concentration value. Primarily because the thicker layers are part of the second aquifer in the Peize-Waalre Formation, which is expected to be the location of the fresh-brackish interface in the majority of the model area. Therefore, these thicker layers were split into smaller layers containing the same geohydrological properties as the original cell (Figure 4.3). The thicker layers were divided such that the maximum thickness of the new layers did not exceed ten meters.

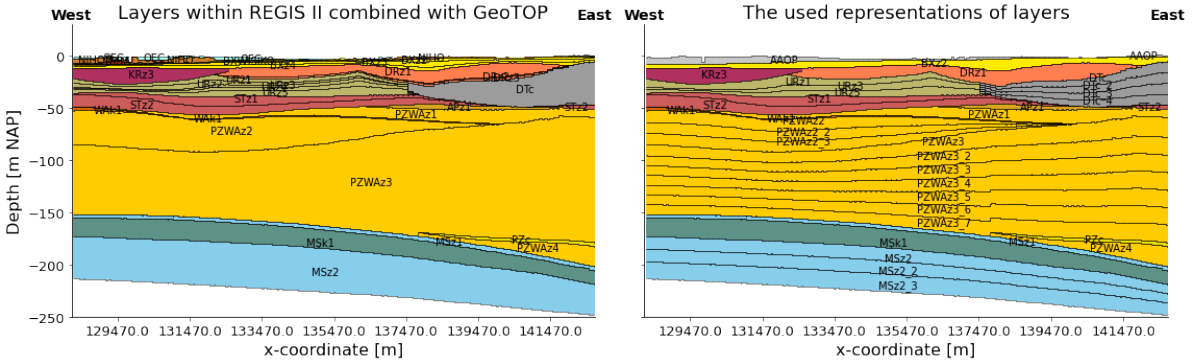

Figure 4.3: Overview of the difference between the original REGIS II + GeoTOP representation of the layers and the used representation after modification. The cross-section is made in the middle of the model area. The abbreviations used in the figure correspond with the abbreviations in Table 3.1 and additional abbreviations of layers in the Holocene Complex.

Although the layer thickness, horizontal and vertical hydraulic conductivity were modelled in great detail, it was chosen to use a constant value for the effective porosity of 0.3, which was used before in Dutch groundwater models [8, 78, 79]. The same approach was used for the anisotropy factor (K_h/K_v), and a constant value of 10 was chosen. This factor was used whenever neither REGIS II nor GeoTOP has a value specified for either K_h or K_v in a cell but did have a value for the hydraulic conductivity in the other direction.

4.2.2. Initial Chloride Concentration

The initial chloride concentration is very influential in the case of variable-density groundwater modelling [80]. In the Netherlands, a nationwide salinity estimate has been developed by Deltares [62]. This model has a grid of 250 x 250 m and is based on all available data on chloride concentration and EC in 2017. The model consists of 39 model layers with a fixed top and bottom, i.e. all cells in a layer have the same thickness and the same heights for the top and bottom of the cell. However, the thickness of the layers varies over the depth from 2 meters to 20 meters at greater depths. Every cell has one chloride value, although since the model is a statistically-based interpolated model, one can choose to use the first-quartile (p25), median (p50), or third-quartile (p75) value. To decide which of these three values should be used, the values were compared with the chloride concentration measurements in DINOloket. As shown in Figure 4.4, the p25-model almost always underestimates the chloride concentration, whereas the p75-model overestimates the chloride concentration at most locations. The p50-model sometimes overestimates and sometimes underestimates the chloride concentration.

The statistics of the error given in Table 4.2 acknowledge the visual conclusions made above. Based on these statistics, the p50-model corresponds best with the measurements since the mean error, the mean absolute error, standard deviations, and maximum absolute error are all the lowest for the p50-model. However, the maximum chloride concentration within the model area in the p50-model is as high as 12585 mg/l, whereas the maximum measured chloride concentration is just 6840 mg/l. Moreover, due to a lack of data on the chloride concentration below the Horstermeer Polder during the creation of the NHI fresh-saline model, the interpolation of the available data has led to

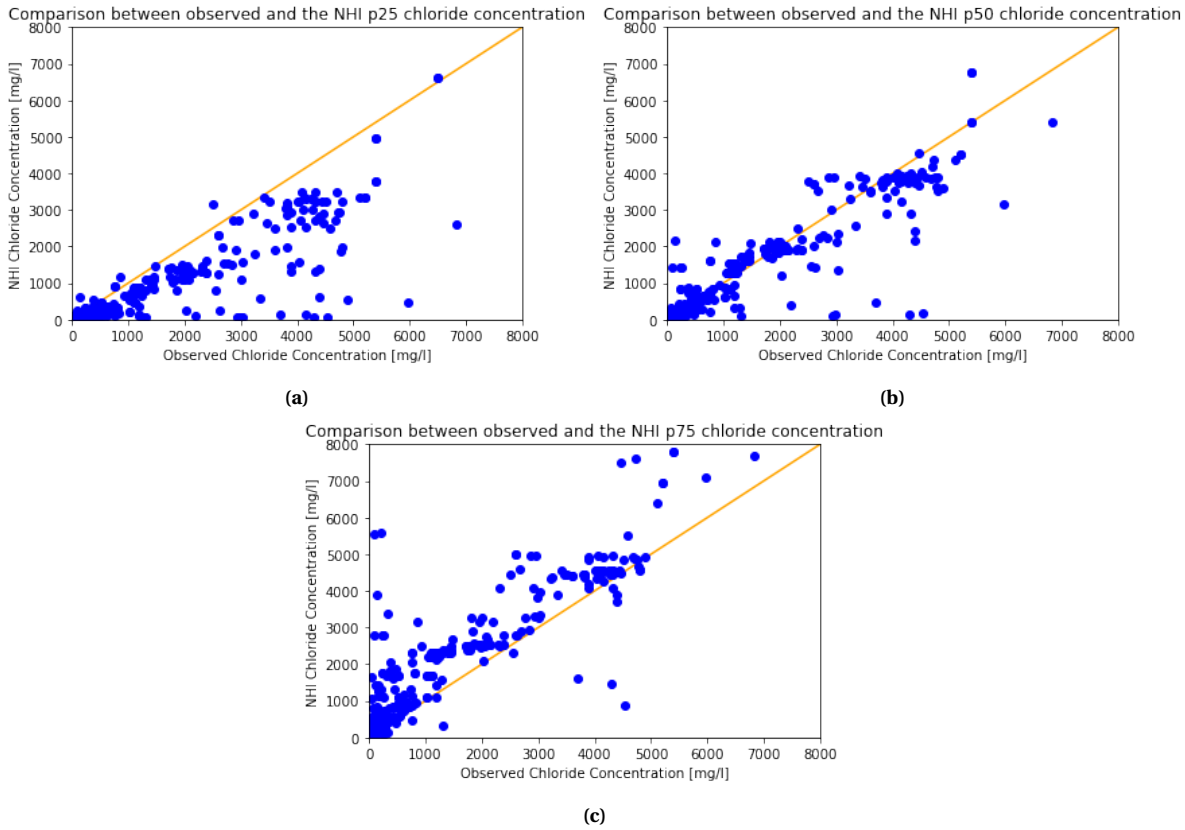

Figure 4.4: Comparison of chloride concentration measurements and the chloride concentration values in the NHI fresh-saline model. In (a) the first-quartile (p25) values of the NHI model are depicted in (b) the median (p50) and in (c) the third-quartile (p75) values. The closer the dots are to the orange line the better the simulated values match with the observed concentration.

an inversion in the salinity distribution in all three models. However, this inversion is not visible in the measurements (Figure 3.5); hence modifications were needed before the p50-model could be used as the initial chloride concentration. These will be explained below. Afterwards, the fitting of the p50 model grid to the model grid of the MODFLOW 6 model will be explained.

Table 4.2: Summary of the characteristics of the error between the chloride concentration values simulated by the NHI fresh-saline models and the observed chloride concentration in the model area.

Error characteristics [mg/l]	p25	p50	p75
Mean error	205	7	-265
Mean absolute error	225	148	292
Standard deviation	563	381	551
Max. absolute error	5493	4374	5438
Max. Cl-concentration	7077	11477	15911

Modification of the NHI Fresh-Saline Model

The inversion below the Horstermeer Polder and the shape of the fresh-brackish interface at the surface of the model, are not in agreement with the measurements. Moreover, the inversion caused model instability. Therefore, it was decided to remove the complete inversion from the model and fill those cells with a chloride concentration of 100 mg/l. In other words, the estimated chloride values below the Horstermeer Polder down to a depth of -50 m NAP have been changed into a value of 100 mg Cl^-/l. Concerning the maximum occurring chloride concentration, it was decided to use the maximum chloride concentration ($\pm$ 7100 mg Cl^-/l) of the p25-model as the maximum occurring chloride concentration. In other words, whenever a cell had a value above 7100 mg Cl^-/l the con-

centration was changed to 7100 mg Cl^-/l. This value is similar to the maximum measured chloride concentration in the area, which is 6840 mg/l.

Model-Grid Fitting

After modifying the p50-model, the model grid was fitted to the MODFLOW 6 model grid. Since the p50-model covers the Netherlands, its extent was first reduced to the model area. Next, four fitting operations were performed: (1) change the cell size of the p50-model grid to 100 x 100 m, (2) fit the x- and y-coordinates to the x- and y-coordinates of the MODFLOW 6 model grid, (3) locate in which layer of the p50-model the top and bottom of each MODFLOW 6 cell are and (4) take the average concentration of all p50-cells that are located within the MODFLOW 6 cell.

The first step was performed by repeating the rows and columns in the p50-model both five times. During this operation the 250 x 250 m cell were split into 25 cells of 50 x 50 m. Next, two neighbouring cells were combined in the y-direction and afterwards in the x-direction. These operations are visualised in Figure 4.5 and, as can be seen, created cells of 100 x 100 m. As only 2.5 cells with cell size 100 x 100 m fit within 250 m, the cells at two edges of the original cell contain the average value of the original cell and the neighbouring cell. Moreover, one cell in every 25 cells contains the average chloride concentration of four original cells.

However, the resulting 100 x 100 m cells did not precisely overlap with the cells in MODFLOW 6. There was a 50 m difference between the centres of each cell in both x- and y-direction, which was resolved by combining the neighbouring cells once more in the same way as before. This modification process was preferred over filling the MODFLOW 6 cells with the value of the cell of the NHI model closest to it, as it made it possible to create a more gradual transition of the chloride concentration between cells. This is expected to lower the number of iterations needed to achieve a numerically stable solution.

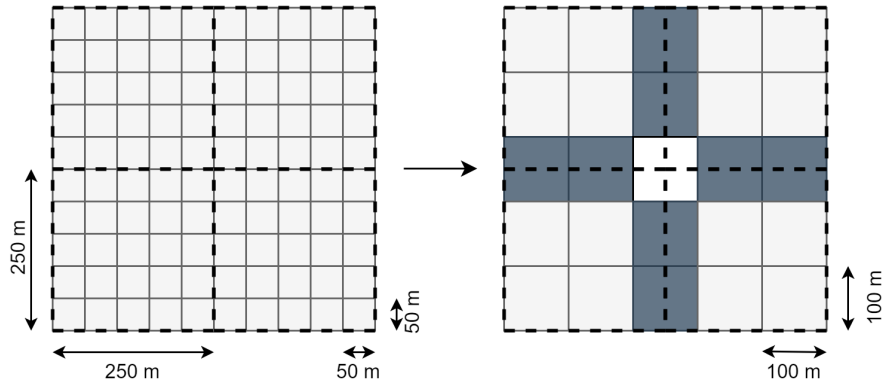

Figure 4.5: Visualisation of the cell-size modification process of the NHI fresh-saline model from 250 x 250 m to 100 x 100 m. The dashed cells represent the original cell size. The dark grey cells are filled with the average chloride concentration of the two neighbouring cells. The white cell in the middle contains the average of all four cells.

After fitting the x- and y-coordinates of the NHI p50-model to the MODFLOW 6 cells, the two matrices were superimposed in the vertical direction. Since the top and bottom of the MODFLOW 6 cells vary in space, it was determined in which NHI layer the top and bottom of the MODFLOW 6 cells are located. Subsequently, it was calculated how many NHI layers are represented within each MODFLOW 6 cell. This was stored temporally for every cell in a 3D matrix with the same dimensions as the MODFLOW 6 model.

Lastly, for every cell, the total chloride concentration of all layers within the NHI-model, that are represented within that cell, was calculated and stored in a new 3D matrix with the same dimensions and orientation as the MODFLOW 6 model. By dividing this total-chloride matrix by the aforementioned matrix containing the number of NHI layers represented in one cell, the average chloride

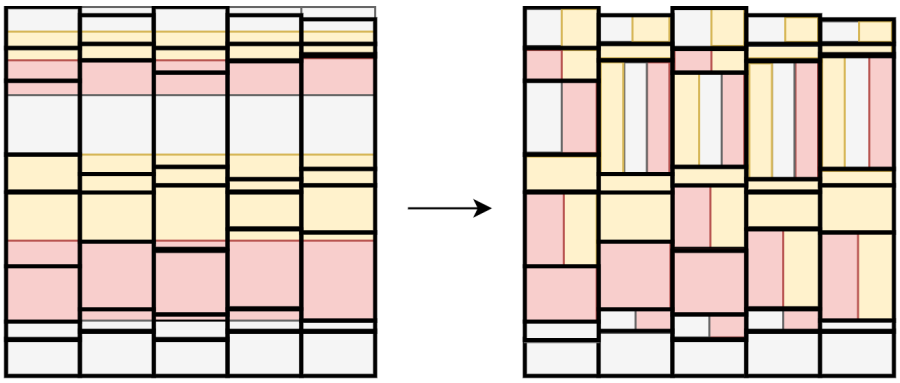

Figure 4.6: Visualisation of the process to determine in which layers within the NHI model the MODFLOW 6 cells are located. The black outlines represent the MODFLOW 6 cells that have a varying thickness in space, whereas the red, yellow, and grey cells represent the NHI layers, which have a constant thickness in space and time. Multiple colors within one MODFLOW 6 cell on the right means that the average is taken from the chloride concentrations corresponding to those layers of the NHI model.

concentration of all cells within the p50-model that are represented by one cell in the MODFLOW 6 model, could be calculated. This process is visualised in Figure 4.6. As shown in the figure, this fitting process means that within one MODFLOW 6 layer some cells have an average value of multiple NHI cells, whereas other cells in the same layer have the value of one NHI cell. Moreover, the ratio between the thickness of the multiple NHI cells, represented within one MODFLOW cell, was not considered within the calculation. In other words, whenever only one cm of the NHI cell was located within the MODFLOW cell, its chloride concentration was used in the averaging process. This is an approximation that required fewer calculation steps.

4.3. Model Set-Up

In this section, the used packages within the MODFLOW 6 model will be explained. The packages simulate different hydrological stresses and solute transport processes that influence groundwater flow. The simulated hydrological processes are recharge, surface water - groundwater interaction, and overland flow. These processes are part of the Groundwater Flow (GWF) Model. The transport processes that are considered are advective transport and sources and sinks resulting from hydrological processes. These are defined within the Groundwater Transport (GWT) Model. The spreading of the chloride is only simulated due to numerical diffusion. Before explaining the two separate models, the basics of the models and the boundaries of the model will be discussed.

4.3.1. Basis MODFLOW 6

MODFLOW 6 was developed to allow multiple groundwater models to be combined in one simulation [50]. For example, with a GWF-GWT Package if a groundwater flow model is combined with a transport model. This means that the basis of a MODFLOW 6 model is always the simulation package that creates the simulation object, which is comparable to the MODFLOW model object in MODFLOW-2005. In contrast with MODFLOW-2005, the discretisation of time is defined in a separate timing module (TDIS). Within the TDIS Package the stress periods, in which stresses are constant, and the time steps per stress period are defined. At each time step, the model is numerically solved to compute the head and flow. Moreover, it is possible to define which stress periods are steady-state and which are transient. Only one timing module per simulation object can be defined [50]. All other packages are specified within the model objects. However, it is important to note that at this moment, the spatial discretisation packages of all models within one simulation should have the same DIS-Package input [51]. Moreover, it is common to use the same Iterative-Model-Solution (IMS)-Package that defines the iterative method that is used to solve the linearised matrix equations of the model [50]. Within this model, Biconjugate Gradient Stabilized (BiCGSTAB) linearised accelerators were used, as this method is used in all available examples of a variable-density model in MODFLOW 6 [81]. The maximum number of iterations was 700 for the outer and 300 for the inner

iteration process. The tolerance of head difference between two iterations was $1 \cdot 10^{-8}$ m, and the tolerance of the flow residual was set to be $1 \cdot 10^{-6}$ m/d. A relaxation factor of 0.97 was used, which is again the commonly used factor in the examples [81].

4.3.2. Boundary of the Model

In practice, the processes defined in the model area will also take place outside of the defined area, depicted in Figure 4.1. As a result, groundwater will flow out and into the system and chloride travels across the borders. Therefore, a boundary condition needs to be set to allow these cross-overs. Fakhari [12] chose to close the northern and southern boundary, i.e. an impermeable 'wall' was placed on those borders to prevent flow and transport from occurring at those borders. This decision was based on an isohypse map simulated by the Regional Groundwater Model of Waternet ($RGWM_{Waternet}$). In this research, it is hypothesised that part of the chloride in the model area originates from the former Zuiderzee in the north. Hence, it was chosen to open all boundaries for both flow and transport.

The aforementioned $RGWM_{Waternet}$ was used to define the hydraulic head values in the cells at the boundary of the model as it includes the boundaries of this model area. However, before it could be used, a modification was needed. First, the model grid was fitted on the MODFLOW 6 grid. The regional model has a grid-cell size of 50 x 50 m. However, the cell centres deviate 50 meters both in x- and y-direction from the MODFLOW 6 cells. Therefore, the neighbouring cells were combined, and the average value was taken. Moreover, the vertical discretisation differs from the MODFLOW 6 model. Both models have spatially varying cell thicknesses and hence different heights of the tops and bottoms of the individual cells. Therefore, it was determined in which layer of the $RGWM_{Waternet}$ the bottom of the MODFLOW 6 cell is located, and the head of that cell was used as the head of the cell in the MODFLOW 6 model. Moreover, the bottom of the $RGWM_{Waternet}$ is at -150 m NAP, whereas the MODFLOW 6 model has a bottom as deep as -260 m NAP (Figure 4.3). Based on rare point-water heads measured in deep drillings below a depth of -150 m NAP, it was approximated that the heads are a factor 0.989 smaller for every layer below the bottom layer of the $RGWM_{Waternet}$.

The boundaries were defined using the General-Head Boundary (GHB)-Package, which requires a conductance term. This term has been calculated using the formula for the conductance term given in Equation 2.11 with the assumption that the horizontal conductivity estimated by REGIS II or GeoTOP is equal to the freshwater-equivalent hydraulic conductivity. Besides the hydraulic head values and a conductance term, this package also requires a chloride concentration in variable-density groundwater models. The modified and fitted NHI p50-model values were used as the chloride concentration at the boundary. The hydraulic-head values are required to be in terms of freshwater heads [22]. However, the $RGWM_{Waternet}$ contains neither point-water heads nor freshwater heads, because the model uses only groundwater-flow modelling and ignores the variable-density within the area and is thus was only calibrated at locations where the influence of the chloride concentration is negligible. It was chosen to transform these heads into point-water heads by using a empirical formula (Equation 4.4). The empirical formula is solely a function of the density since the heads in the model are overestimated with increased density, and the inclusion of a depth term did not result in better correspondence with the measurements.

$$h_{rm_{new},i} = h_{rm,i} - 49.32 \cdot \frac{\rho_i - \rho_f}{\rho_f} \tag{4.4}$$

where $h_{rm_{new},i}$ $[L]$ is the modified point-water head at location i, $h_{rm,i}$ $[L]$ is the original point-water head simulated by the regional model at location i, ρ_i $\left[ML^{-3}\right]$ is the density at location i based on NHI and ρ_f $\left[ML^{-3}\right]$ is the freshwater density.

The factor of 49.32 has been determined using Monte-Carlo simulations with a changing factor and the objective function: Root Mean Square Error (RMSE), given in Equation 4.5. The best achievable

RMSE was 0.27, which means the newly created point-water heads show reasonable goodness of fit with the measurements.

$$\text{RMSE} = \sqrt{\frac{\sum_{i=1}^{n} \left(h_{rm_{new},i} - h_{o,i}\right)^2}{n}} \tag{4.5}$$

where $h_{o,i}$ $[L]$ is the observed head at location i, and n is the number of measurement locations.

The modified point-water heads were transformed into freshwater equivalents by applying Equation 2.5. However, these boundary conditions resulted in "loops" at the boundary, i.e. groundwater enters the model domain at the deeper boundary cells, then flows upwards and leaves the model domain again in the shallow boundary cells. This occurred especially at locations where density difference plays a significant role in the flow pattern. Since there is no physical explanation of the loops, it was chosen to change the boundaries to hydrostatic-over-the-depth boundaries. The modified point-water heads were used as the phreatic surface and with the help of the freshwater-equivalent of Equation 2.1 and calculation of the weight above the centre of every cell, the hydrostatic groundwater heads were determined. This is explained in more detail in Appendix C.

To make sure that the boundary remained hydrostatic throughout the simulation, the Constant Concentration (CNC)-Package was applied on all boundary cells. This package ensures that the chloride concentration stays constant in all boundary cells. The used chloride concentration is equal to the initial chloride concentration.

4.3.3. Groundwater-Flow Model

Within the GWF Model, the hydrological processes are defined. Besides these processes, also the spatial discretisation in all directions (DIS-Package) and the hydraulic conductivity per cell are specified (NPF-Package) within this model based on the input described above. Every cell has its own IDOMAIN value that determines whether a cell is active (1), inactive (0), or acts as a "vertical pass-through cell" (-1) [49], as explained in Section 2.5. Cells with a thickness less than one meter were changed to "vertical pass-through cell" by setting the IDOMAIN value to -1. Only when the top cell of a column is thinner than a meter, the cell was excluded from the model and made inactive (IDOMAIN = 0). The hydrological stresses explained below were always placed on the first-active cell of a column, if the column is subjected to that stress. Lastly, as said before in Section 2.5, within the GWF Model, it is necessary to include the BUY-package to use the variable-density form of Darcy's law (Equation 2.3) for all flow calculations.

Groundwater Recharge

Recharge varies between 0 and 0.0014 m/d (Figure 4.7). The data set that was used in the model originates from the LHM4.1 model, the latest version of the nationwide hydrological model of Deltares. Within the model, three models were coupled: MODFLOW, to simulate groundwater flow, metaSWAP, to simulate the unsaturated zone, and MOZART-DM, to simulate surface waters. The recharge estimates are an interim result of this model, which was calculated by subtracting the evaporation from the precipitation and adding irrigation. Moreover, this data set was also used in the NHI fresh-saline model [62]. It was chosen to use the data set that represents the long-term average recharge of the years 2011-2018 AD, as the simulation of the current situation is the objective of this research.

However, in Figure 4.7, a clearly defined square within the Horstermeer Polder is visible in which the recharge is significantly lower than the surrounding areas. A reason for this reduced recharge in this specific area is the top layer in that area; The square-shaped area is located at the same place as the small clay area in the northwest of the polder (Figure 4.10). Hence the limited recharge could be a result of a very low infiltration capacity. Yet, in other clayey areas in the model area, groundwater recharge does occur. However, there are many ditches at this specific location, and due to the low infiltration capacity overland, flow occurs quickly. Subsequently, retention at the

location with a lower infiltration capacity is unlikely as it will flow towards one of the ditches. As a result, the recharge could be limited in this specific square in the Horstermeer Polder and therefore the data set has not been altered.

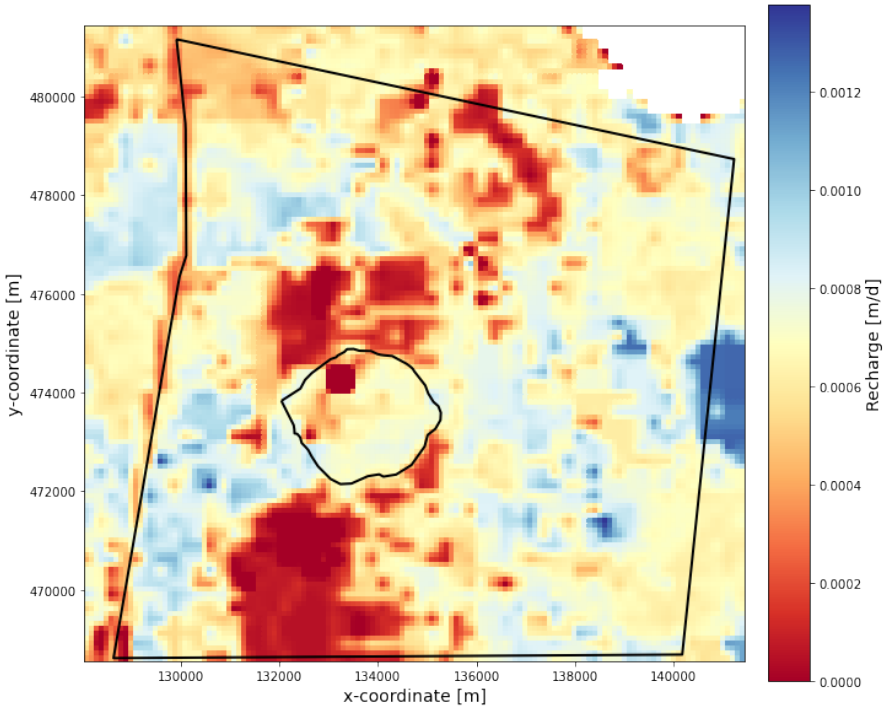

Figure 4.7: Spatial distribution of the recharge. The Horstermeer Polder and the model area are indicated with a black outline.

Surface Water-Groundwater Interaction

The interaction between the aquifer and the surface waters not has a significant influence on the magnitude of flow in surface waters and on the flow patterns in the aquifer [82]. Therefore, this interaction needs to be taken into account when modelling the groundwater flow.

Within MODFLOW 6, these head-dependent flux boundaries can be modelled by either using the Drain (DRN)-Package or the River (RIV)-Package. The difference between the two is that the DRN-Package can only simulate drainage from the aquifer into surface water, whereas the latter can simulate both infiltration and drainage. The conductance term of both processes in the RIV-Package is equal. However, in practice, the conductance of leakage from the aquifer is often higher than the infiltration from surface waters into the aquifer [83]. One of the reasons for this is that drainage into the river occurs both through the riverbank and the base of the river, whereas infiltration primarily occurs through the bottom sediments and lower riverbank parts [82]. On top of that, the hydraulic conductivity is generally lower during infiltration due to clogging by fine bed sediments [84]. Moreover, at the upper part of the river banks clogging is not common, and hence the hydraulic conductivity of those parts is higher. However, very little research has been done on this phenomenon, and, in some cases, no difference was found between the hydraulic conductivity while infiltrating and exfiltrating [85]. Nevertheless, in the Netherlands, it is relatively common to use a different conductance for both processes within polders [83]. Therefore, different conductance terms were used by combining a DRN-Package with a RIV-Package with the same drainage level at one location. The conductance term is the same in both packages, but since the DRN-Package only simulates drainage into surface waters, the conductance term for seepage into the surface waters is twice as high compared to the infiltration value.

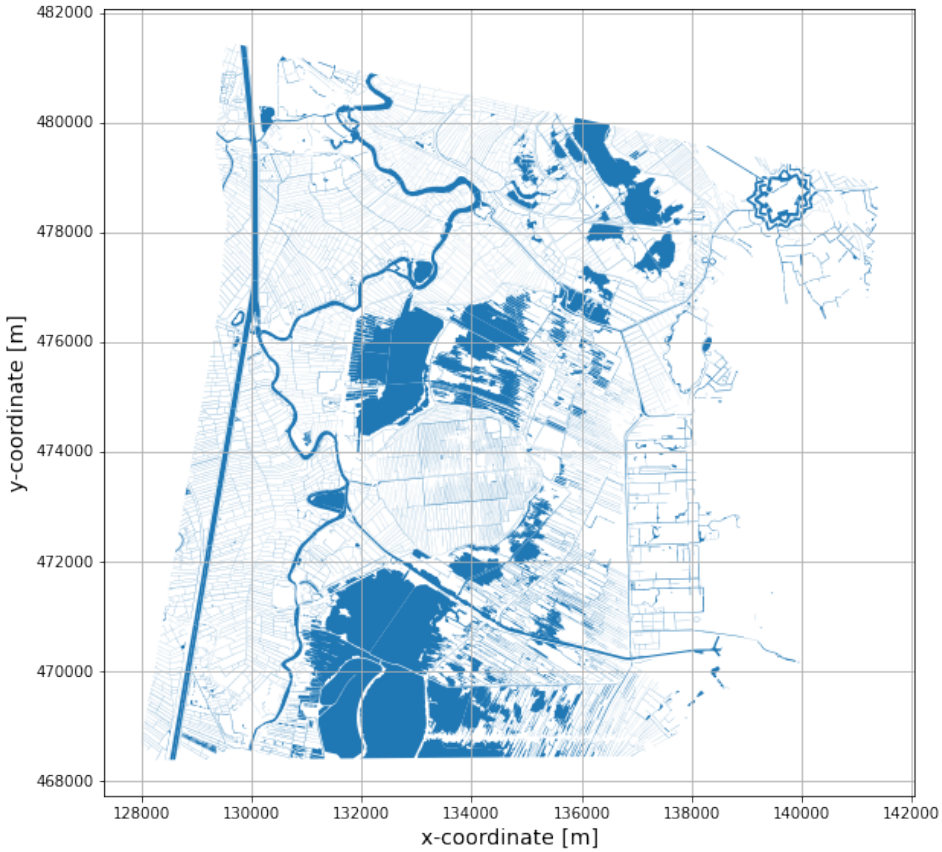

Figure 4.8: Overview of the controlled surface waters within the model boundary that were used in the simulation.

To determine on which cells the DRN- and RIV-Package should be applied, a shapefile of Waternet, containing all controlled surface waters, was used. As shown in Figure 4.8, the shapefile has a very high level of detail, and every controlled ditch in the area is taken into account. This shapefile was superimposed over the model grid with the help of an algorithm of NLMOD, and, per cell, the area covered by surface waters could be quantified as well as the corresponding stage and bottom elevation. Since every surface water has its own defined stage and bottom elevation, the area-weighted average was taken as the stage and bottom elevation in every cell. The only parameter that still needed to be defined to calculate the conductance is the representative bottom resistance of those surface waters in every cell. The LHM4.1 model has, besides a recharge data set, also a data set of the estimated bottom resistance, visualised in Figure 4.9. This data set is based on the classification of the top layer (Figure 3.3). The conductance was calculated by dividing the total area covered by surface waters in the specific cell by the bottom resistance.

This calculation method neglects the head loss in the aquifer due to the surface water - groundwater interaction [86]. The importance of this aquifer resistance depends on its hydraulic properties in relation to the properties of the streambed and the geometry of the surface water [87]. Pauw *et al.* [86] showed that the aquifer resistance is significant in the case of a low grid resolution and should be taken into account. In this research, a grid-cell size of 100 x 100 m is used. Therefore, using the formulation of De Lange [88] would lead to better results since the negligence of the aquifer resistance results in an overestimation of the flux towards surface waters [86]. This formulation is included in NLMOD and can easily be adopted, although it does require a significant amount of additional parameters, i.e. the resistance of the top system, the resistance of the surface water bottom, the submerged height at the banks of the surface water, and the width of the bottom of the surface water. However, these parameters are not known in the model area and hence should all be estimated. Therefore it was chosen to use the simplified version for the calculation of the conductance.

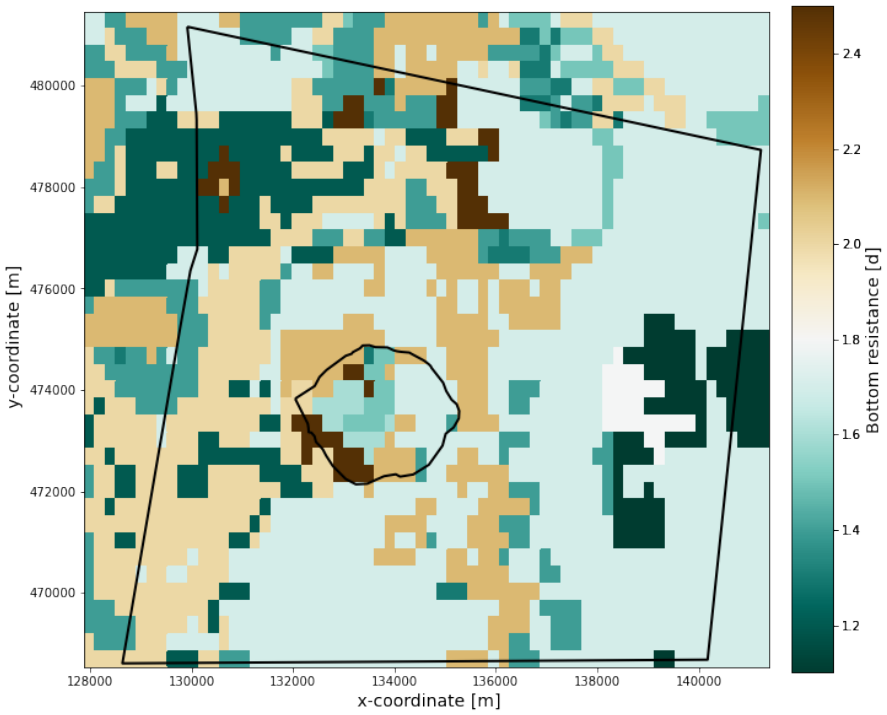

Figure 4.9: Spatial distribution of the bottom resistance based on the LHM4.1 model.

Overland Flow

Whenever the hydraulic head rises above the surface level or when the rainfall intensity exceeded the soil's infiltration capacity, water would drain overland with the help of gravity. Most of the time, the water will eventually drain into surface water or a sewage system. This process is taken into account in the model with the help of another DRN data set. This inhibits the occurrence of high water tables above the surface level. Those high water tables should be avoided since they are not realistic to occur in a time window of a year, which is the time step of the model. The stage that is used in this DRN data set is equal to the surface level. If in one cell both DRN data sets are present, the lower stage value is determinative.

In the Netherlands, a digital version of the surface level is available in a digital elevation map: Actueel Hoogtebestand Nederland (Up-to-date Height Model of the Netherlands) (AHN). For every cell, the average surface level was calculated with the help of code from NLMOD. Since the AHN has no values whenever water is present, some cells in which a significant fraction is water, have no stage and no DRN data set representing overland flow. However, most of those cells have a DRN data set value due to groundwater-surface water interaction, and, therefore, the head in those cells will never rise above the surface level.

Effect Variable Density on Groundwater Flow

Differences in density heavily influence groundwater flow; thus, to simulate variable-density groundwater flow correctly, it is necessary to take the density into account. In MODFLOW 6, this is done by including the BUY-Package. In this package, the parameters of Equation 2.7 are defined. In this research, the reference concentration is 0 mg Cl^-/l, whereas the volumetric concentration expansion coefficient divided by the reference density (DRHODC) is set to be $1.32 \cdot 10^{-3}$.

4.3.4. Groundwater-Transport Model

The GWT Model includes the same DIS and IMS-Package as the GWF Model. The initial chloride concentration is used as the initial condition of the GWT Model. Moreover, it is necessary to define the porosity of the cells by applying the Mobile Storage and Transport (MST)-Package. Additional to these requirements, it is possible to define other chemical processes to be modelled. The transport

process advection and sources and sinks are explained below. Moreover, the decision to exclude diffusion and dispersion from the model, and, thus, only use numerical diffusion as a spreading mechanism is elaborated.

Advection
Advection can be simulated by applying the Advection (ADV)-Package, which is solved by either centre-in-space weighting, upstream weighting or an implicit second-order total variation diminishing scheme [89]. These approaches are not particle-based (Method of Characteristics) and hence require a higher level of spatial discretisation. It appeared that only the upstream weighting results in a stable numerical solution with the used spatial discretisation.

Sources and Sinks
Hydrological stresses not only influence groundwater flow physically, but they also act as sources and sinks of solutes. Therefore, every hydrological-stress package has a chloride concentration defined per cell, used whenever groundwater enters the aquifer. For recharge, this value was set to 50 mg Cl^-/l, which is the same value as was used to create the NHI fresh-saline model [62]. In the RIV- and DRN-packages the cells got the same chloride concentration as the initial value.

Diffusion and Dispersion
Both diffusion and dispersion cause a spreading of solutes in the system. In other words, these processes influence the sharpness of the interface between fresh and brackish groundwater [90]. However, these processes are influenced by many mechanisms and aquifer characteristics, e.g. spatial heterogeneity of the geology, variability in groundwater recharge, and pumping activities [3]. Moreover, the relative contribution of these factors to the spreading of solutes is still not fully understood. Therefore, defining the parameters belonging to these processes is challenging, and a wide range of values is used.

At the same time, in numerical models, numerical diffusion occurs as a result of the truncation error of the used solution scheme[2] [91]. Numerical diffusion can be significant, and estimating the physical parameters in relation to numerical diffusion is hard and time-consuming. Therefore, it is often chosen to exclude physical diffusion and dispersion and only use the numerical diffusion to simulate spreading in the model. Although it was tried to include an appropriate physical diffusion and dispersion parameter, the physical processes were eventually excluded from the model.

4.4. (Un)Steady Chloride Distribution and Calibration

It was expected that the used initial chloride concentration data set has not reached a steady position under the current boundary conditions. Hence, the spatial distribution of chloride will change when the model is running. However, to analyse the effect of the pilot well in the Horstermeer Polder, it is necessary to have a steady chloride distribution. At the same time, in practice, the spatial distribution of chloride never corresponds to the current hydrological stresses, and autonomous salinisation occurs [8, 38, 47, 48]. Therefore, the model will be considered steady enough to run the scenarios whenever the average difference of the chloride concentration in one cell between two consecutive years is more or less constant.

The spatial distribution of chloride is influenced by hydrogeological parameters and the boundaries of the model. Although the boundaries are important, this research will only focus on the calibration of the K_v of the Holocene complex, as this appeared to be a very influential parameter. One of the objectives was to achieve fluxes in a reasonable agreement with the estimated fluxes by water balance calculations [92]. Since the Holocene layer is a combined layer, the calibration will be on the minimum and maximum occurring K_v. It appeared that the constant-in-space limit on the minimum occurring K_v resulted in fluxes in the polders in the model area, which did not correspond

[2] The truncation error is the error in approximating the differential equations by the numerical scheme [91].

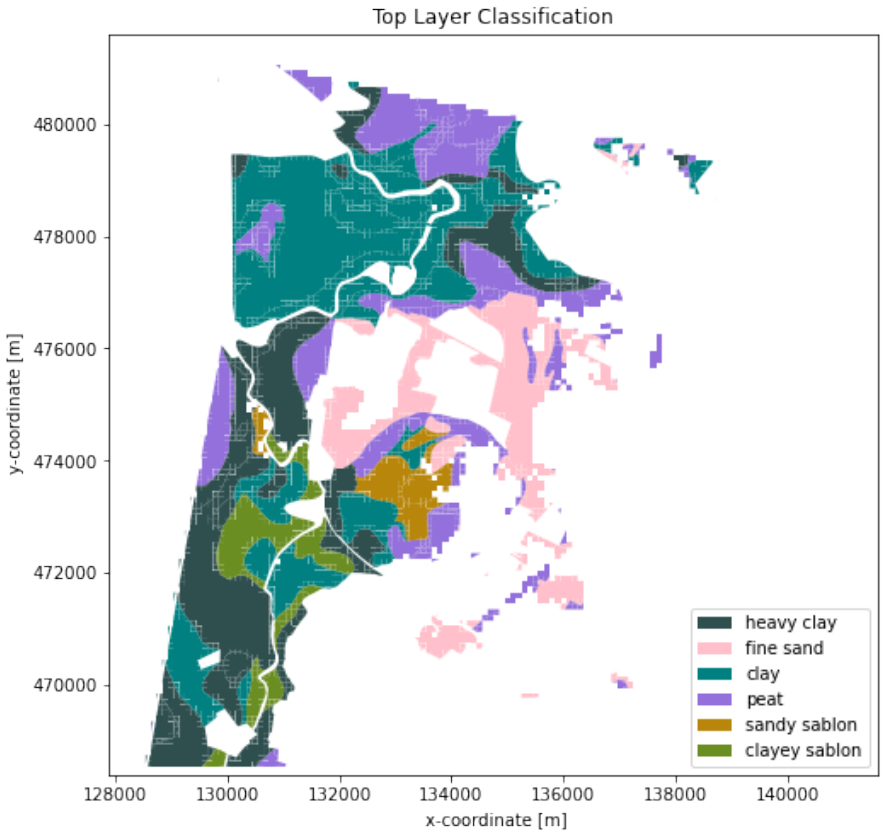

Figure 4.10: The classification of the top layer used for the limit on the vertical hydraulic conductivity of the Holocene complex.

with the water balance calculations. In specific polders, the flux was too high, whereas, in others, including the Horstermeer Polder, the simulated flux was too low. Therefore, a limit based on the top layer classification (Figure 3.3) was determined. However, as given in Figure 3.3, the classes were first lumped together since that level of detail would be too time-consuming. The used classification can be seen in Figure 4.10. Whenever no top layer classification was present, because there is water or urban area, the previous limit on the minimum K_v of $K_{h,min}/10$ is used. Moreover, at some locations, the K_v was unrealistic high. At these locations, the maximum K_v was limited to 1.5 times the minimum K_v of the top layer.

Table 4.3: Overview calibrated limits vertical hydraulic conductivity per soil type.

Type of Sediment	$K_{v,min}$ **[m/d]**	$K_{v,max}$ **[m/d]**
heavy clay	0.002	0.003
clay	0.0025	0.00375
clayey sablon	0.008	0.012
sandy sablon	0.05	0.075
peat	0.08	0.12
fine sand	0.5	0.75
Undefined	0.005	-

In Table 4.3, the calibrated limits of K_v are presented. It was determined that in the peat areas, located in the west of the model area between 473900 and 476000 meters and between 477900 and 479000 meters, large fluxes towards the local surface waters were simulated. These large fluxes were, however, never observed in practice. Therefore, the minimum K_v of those areas was decreased to 0.02 m/d.

4.5. Scenarios Pilot Well

A transient groundwater model is needed to model time-dependent groundwater flow resulting from pumping of the well [93]. Although the pumping rate is constant in time in these scenarios, and, thus, there is no time dependency, the model was set up such that time-dependent rates are easily implementable. In other words, the model was extended with two years that were run transient. Moreover, all boundary conditions were kept constant over these two years, and, thus, the effects of climate change and subsidence are ignored. In other words, the resulting fluctuations of the phreatic surface [8, 62] were neglected. As a result, the scenarios are not realistic for the future. They, however, clearly visualise the effect of a well on the brackish upconing. Inclusion of the effect of subsidence and climate change would overshadow this effect, and, thus, the conclusions on the effects would be a mixture of the effect of the wells with the changed boundary conditions. Since determining the effect of the wells on the brackish upconing is the purpose of this research, it is preferred to ignore the expected future changes in boundary conditions.

An additional package is required to run the model transient: the Storage (STO)-Package. This STO-Package is needed to simulate the compression of the grain skeleton as a result of the decreasing pressure due to the pumping of the well. The STO-Package is established with the help of the NLMOD algorithm and the default values for the specific yield (S_y) and the specific storage coefficient (S_s), which are 0.2 and 0.000001 m^{-1}.

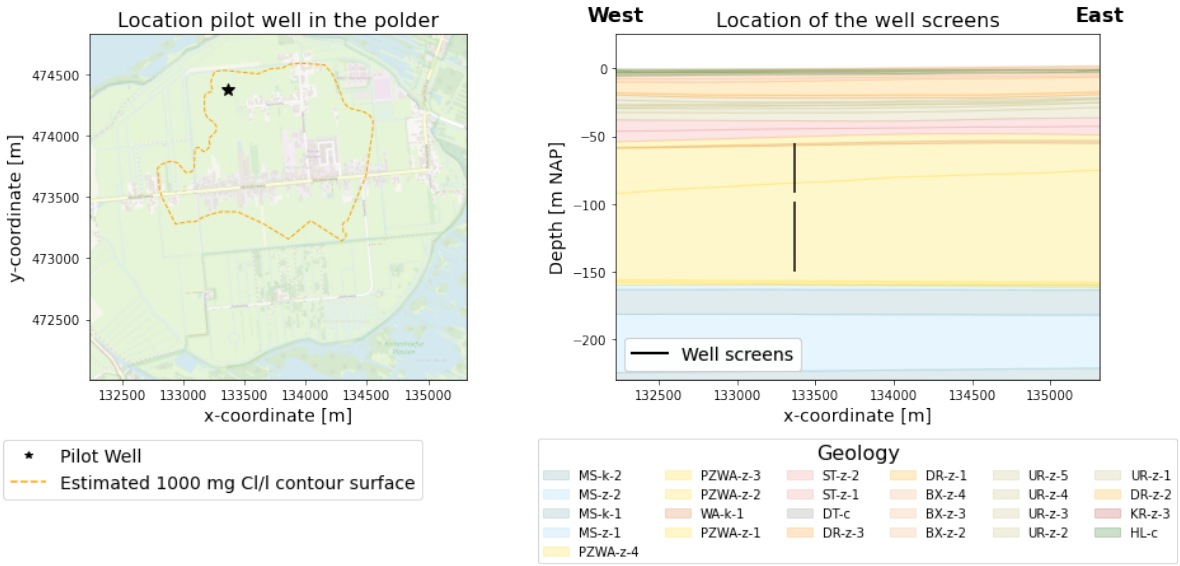

Figure 4.11: Location of the pilot well and the two well screens.

The pilot well was placed in March 2021, both at x-coordinate 133366 m and y-coordinate 474375 m in the north of the Horstermeer Polder [94]. The well has two well screens: a shallow well screen starting at -55 m NAP with a length of 37 meters and a deeper screen that starts at a depth of -98 m NAP and ends at -150 m NAP. The location of the pilot well and its screens are given in Figure 4.11. Both well screens are located within the Peize-Waalre Formation. The well has a radius of 15 cm. The reverse osmosis system, which is used to remove chloride and other ions from the well water, has a capacity of 55 m^3/h. Hence, pumping can occur through one of the two well screens with a constant pumping rate of 55 m^3/h. However, the total well can pump up to 100 m^3/h during pump tests. This can be split over the well screens or be pumped through one well screen. The well screens were added to the model by applying the Multi-Aquifer Well (MAW) Package. The MAW has an inactive status during the first stress period and was set to be active in the second stress period. This needs to be explicitly defined to prevent the well from influencing the hydraulic heads and chloride concentration in the surrounding area of the well, due to the connection of the cells in the well package. The Thiem conductance equation was used to calculate the saturated conductance of the

multi-aquifer well. Moreover, a Multi-Aquifer Well Transport (MWT) Package is used to determine the concentration of the well water. In total, six scenarios were run, five in which at least one of the wells is operating and one scenario in which the wells are inactive (baseline). The latter is used to distinguish between autonomous salinisation and the effects of the well. The operational settings used in these scenarios are given in Table 4.4

Table 4.4: Overview of the operational settings used in the six scenarios.

Scenario	Pumping Rate [m^3/h]		Total Withdrawal [m^3/h]
	Shallow Well Screen	Deep Well Screen	
Baseline	-	-	0
1	55	-	55
2	-	55	55
3	50	50	100
4	100	-	100
5	-	100	100

5

Results Regional Aquifer System Analysis

This chapter will present the results of the calibrated model. The model is used to determine the effect of the pilot well in the next chapter. The chloride distribution in the model has to be steady to be useful for this analysis. Therefore, the changes during the warm-up period of the model will be described first. Next, the outcome of the model will be presented. The outcome gives insights into the flow regime in the area, the spatial distribution of fresh and brackish groundwater, and the characteristics of the fluxes out of the polders in the model area. The last part of the chapter will focus on the degree of agreement with the measurements presented in Chapter 3 and the water balance calculations of the polders.

5.1. Model Warm-Up

Due to the high variety of input data sets, which potentially differentiate from the data sets used in the NHI fresh-saline model, and the modification of the NHI model, it is very likely that the spatial distribution of the chloride concentration will change significantly once the model is run. However, autonomous salinisation also influences the distribution [8], and, thus, a completely steady model is not realistic. As shown in Figure 5.1, the average difference of a cell's chloride concentration between two consecutive years is more or less constant, and, thus, the change has a constant rate after a run time of 400 years. Moreover, the maximum difference is only 60 mg Cl^-/l around the same time. Since this value is in this research negligible, it is concluded from these results that a run time of 450 years is long enough to reach approximately a steady chloride distribution.

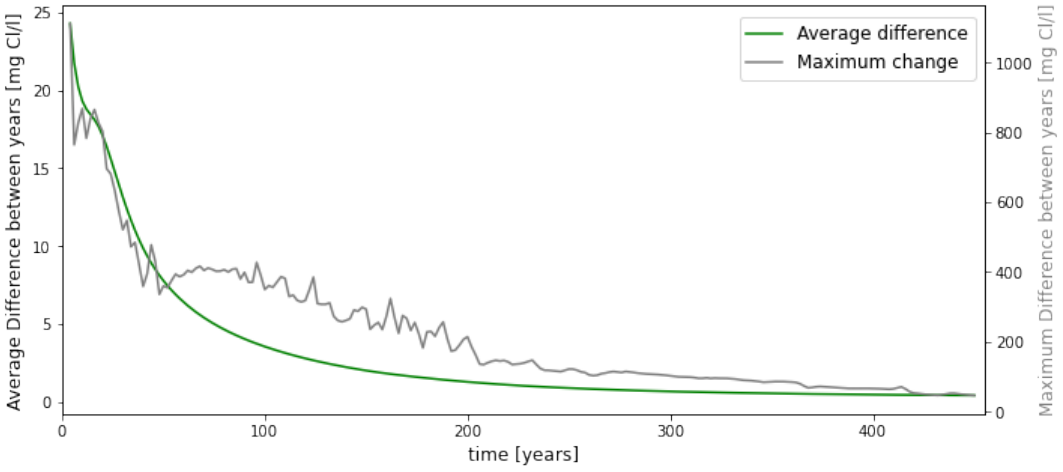

Figure 5.1: Time series of the average difference of the chloride concentration in one cell between two consecutive years and the maximum occurring difference within the model grid.

Figure 5.2 shows the changes in the spatial distribution of the chloride concentration over time. From the figures can be concluded that the difference between the initial distribution and the distribution after a run time of 100 years is significant. After 100 years, the chloride concentration below the Horstermeer Polder increases. The difference between the outcome after 250 years and after 450 years is less profound. However, the chloride concentration below the Horstermeer Polder still increases with time. Furthermore, the figures show that the interface below ± -160 m NAP, i.e. below the upper clay layer of the Maassluis Formation, moves slowly eastwards and southwards with time.

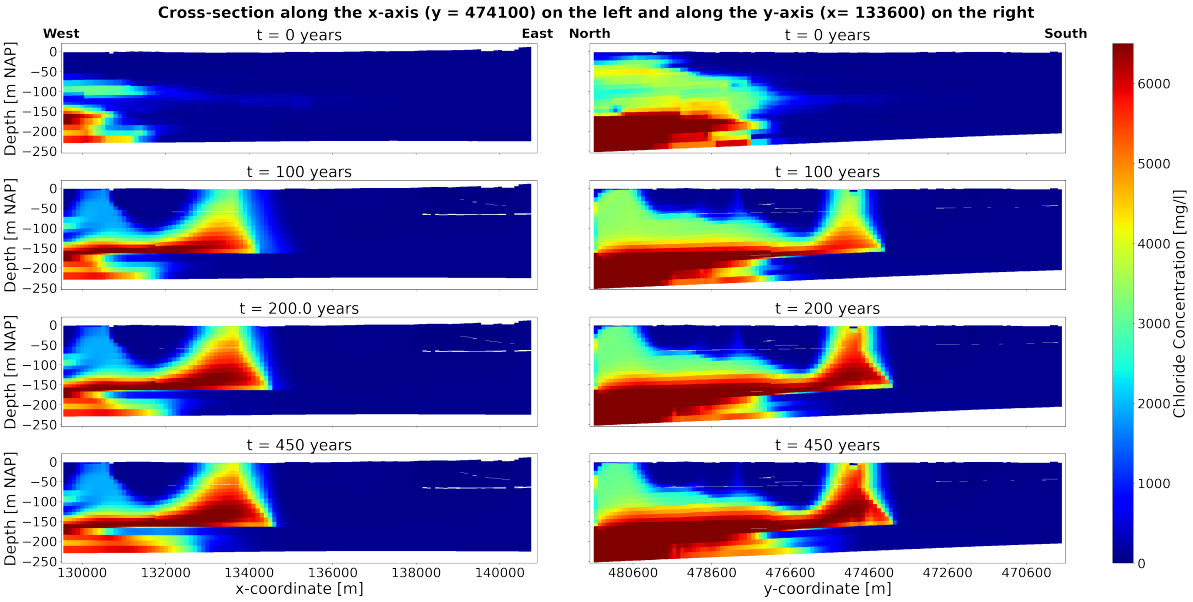

Figure 5.2: Visualisation of the change in the spatial distribution of the chloride concentration over the model time in two cross-sections going through the middle of the Horstermeer Polder. The upper image shows the initial distribution based on the modified NHI p50-model, the second image shows the distribution after a run time of 100 years, the next after 200 years, and the lower image shows the distribution at the end of the run time.

As shown in Figure 5.3, the biggest change of the chloride concentration occurs below the Horstermeer Polder above the upper clay layer of the Maassluis Formation (± -160 m NAP) during the warm-up period. However, just northwest of the Horstermeer Polder, the chloride concentration also increases over time, especially below the polders. Moreover, two figures on the left show that in the shallow subsurface in the north, the chloride concentration decreases below surface waters. Lastly, the movement of the interface below the upper clay layer of the Maassluis Formation, as mentioned before, is also visible in the left figure.

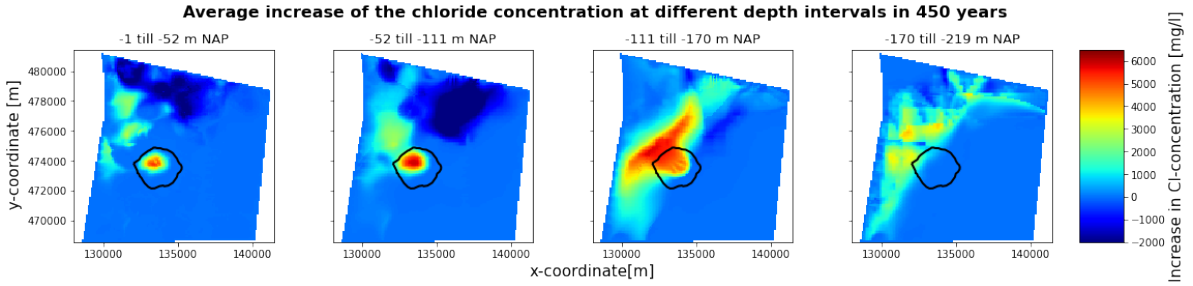

Figure 5.3: Visualisation of the average increase in chloride concentration in four different depth intervals in the 450 years warm-up period of the model. In black, the delineation of the polder is given.

5.2. Current Situation

From measurements, it is known that brackish upconing takes place below the Horstermeer Polder. The brackish upconing is the result of the reclamation of the deep lake Horstermeer with a relatively low controlled phreatic surface compared to the surroundings. The difference in the phreatic surface within and outside the Horstermeer Polder is approximately two meters. In this section, the model outcome is presented in terms of the flow regime, the spatial distribution of the fresh and brackish groundwater, and the fluxes into or out of the polders in the area.

5.2.1. Flow Regime

The effect of the low controlled phreatic surface is visible in the model result given in Figure 5.4. The phreatic surface is simulated to be between -3 and -4 m NAP, whereas the surrounding area has a phreatic surface of at least -1.5 m NAP. The minimum simulated point-water head is -3.43 m NAP in the Polder, whereas the maximum simulated point-water head is 0.53 m NAP in the east of the model area. The river Vecht and the Amsterdam-Rhine Canal (ARC) have water levels (-0.4 m NAP) far above the phreatic surface in the polders in the model area. As a result, the water from the rivers will infiltrate into the aquifer and supply freshwater. Likewise, the groundwater will drain into the surface waters in the Horstermeer Polder.

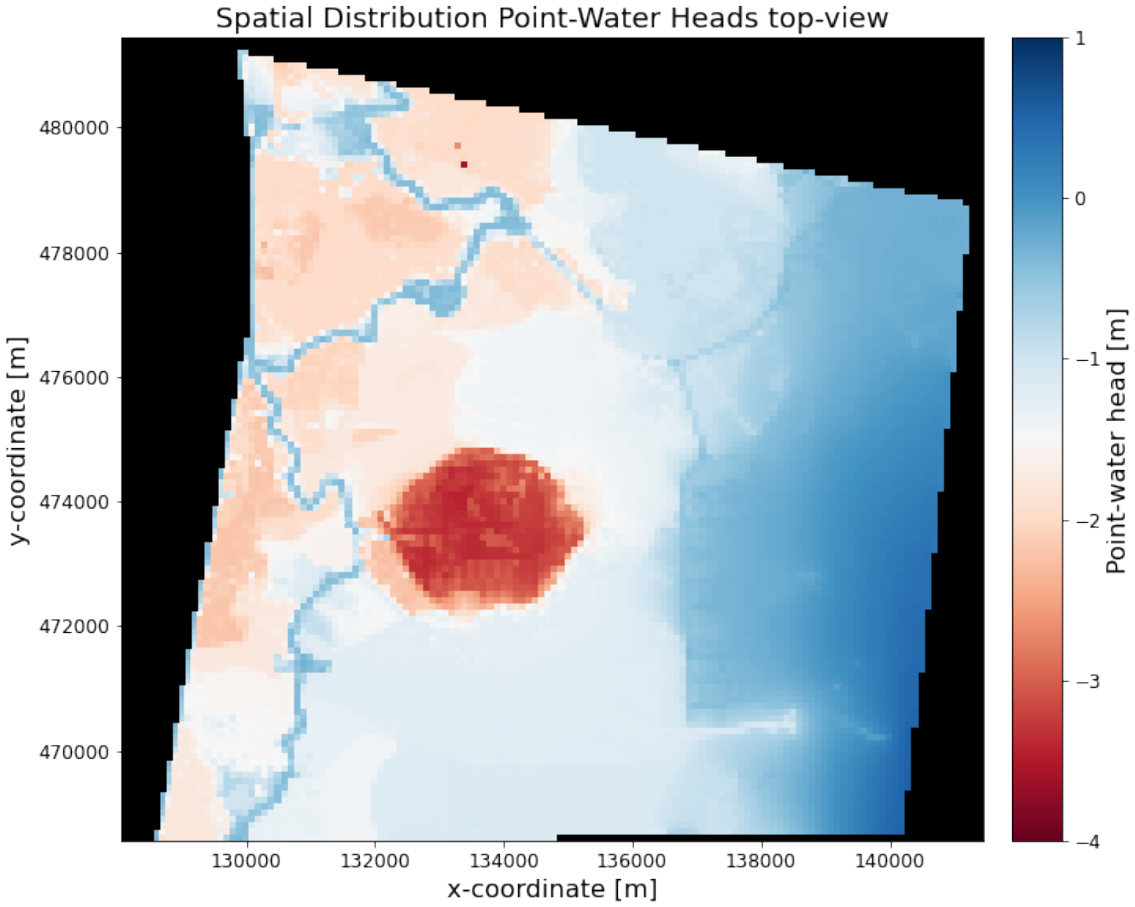

Figure 5.4: The simulated point-water head distribution in the top layer.

Moreover, due to the man-controlled lower phreatic surface in the Horstermeer Polder, the freshwater heads below the polder until the upper clay layer of the Maassluis Formation (± -150 m NAP) are lower than the surroundings (Figure 5.5). Below this clay layer, the effect of the Horstermeer Polder is significantly less apparent.

The two upper clay layers in the area significantly influence the spatial distribution of the freshwa-

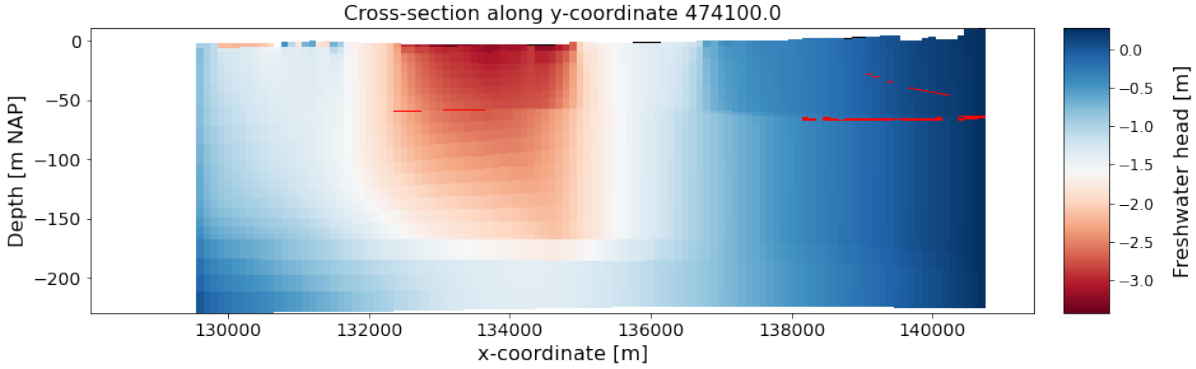

Figure 5.5: The spatial distribution of the simulated freshwater head over the depth in the cross-section along y-coordinate 474100 m. With bright-red vertical pass-through cells are indicated.

ter heads and hence the flow regime. In Figure 5.5, the upper clay layer of the Maassluis Formation (± -150 m NAP) and the clay layer in the Waalre Formation (± -55 m NAP) can be easily identified by the deviation of the freshwater head above and below layer. The deviation in the freshwater head resulting from both the upper clay layer of the Maassluis Formation and the clay layer in the Waalre Formation is as large as 80 cm below the Horstermeer Polder. The Waalre Formation only influence the freshwater head distribution at the southeast of the polder, since in the northwest, the clay layer has a thickness of below 1 meter, i.e. these cells are vertical pass-through cells. In terms of point-water head, the deviation caused by the upper clay layer of the Maassluis Formation is larger than by the clay layer in the Waalre Formation, 1.0 m and 0.65 m, respectively. The effect of the clay layers is even more apparent in Figure 5.6, which shows that the groundwater flows parallel to the clay layer in the Waalre Formation until the clay layer is less thick, and, thus, its influence reduces. Therefore, the groundwater flows slightly diagonally upwards from the Maassluis Formation towards the surface. More precisely, it flows from the east somewhat to the west in its way up due to the Waalre Formation. As a result of the clay layer in the Maassluis Formation, groundwater exchange above and below the layer is very low, i.e. the maximum simulated vertical specific discharge is 0.11 mm/d. Maps of the differences of the point-water heads and freshwater heads and vertical specific discharge over the clay layers can be found in Appendix D.

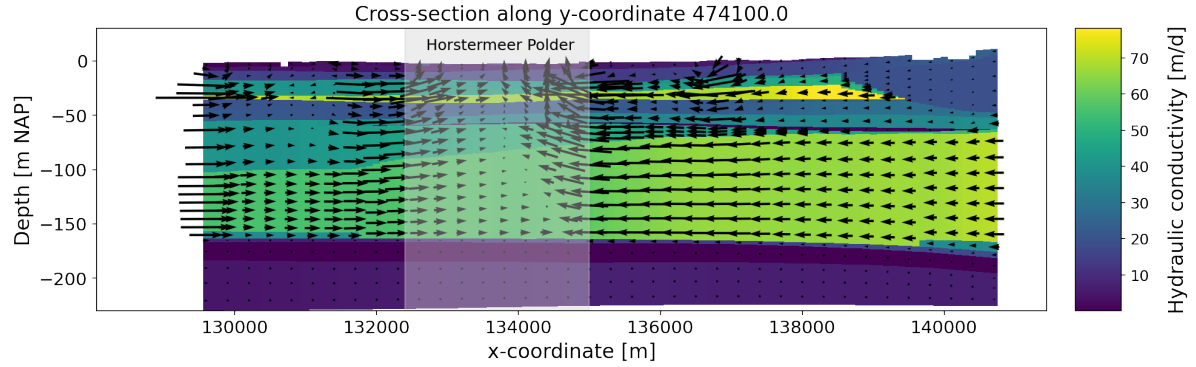

Figure 5.6: Specific discharge vectors and the hydraulic conductivity in all layers of the model present in the cross-section along y-coordinate 474100 m. In light grey, the Horstermeer Polder is indicated.

Not only low conductivity layers influence the groundwater flow, but also high conductivity layer. As said before, within the model area, a "race layer" is present between -25 and -35 m NAP. This layer is visible in Figure 5.6 by its high hydraulic conductivity. In this layer, the specific discharge is significantly larger than in the surrounding layers. This layer facilitates the faster movement of fresh infiltrated water towards the polder, as shown in Figure 5.6. Hence, most likely, this layer causes the brackish upconing to be further to the middle.

Although the clay layers and "race layer" affect the flow paths in the subsurface, the strong influence of the Horstermeer Polder still creates a flow of the deeper (brackish) groundwater towards the polder (Equation 2.3). Figure 5.7 shows that most of the water arrives from the east, followed by the southwest and the northwest. Over the south boundary, there is almost no groundwater flow occurring.

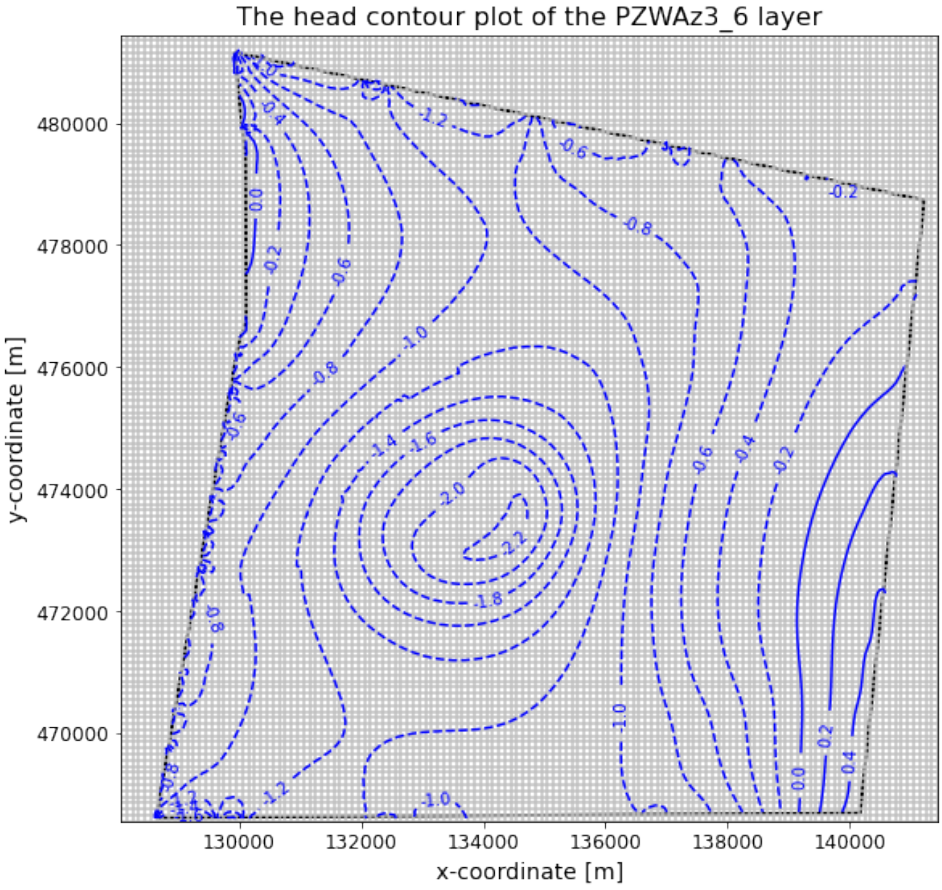

Figure 5.7: A contour plot of the freshwater head in the third sand layer within the Peize-Waalre Formation. The groundwater flow is perpendicular to the contour plot.

5.2.2. Spatial Distribution of Fresh and Brackish Groundwater

The spatial distribution of fresh and brackish groundwater influences the groundwater flow regime and vice versa. Since the aquifers above and below the upper clay layer of the Maassluis Formation are almost disconnected, the spatial distribution of chloride in both aquifers will be presented separately.

First, in Figure 5.8, the 1000 mg Cl^-/l contour surface in all layers above the Maassluis Formation, and the chloride concentration in the first active layer is given. In all figures, it is evident that the southeastern part of the model area is entirely fresh. In the northeastern and the southwestern part of the model area, brackish groundwater is only present in the deeper layers, whereas in the remaining part of the model area, brackish groundwater is present over the complete depth at many polders within that area. However, the infiltrating nature of the Vecht river creates freshwater lenses in between the polders. This creates an interesting pattern of brackish upconing in the northwest of the model area (Figure 5.8a and Figure 5.8b). Besides the Vecht, also other surface waters influence the interface. There is a dip in the interface apparent at the north side of the Horstermeer Polder, which is a result of the drainage of fresh groundwater that originates from the deep surface waters, e.g. Spiegelplas, north of the polder. Likewise, in the north, the Naardermeer Lake creates a dip in the interface pattern.

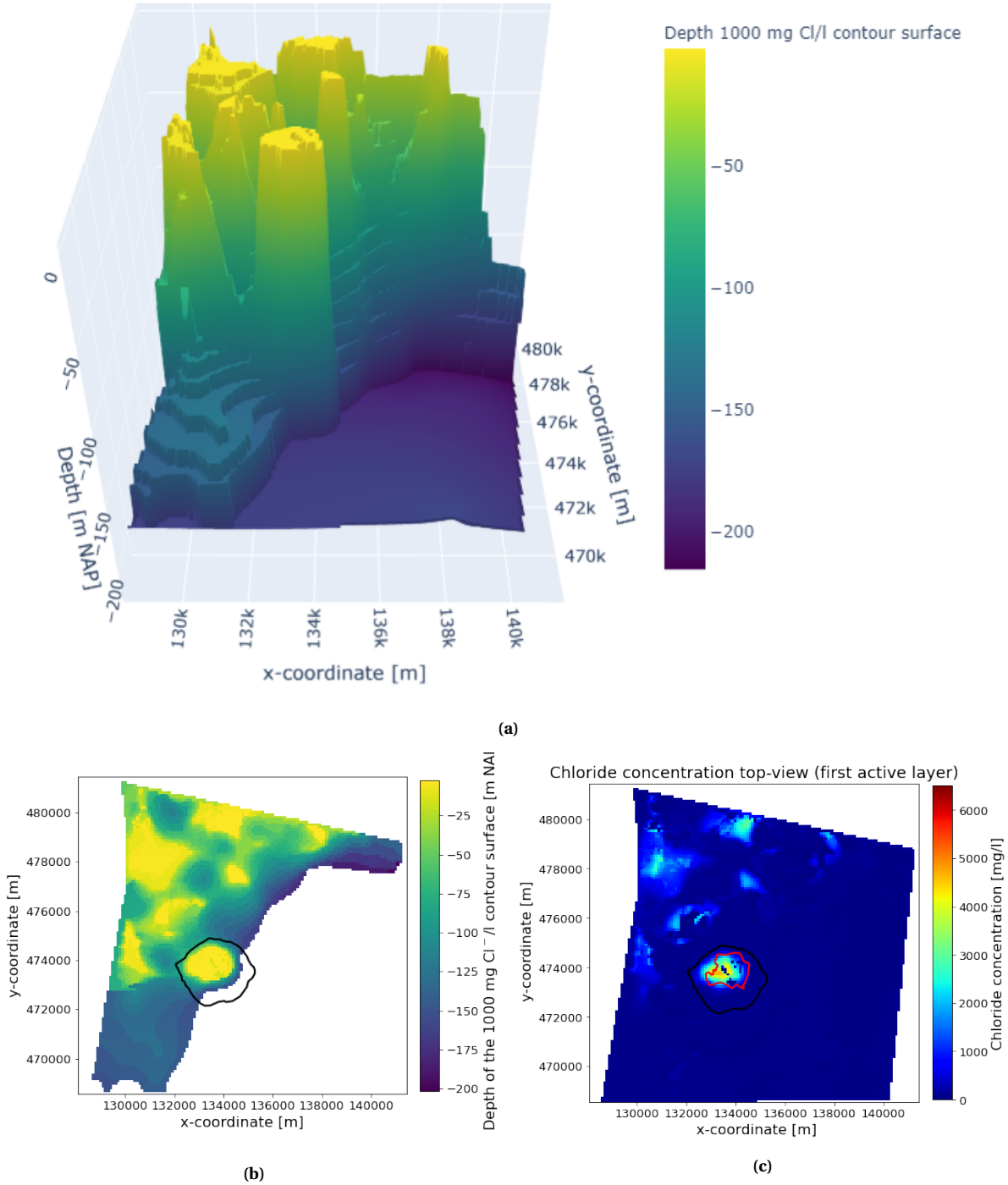

Figure 5.8: Spatial distribution of the chloride concentration above the upper clay layer of the Maassluis Formation (MSk1). In (a) the depth of the 1000 mg Cl^-/l contour surface is visualised in 3D. Whenever the concentration is lower than 1000 mg Cl^-/l over the whole depth, the top of the MSk1 is given. The colours depict the depth of the contour surface and are equal to the legend used in (b). In (b), the depth of the same contour surface is visualised in 2D, including the delineation of the Horstermeer Polder, the river Vecht and the measured 1000 mg Cl^-/l contour surface of Van Wielink [11] and Jain et al. [18], and in (c), the chloride concentration in the top layer is given.

Although brackish upconing occurs in almost all polders north of the Horstermeer, the concentration of the brackish upconing in the Horstermeer Polder is significantly higher (Figure 5.8c), and, thus, this upconing is problematic. Moreover, the interface of the brackish upconing below most polders is less steep compared to the upconing below the Horstermeer Polder. It appears that the interface in the Horstermeer Polder is very sharp, i.e. the upconing has almost a vertical interface at the east side.

Second, the depth of the 1000 mg Cl^-/l contour surface below the upper clay layer of the Maassluis Formation is given in Figure 5.9. The figure shows that the aquifer is fresh below the Horstermeer Polder except in the far west. This means that an inversion of the chloride concentration is present below the Horstermeer Polder. This emphasises the disconnection of both aquifers. Moreover, Figure 5.9a shows that the interface is again sharp below the east and south of the Horstermeer Polder. The interface becomes more gradual in the north. Lastly, in the far northwest, the chloride concentrations are significantly higher than in the remaining part of the model area.

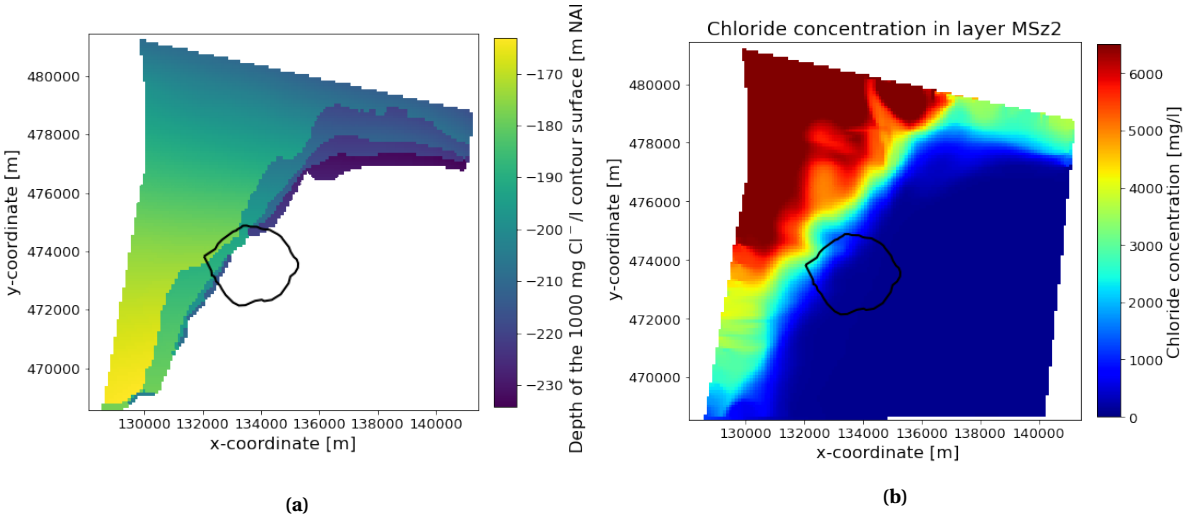

Figure 5.9: Spatial distribution of the chloride concentration below the upper clay layer of the Maassluis Formation (MSk1). In (a), the depth of the 1000 mg Cl^-/l contour surface is visualised in 2D including the indication of the Horstermeer Polder, and in (b), the chloride concentration in the first layer below the clay layer is given.

5.3. Model Performance

The model outcomes presented in the previous section will be compared with the point measurements in this section. The degree of compliance with these measurements is the benchmark of the model. As said before, a distinction will be made between head, chloride concentration, and flux measurements.

5.3.1. Hydraulic Heads

The output of MODFLOW 6 is in terms of point-water heads. In other words, the output can directly be compared with the measurements (Figure 5.10a). However, in the area in and around the Horstermeer salinity has a significant influence on the groundwater density,and, thus, on the freshwater equivalent of the head. Therefore, the model results will also be evaluated in terms of freshwater head (Figure 5.10b). There are 149 measurement locations of which an average hydraulic head has been calculated over the period 2000 to 2020 AD. At 59 of these measurement points, the chloride concentration was measured, which enables comparison of the freshwater head.

As shown in Figure 5.10, the point-water head fluctuates heavily in some locations causing the simulated head to be in the 95%-confidence interval of the measurement location, although the average measured point-water head deviates from the simulated value. On average, the standard deviation of the observed point-water heads is 10 cm, however, fluctuations of the point-water head up to 33 cm are observed. Fluctuations of the freshwater head are equal to the fluctuations of the point-water head since time series of the chloride concentration are not available. This is probably not the case in practice since freshening and salinisation occur in the area [59]. Nonetheless, the difference between the modelled and the average observed point-water head was in 41% of the cases less than 10 cm, in 70% of the case less than 30 cm and 89% of the measurement points have a deviation of 50 cm or less. In terms of freshwater head, 32% of the cases have a difference of less than 10 cm, 51%

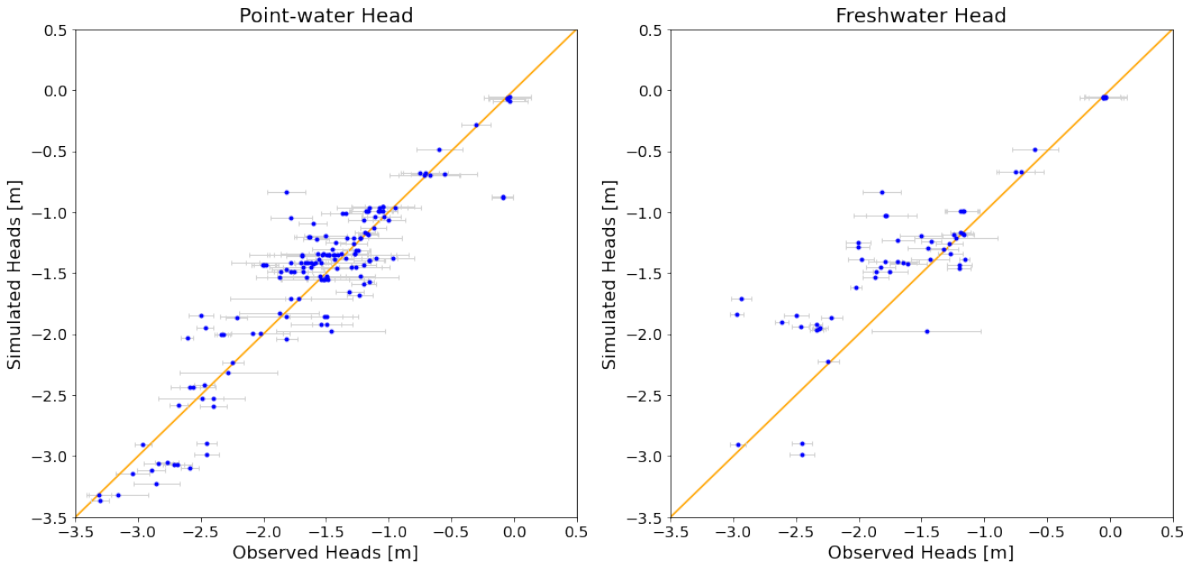

(a) (b)

Figure 5.10: Comparison between the simulated and average observed hydraulic heads: a) in terms of point-water head and b) in terms of freshwater head. The average observed head based on measurements between 2000 and 2020 AD. The figure includes the 95%-confidence interval of the observed measurements. The closer the dots are to the orange line the better the simulated values match with the observed concentration.

less than 30 cm, and 75 % less than 50 cm.

Table 5.1: Summary of the characteristics of the error between the measured point-water heads and freshwater heads and the simulated values of these types of hydraulic heads.

Error characteristics [m]	Point-water head	Freshwater head
Mean error	0.04	0.13
Mean absolute error	0.21	0.29
Standard deviation	0.29	0.36
Max. absolute error	0.98	0.98
RMSE	0.29	0.39

In Table 5.1 the error characteristics are summarised. In this case, the error is defined as the difference between the modelled versus the observed value. In general, the model slightly overestimates the hydraulic heads. Since the RMSE is biased towards the more negative values, the freshwater heads perform less well in the lower range of the hydraulic heads compared to the point-water heads.

Besides the general trend of the model performance, the local performance is of interest. In Figure 5.11 the measured freshwater heads including the error of the model output are plotted. The size of the spheres shows that although measurement locations are close to each other the model performance differs significantly. In some locations, there is an underestimation of the freshwater head whereas, in other locations, the model overestimates the freshwater head. The model performance is the lowest in the north(west), characterized by brackish groundwater. Since a time series of the chloride concentration is lacking in most locations, it is impossible to determine whether the model outcome of the chloride concentration or point-water head is deviating from field observations, or if the latest chloride measurement is no longer representative. Large deviations of the model performance are also visible within the Horstermeer Polder: in the fresher south, the model underestimates the freshwater head, whereas at the location of the deep drilling in the west, the freshwater head is overestimated. The chloride concentration at that specific location was mea-

sured in 2018 AD. Therefore, the deviation in the west can only be due to an overestimation of the simulated chloride concentration, an overestimation of the point-water head, or a combination of both. Moreover, the results show that the overestimation of the simulated freshwater head increases with depth at the location of the deep drilling in the Horstermeer Polder. On the contrary, the freshwater head is underestimated below the upper clay layer of the Maassluis Formation.

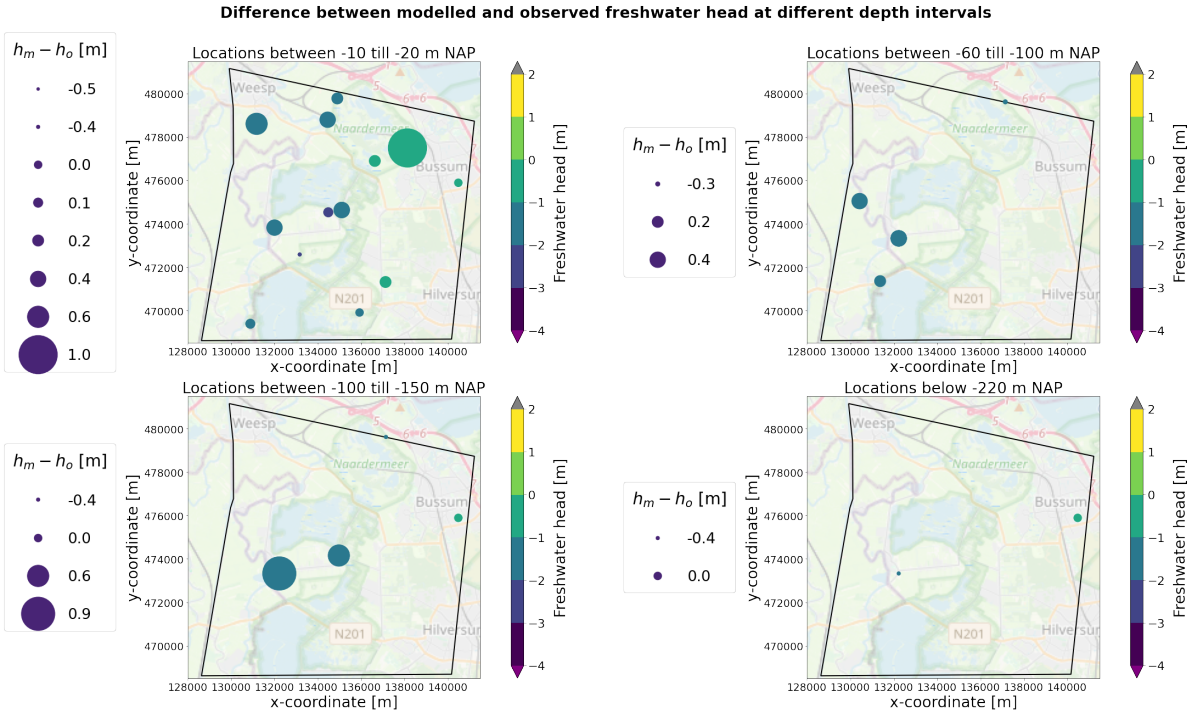

Figure 5.11: The simulated freshwater heads and the error of the model results in the shallow subsurface (-10 to -20 m NAP), in the upper part of the Peize-Waalre Formation (-60 to -100 m NAP), in the lower part of the Peize-Waalre Formation (-100 to -150 m NAP) and below the upper clay layer of the Maassluis Formation (< -220 m NAP).

5.3.2. Chloride Concentration

Figure 5.8b and Figure 5.8c already showed that the modelled 1000 mg Cl^-/l contour surface within the polder does not entirely match the contour surface based on the measurements of Van Wielink [11] and Jain *et al.* [18]. Nonetheless, in 64% of all measurement locations in the model area, the simulated chloride concentration deviates less than 100 mg Cl^-/l from the measured chloride concentration, 80% of the points measurements have a deviation of less than 200 mg Cl^-/l off, and 86% have a deviation of less than 500 mg Cl^-/l. In some locations, the deviation is more than 1000 mg Cl^-/l. Figure 5.12 gives an overview of the error. In most cases, when the model results deviate from the chloride measurements, the model underestimates the chloride concentration. Within the polder, the maximum underestimation is even 4600 mg/l. The only location in which the model extremely overestimates the chloride concentration is at the location of the measurement within the upper clay layer of the Maassluis Formation below the Horstermeer Polder. This is because this layer is slightly lower in REGIS II than in practice.

In general, the simulated chloride concentration is less accurate than the simulated hydraulic heads. The RMSE-values depicted in Table 5.2 indicate this lower accuracy. The model is less in agreement with the shallow subsurface measurements than with the measurements retrieved from DINOloket. Although the simulated chloride concentrations do not perfectly match the observed chloride concentrations at specific locations, the model does match the general observed spatial distribution of chloride in the area. This is depicted in Figure 5.13 and in Appendix E.

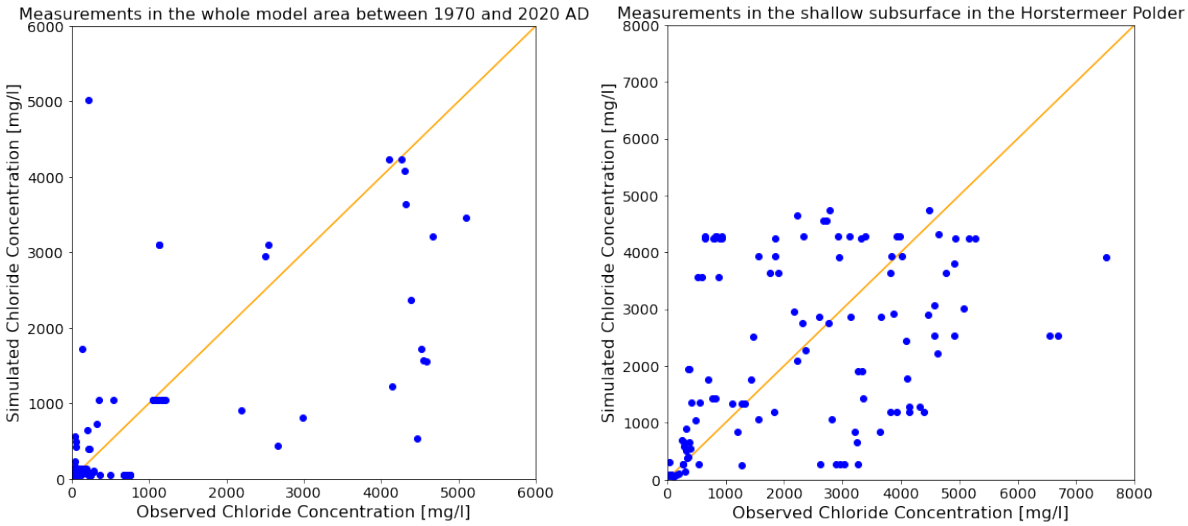

(a) **(b)**

Figure 5.12: Comparison between the simulated and observed chloride concentration: a) in the whole model area and b) in the shallow subsurface (>-5 m NAP) of the Horstermeer Polder. The closer the dots are to the orange line the better the simulated values match with the observed concentration.

There are four locations where the model is slightly off; (1) in between the river Vecht and the lake Naardermeer in the north of the model area, (2) just south of the city of Weesp, (3) the upconing below the Horstermeer Polder in the east and especially the west and (4) the chloride concentration below the upper clay layer of the Maassluis Formation at the location of the deep drilling in the polder. Since the Horstermeer Polder is the focus this research, the off-set at the polder is shown in Figure 5.13b, the deviation at the north side of the model area can be found together with more cross-sections in Appendix E. Figure 5.13b shows that compared to field observation, the simulated upconing should be moved a couple of hundred meters to the east. In other words, in the model brackish groundwater is also present in the shallow subsurface in the west of the polder, which is not observed in the field. In the north and south, the shape of the upconing corresponds to the observations.

If the spatial distribution of the chloride concentration within the upconing below the Horstermeer polder is examined in more detail (Figure 5.14), it can be seen that the location of the maximum chloride concentration should also be located more towards the east. Moreover, large rainwater lenses are visible within the upconing.

Table 5.2: Summary of the characteristics of the error between the modelled chloride concentration and observed chloride concentration. For the whole model area the observed chloride concentration is based on the data in DINOloket and for the shallow subsurface the chloride values were acquired by Van Wielink [11] and Jain et al. [18].

Error characteristics [g/l]	**Cl-concentration Whole Model Area**	**Cl-concentration Shallow subsurface of the Horstermeer**
Mean error	-0.128	0.346
Mean absolute error	0.320	0.922
Standard deviation	0.778	1.435
Max. absolute error	4.683	4.633
RMSE	0.790	1.475

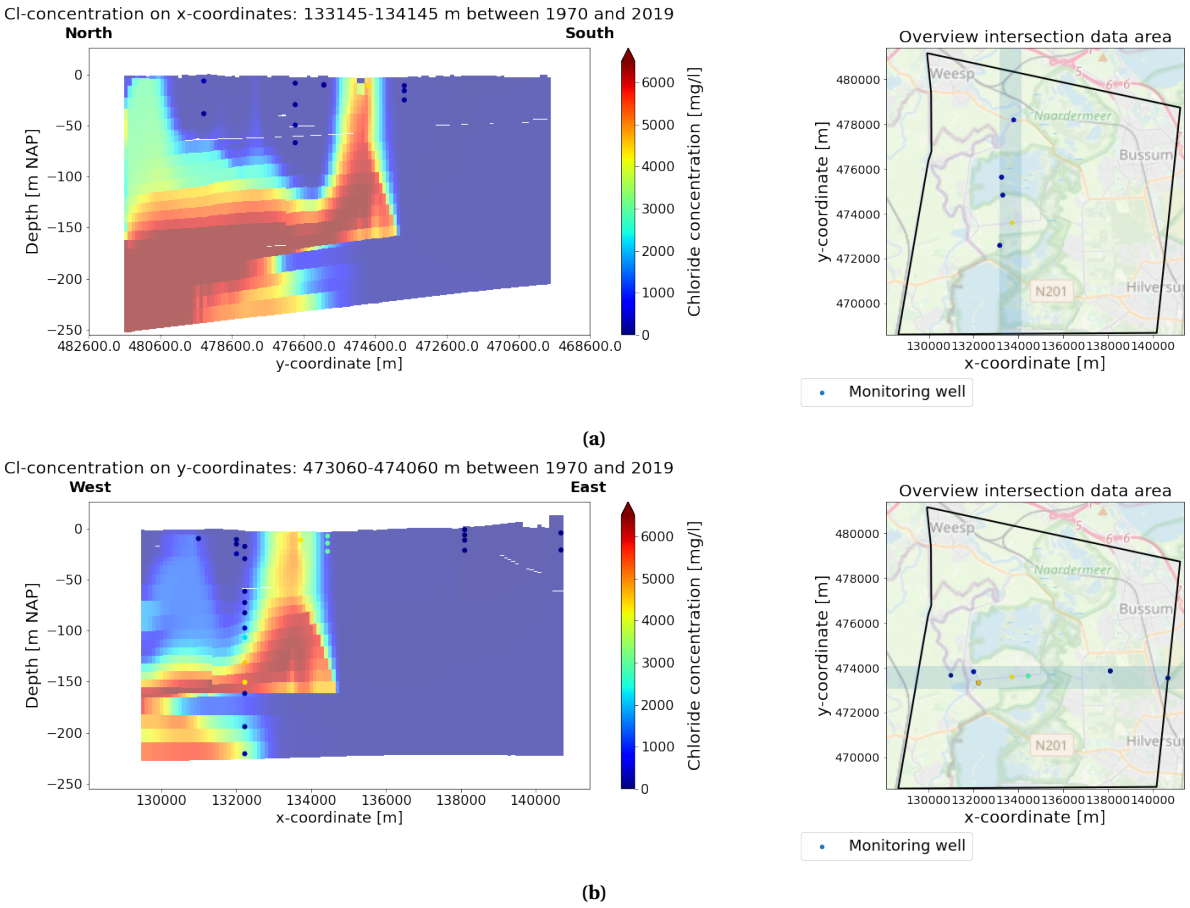

Figure 5.13: Chloride concentration distribution over the depth of the model and the measurements from (a) from north to the south at the x-coordinate corresponding to the middle of the Horstermeer Polder and (b) west to east at the y-coordinate corresponding to the middle of the Horstermeer Polder. The measurements of the chloride concentration were retrieved from DINOloket [55]. In the right figures, the locations of the cross-sections are given as well as the model boundary.

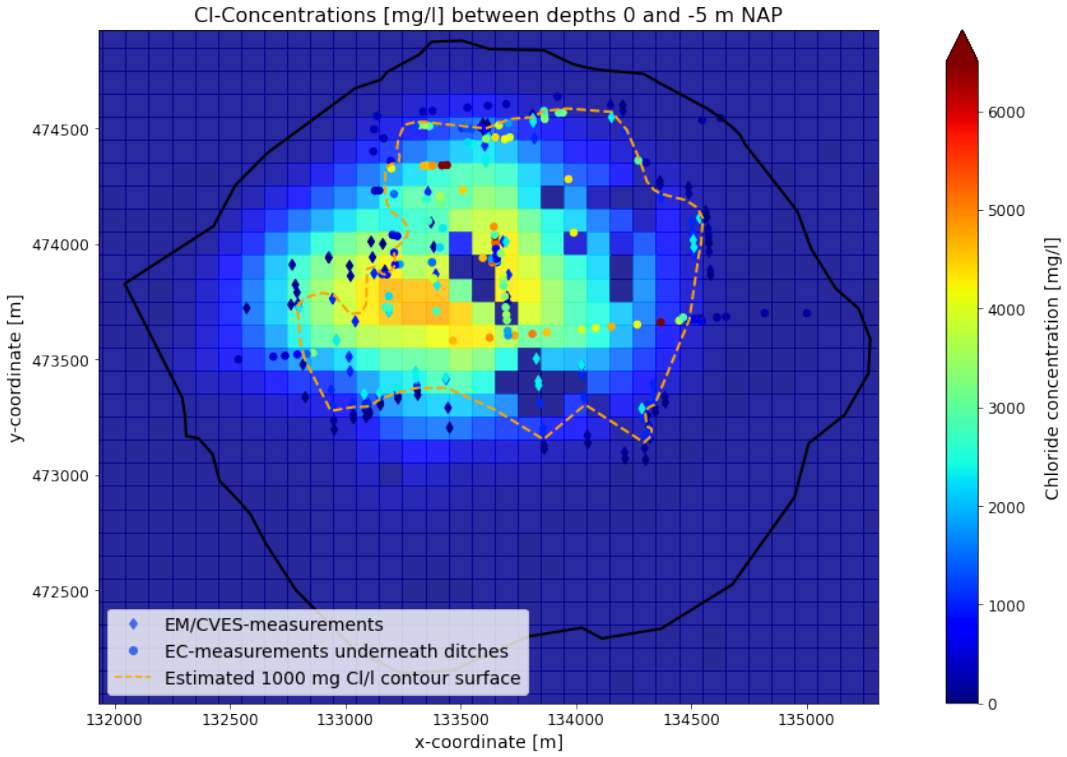

Figure 5.14: Chloride Concentration distribution in the Horstermeer Polder. The background depicts the model output whereas the measured and estimated chloride concentrations by Van Wielink [11] and Jain et al. [18] are illustrated with diamonds and dots respectively. In black the delineation of the Horstermeer Polder is given.

5.3.3. Fluxes

Besides comparison with point measurements, like the hydraulic heads and chloride measurements, it is beneficial to compare the model output with measurements that capture larger areas. One of the most valuable measurements is flux measurement. Many polders have pumping stations where the fluxes and corresponding chloride concentration are measured. With these measurements, water balances have been made for the polders by Voort [92]. The outcomes of these water balances should correspond to a certain degree with the average flux drained and infiltrated in the model. However, in the calculation of the water balances, many assumptions are made. Some of those assumptions, e.g. the amount of seepage and infiltration, are based on the Regional Groundwater Model of Waternet ($RGWM_{Waternet}$). Hence, the water balances have much uncertainty. Nevertheless, the water balances and the model outputs should be in the same order, and large deviations could indicate mistakes in the model. Therefore, the model results were still compared to these water balances.

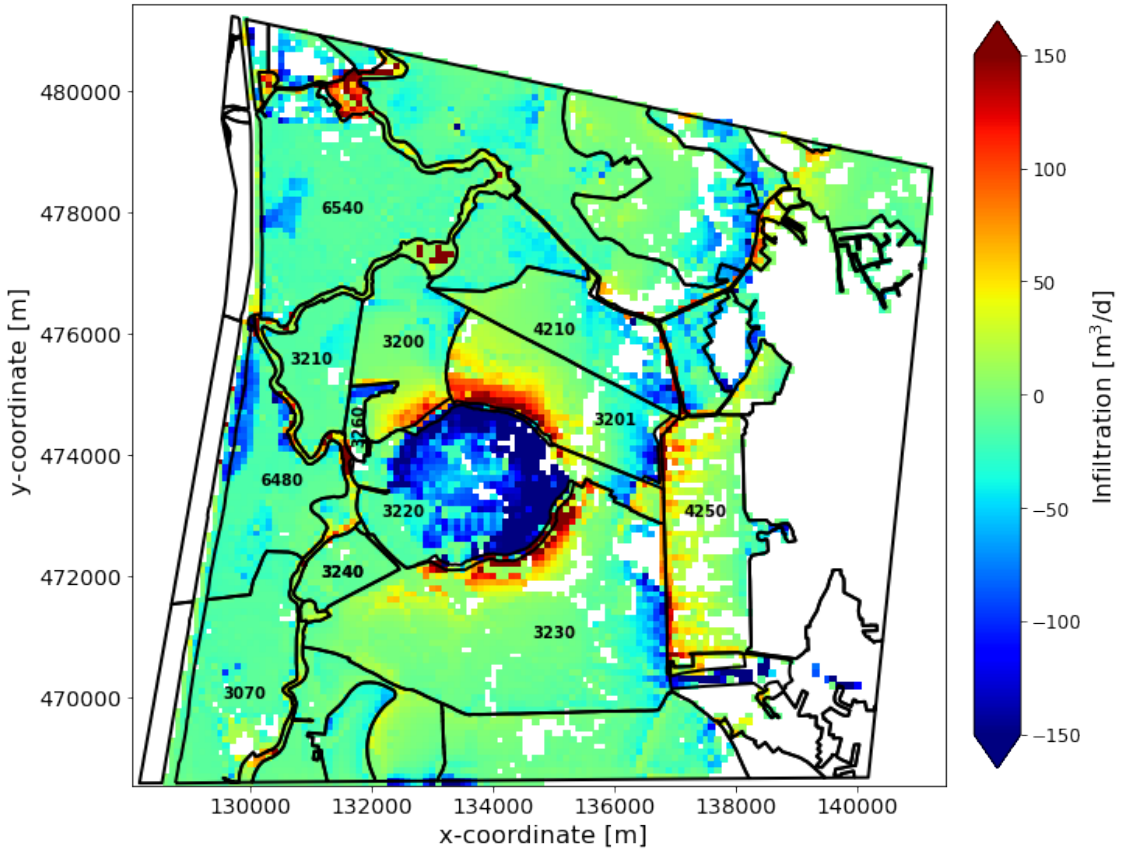

Figure 5.15: Infiltration into the groundwater system simulated by the model. Negative values mean the water exfiltrates into the surface water. In black the catchment zones of the measurement locations are depicted. The used zones for the comparison are indicated with their zone ID. White cells within the model area mean neither a DRN- nor a RIV-Package has been applied in the cell or no overland flow occurred.

Figure 5.15 depicts the average simulated flux of drained and infiltrated groundwater per cell. Whenever a cell is white, either no DRN or RIV-Package was applied on that cell, or no overland flow occurred at that location. In most polders, at one side, drainage occurs, whereas, on other sides, infiltration into the next polder occurs. Only the Horstermeer is solely a draining location, although spatial differences can still be seen: In the southwest, the drainage rate is significantly less than in the east. Moreover, the polders surrounding the Horstermeer infiltrate large amounts of water into the aquifer that exfiltrates again in the polder.

Table 5.3: Overview of the estimated average flux, based on water balance studies, and the simulated average flux infiltrating into the aquifer (positive numbers) or draining (negative numbers) into the surface waters.

Zone ID	Name Polder	$Q_{waterbalance}$ [12, 92] [MCM*/y]	$Q_{modelled}$ [MCM*/y]	Difference [MCM*/y]
3070	Holland, Sticht Voorburg and 't Honderd Oost Polder	-4.63	-2.17	2.46
3200	Spiegelpolder	1.58	0.43	-1.15
3201	Stichtsch Ankeveensche Polder	1.19	2.72	1.53
3210	Horn and Kuijer Polder	-0.93	-0.74	0.19
3220	Horstermeer and Meeruiterdijksche Polder	-32.65	-26.07	6.58
3230	Polder Kortenhoef	3.29	2.80	-0.59
3240	Polder Dorssewaard	0.02	0.01	0.01
3260	Blijkpolder	0.08	-0.18	-0.10
4210	Hollandsch Ankeveensche Polder	1.12	-1.76	-2.88
4250	's Gravelandsche Polder	1.29	3.94	1.65
6480	Hoeker-Garsten Polder	-3.87	-4.77	-0.90
6540	Aestveldse Polder Oost	-4.85	-4.90	-0.05

* MCM: Million Cubic Meters

Furthermore, in Table 5.3, per zone, the sum of the outcome depicted in Figure 5.15 is given. The zone IDs in the table correspond with the number given in the figure. Based on the water balances, some polders are, on average, draining areas, e.g. 3070, 3210, 3220, 6480, and 6540, whereas the others are infiltrating areas. The Horstermeer Polder drains up to 32.65 million m^3/y towards its surface waters. These seepage rates are at least a factor 8 higher than the seepage/infiltration rates in all surrounding polders. Compared to the water balance calculation, the model underestimates this seepage rate. The average simulated seepage rate is 12 mm/day. This is only slightly less than the estimated seepage rate of 14 mm/day by Van der Linden and Appello [56]. Moreover, some of the polders, which are, based on the water balance calculation, considered an infiltration area, are based on the model a drainage area. The absolute difference is limited, except the Hollandsch Ankeveensche Polder. The difference between the outcome of the water balance and this research of the Hollandsch Ankeveensche Polder can be explained by the fact that the regional model simulates infiltration in the southwest of the polder [95], and the model of this research does not simulate this (Figure 5.15). In general, all modelled fluxes are in the same order, and hence the model performance in terms of flux is reasonable. Especially because the total simulated infiltration from all infiltration zones is 10.0 million m^3/y and the estimated infiltration based on the water balances is also 10.0 million m^3/y [12].

Lastly, the modelled chloride concentration of the seepage out of the aquifer were determined. These values were compared with measurements that capture the chloride concentration of these seepage fluxes. The measurements are performed within the main surface water draining the polders. However, this is not measured in every polder or only in a part of the polder. Therefore, only of a few polders, the measured chloride concentration is given in Table 5.4. In all those polders, the measurements correspond very well with the simulated concentrations.

Table 5.4: Overview of the observed and simulated chloride concentration of the flux out of the aquifer.

Zone ID	Name Polder	$Cl_{observed}$ [mg/l]	$Cl_{modelled}$ [mg/l]
3070	Holland, Sticht Voorburg and 't Honderd Oost Polder	-	73
3200	Spiegelpolder	-	525
3201	Stichtsch Ankeveensche Polder	77	84
3210	Horn and Kuijer Polder	-	585
3220	Horstermeer and Meeruiterdijksche Polder	552	627
3230	Polder Kortenhoef	65	69
3240	Polder Dorssewaard	75	56
3260	Blijkpolder	-	608
4210	Hollandsch Ankeveensche Polder	73	115
4250	's Gravelandsche Polder	-	63
6480	Hoeker-Garsten Polder	-	436
6540	Aestveldse Polder Oost	-	879

6

Effects Pilot Well Scenarios

The pilot well has several modes of operation, of which five were simulated with the model presented in the previous chapter: (1) an active shallow well with a constant pumping rate of 55 m^3/h, (2) an active deep well with a rate of 55 m^3/h, (3) both the shallow as well as the deep well are active with a constant pumping rate of each 50 m^3/h, (4) an active shallow well with a constant pumping rate of 100 m^3/h and finally (5) an active deep well with a constant rate of 100 m^3/h. The effects of these five operational modes will be presented in this chapter. However, since the results of (1) and (4) and the results of (2) and (5) were often similar; only one of them will be shown in this chapter, and the results of the other scenario can be found in Appendix F. The effects are split in effects on the flow regime, including the drawdown and the flow paths, the chloride distribution, and the flux out of the Horstermeer Polder.

6.1. Flow Regime

Due to the pumping of the well, the groundwater flow regime will change. Because of the different discharge, the drawdown and the change in flow regime differ per scenario. This will be shown below.

6.1.1. Drawdown

The simulated effect on the point-water heads surrounding the well is given in Figure 6.1. The figures show that in all three scenarios, the largest drawdown is simulated at the bottom of the well screen, i.e. PZWAz3 for the shallow well screen and PZWAz3_6 for the deep well screen. However, whenever all layers are taken into account, the largest overall drawdown of 30 cm drawdown is simulated at 2/3 of the deep well screen, i.e. -121 to -132 m NAP, in scenario 5. In scenario 2, the maximum overall drawdown is only 17 cm at the same location. For scenarios 1 and 4, a similar pattern is observed, although the maximum overall drawdown is 25 cm at 2/3 of the shallow well screen, i.e. -70 to -86 m NAP, in scenarios 1 and 4, the maximum drawdown of 45 cm occurs slightly higher between -68 and -77 m NAP. The different depth of the maximum occurring drawdown in both scenarios is the result of the chloride concentration since the maximum freshwater-equivalent drawdown occurs in both scenarios between -59 and -68 m NAP. The deviation in drawdown over the well screens demonstrates that the groundwater is not pumped out evenly distributed over the screens. Moreover, the drawdown caused by the shallow well is higher than the drawdown caused by the deeper well. In scenario 3, in which both wells are pumping, the maximum overall drawdown of 26 cm occurs between -68 and -77 m NAP. Besides a different depth of the maximum drawdown, the drawdown also evolves differently over time in the deep and shallow well. The drawdown slightly decreases with time in most depths with an active deep well, whereas the drawdown slightly increases with time with an active shallow well.

Figure 6.1 reveals that the well also slightly influences the heads in the Maassluis Formation, i.e. MSz2. However, the drawdown is limited below the upper clay layer of the Maassluis Formation, i.e. only 2 cm in all scenarios. Furthermore, the flux over the thick clay layer slightly increases below the

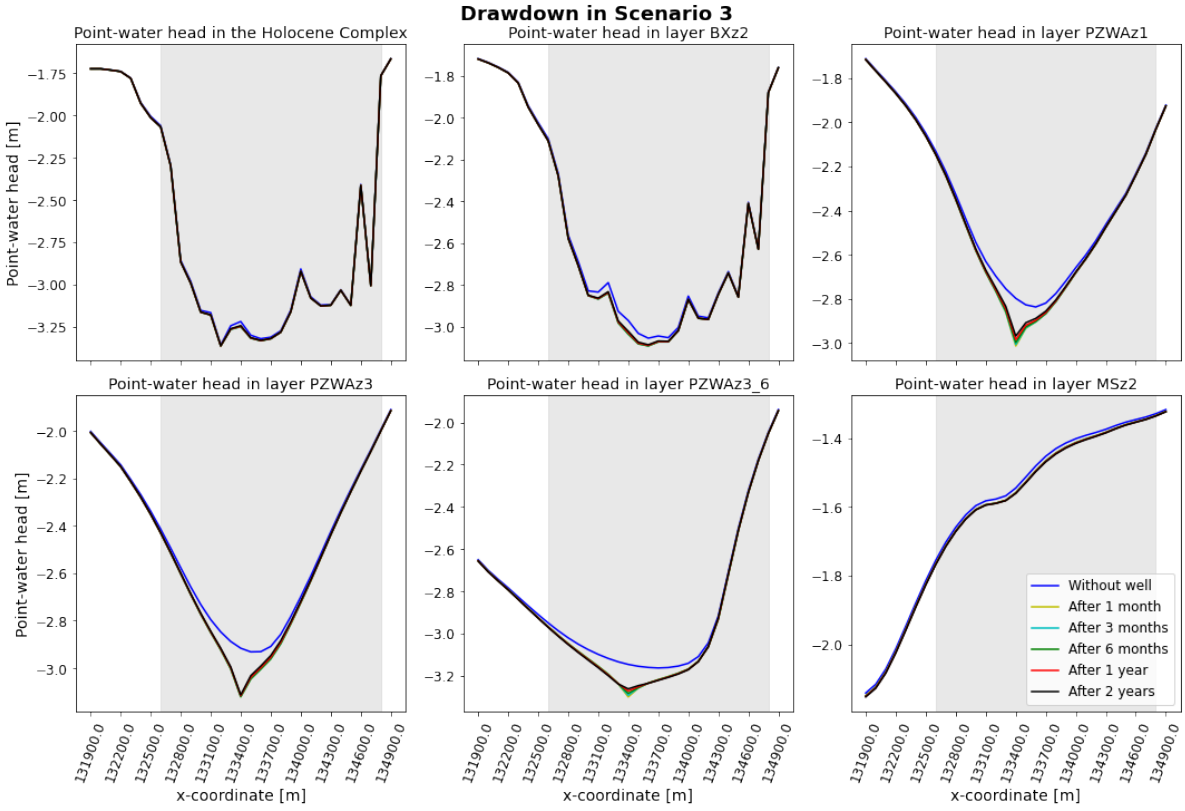

(a)

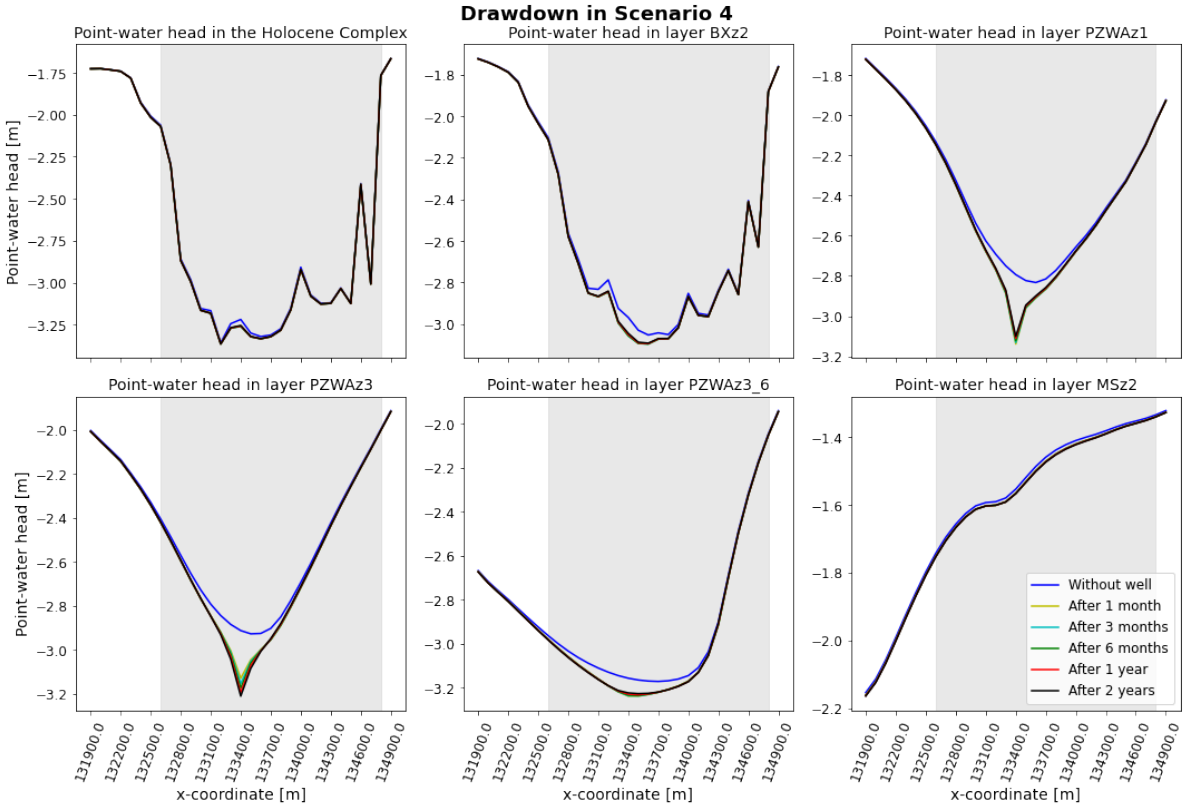

(b)

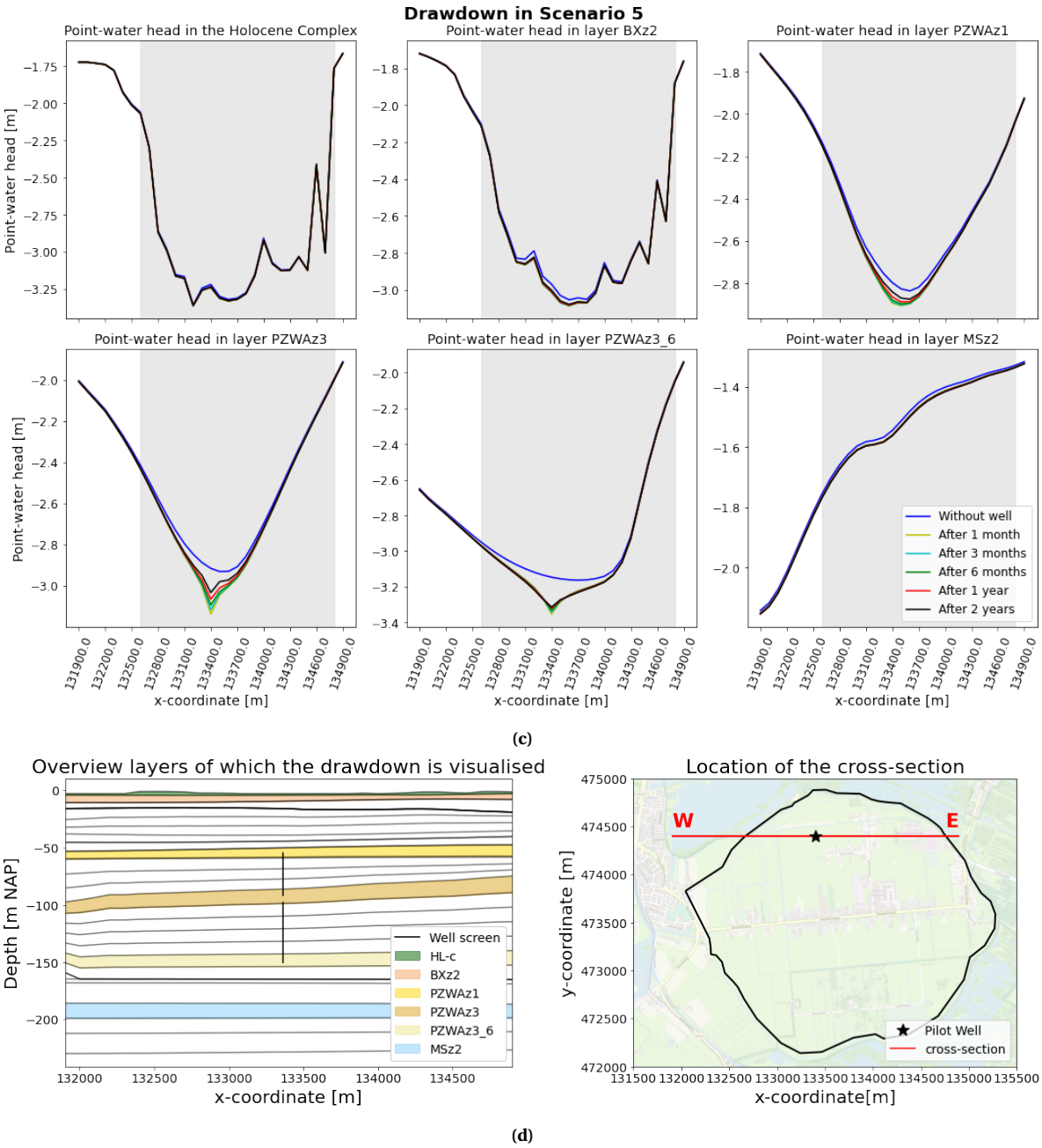

Figure 6.1: The drawdown in terms of point-water heads in different layers in a cross-section of 3.0 km going through the well (x,y = 133400,474400 m). In (a), the simulated drawdown in scenario 3, i.e. pumping from both well screens with a rate of 50 m^3/h, is given, in (b), the simulated drawdown in scenario 4, i.e. pumping from the shallow well screen with a rate of 100 m^3/h, is given, and in (c), the simulated drawdown in scenario 5, i.e. pumping from the deep well screen with a rate of 100 m^3/h, is given. In grey, the delineation of the Horstermeer Polder is indicated. In (d), the layers in which the drawdown is given are visualised, including the location of the well screens.

well screens, but the flux rate is still limited to 0.11 mm/day. The influence at the surface level, on the other hand, is higher in the case of an active shallow well compared to an active deep well. With an active shallow well the maximum drawdown at the surface level is 4 cm. Moreover, as shown in the figures, the influence of the well is limited to the proximity of the wells and especially more towards the middle of the polder at all depths.

6.1.2. Flow Paths

Figure 6.2 shows the simulated effect of the well on the flow paths in the lower aquifer. It can be seen that the shallow well is located just above and below the clay layer in the Waalre Formation

(Figure 6.2a). However, the clay layer is very thin at the location of the well. Hence, the groundwater naturally flows upwards at the location of the well, and the well collects part of the brackish seepage. The deeper well, on the other hand, is located in the lower part of the aquifer. Nevertheless, also towards the deeper well screen, radial flow is simulated, shown in Figure 6.2b.

Moreover, it can be seen that the largest flux towards the wells takes indeed place in the middle of the well screen with an active shallow well and at 2/3 of the well screen of the deep well. This is the case, although the hydraulic conductivity over the whole deep well screen is equal since the whole well screen is located in the PZWAz3 layer. In scenario 3, the largest flux takes place through the shallow well screen. This was already expected due to the location of the largest drawdown. Nonetheless, also through the deeper well screen, groundwater is pumped up.

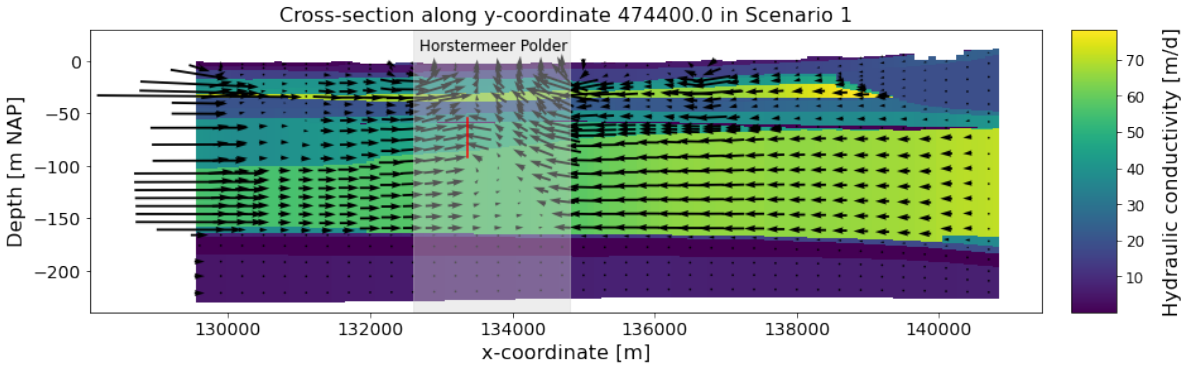

(a)

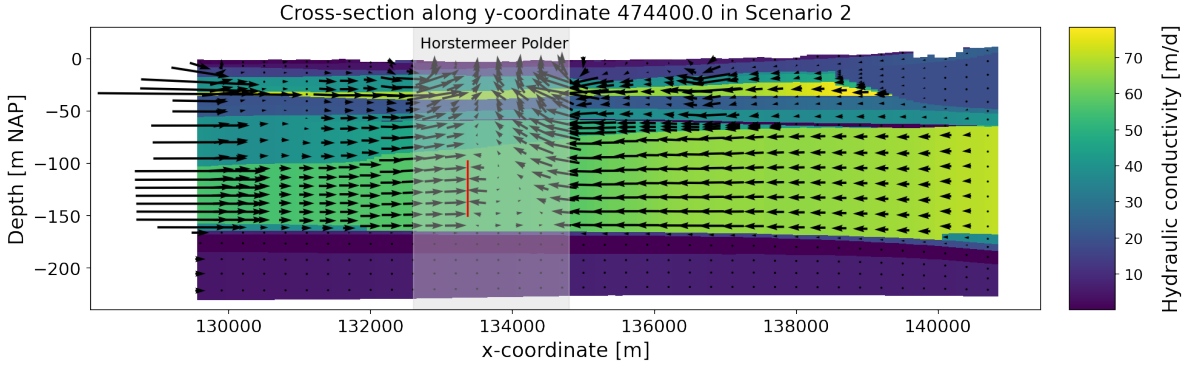

(b)

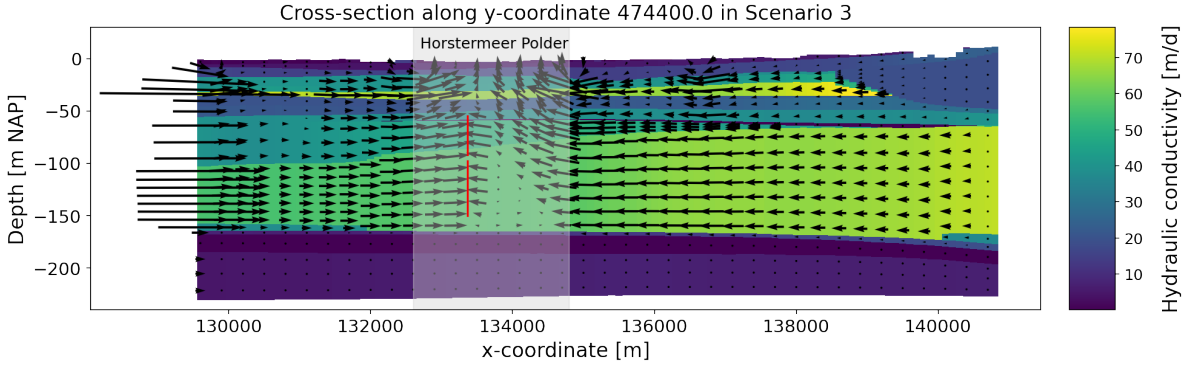

(c)

Figure 6.2: The new flow paths as a result of the wells in the cross-section through the well location. In (a), the shallow well pumps with a pumping rate of 55 m^3/h (scenario 1), in (b), the deep well has a pumping rate of 55 m^3/h, and in (c), both the deep and the shallow well pump with 50 m^3/h. In red, the location of the active well screen is depicted, and in light grey, the Horstermeer polder is indicated.

6.2. Chloride Distribution

The pumping of the well influence not only the flow regime but also the spatial distribution of chloride. In this section, the change in chloride concentration due to the wells will be visualised and the simulated chloride concentration of the well water will be presented.

6.2.1. Top layer

Figures 6.3a, 6.3b and 6.3c visualise the effect of the wells on the chloride concentration in the top layer in the Horstermeer Polder and north of the polder. It can be seen that the shallow well leads locally to a higher decrease in chloride concentration. The model simulates a decrease in the concentration of up to 355 mg Cl^-/l close to the well in the case of an active shallow well. The maxi-

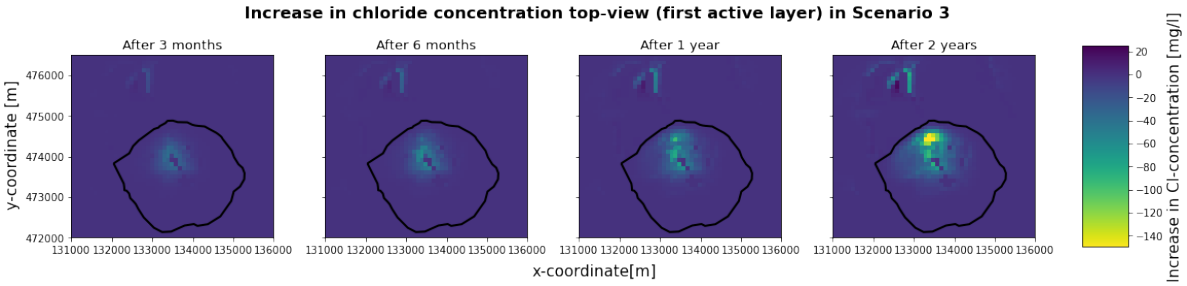

(a)

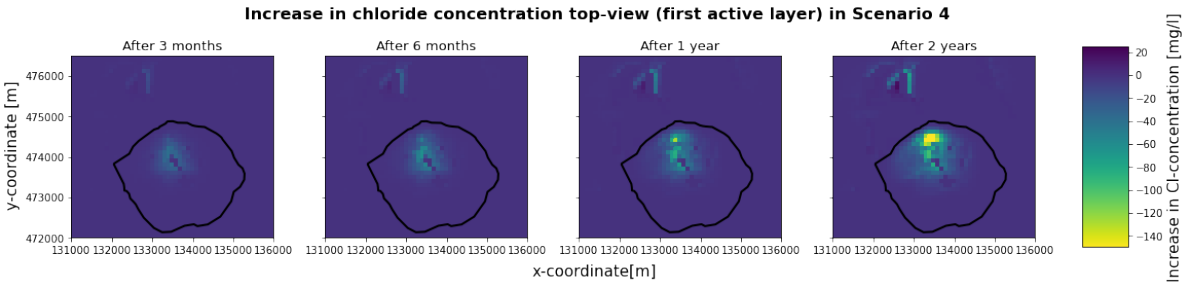

(b)

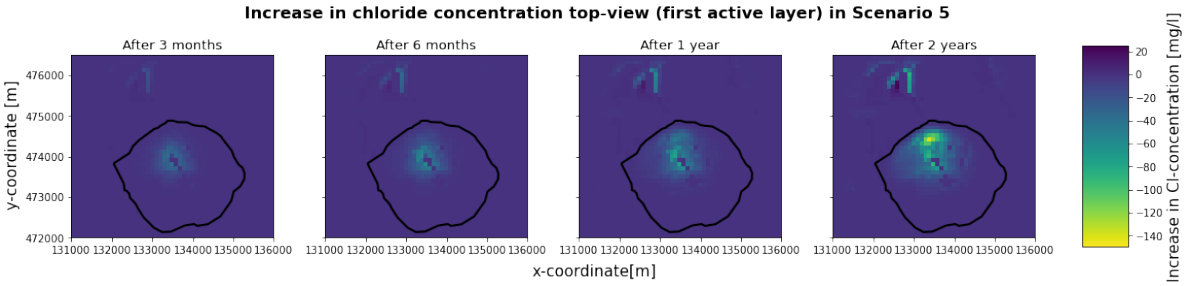

(c)

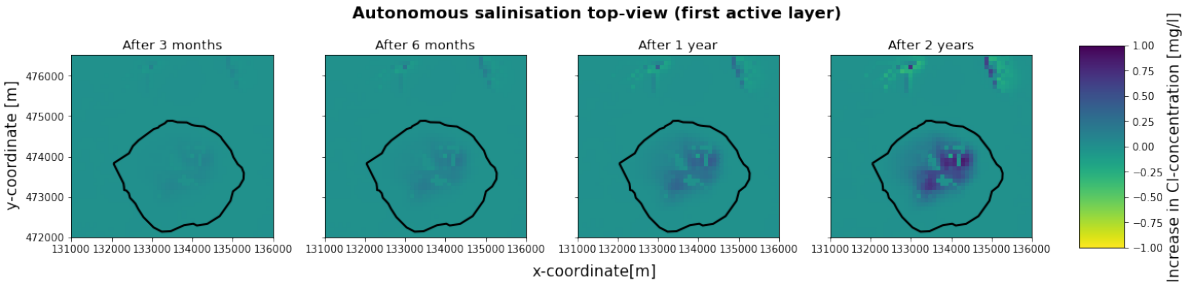

(d)

Figure 6.3: The change in chloride concentration over time compared to before the placement of the well. In (a) both the shallow and the deep well pump with a constant rate of 50 m^3/h, in (b) the shallow well pumps with a constant rate of 100 m^3/h, in (c) the deep well pumps constantly with the same rate and in (d) the autonomous salinisation over the 2 years is given (inactive wells). In black the delineation of the Horstermeer Polder is visualised.

mum decrease of the chloride concentration due to the deep well is, on the other hand, only 135 mg Cl^-/l. Moreover, autonomous salinisation occurs slightly in the Horstermeer Polder, as shown in Figure 6.3d. Although the rate is negligible compared to the effect of the wells, it indicates that the chloride load in the discharge out of the polder will increase over time whenever no mitigation measures are taken.

Besides a change of the chloride concentration within the Horstermeer Polder, a change is visible in the Spiegelplas located northwest of the polder. Figure 6.3 shows that locally the chloride concentration at the bottom of the Spiegelplas increases or decreases if a well is active. The decrease is, however, higher in magnitude and stretches over a larger area. Hence, the wells in the Horstermeer Polder will most likely also slightly reduce the chloride concentration in the Spiegelplas.

6.2.2. Brackish Upconing

Besides the chloride concentration in the top layer of the Horstermeer Polder, the wells also affect the brackish cone of the upconing. Figures 6.4a and 6.4b show that the reduction of the chloride concentration within the cone is less if the shallow well is pumping compared to the effect of the

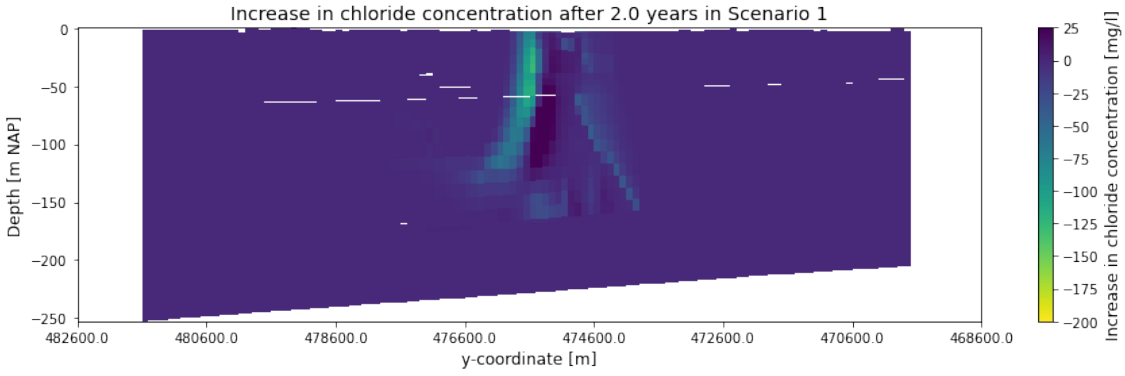

(a)

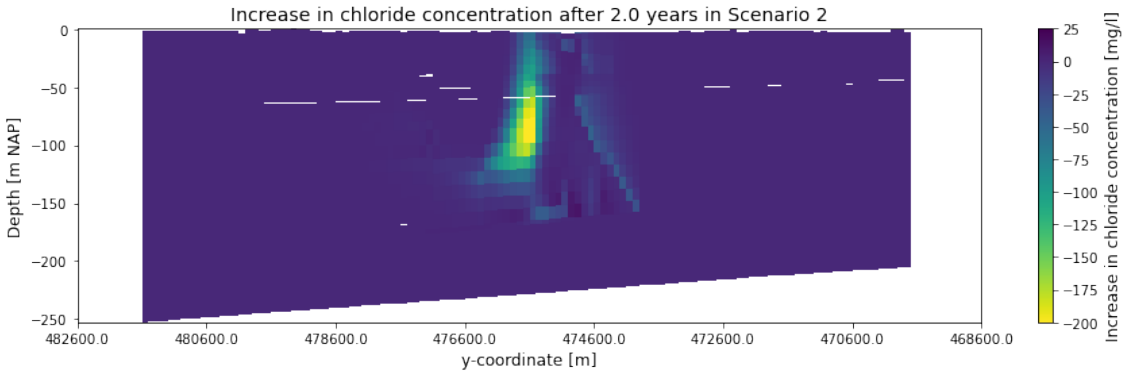

(b)

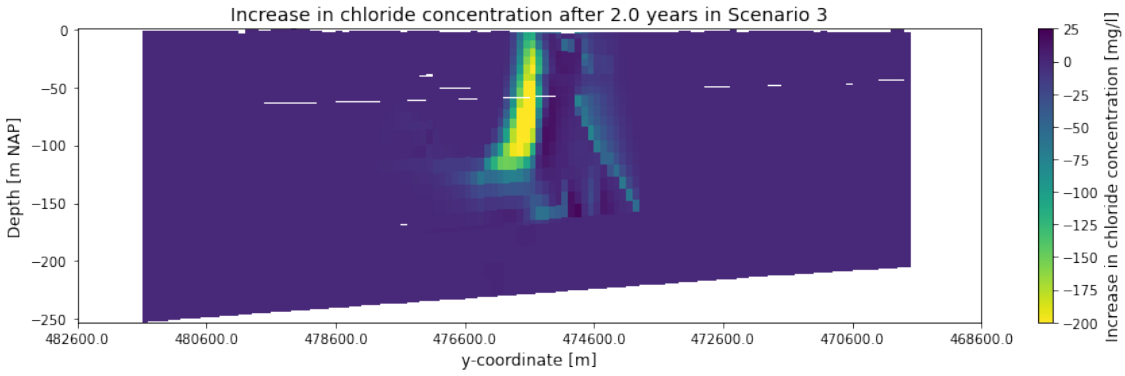

(c)

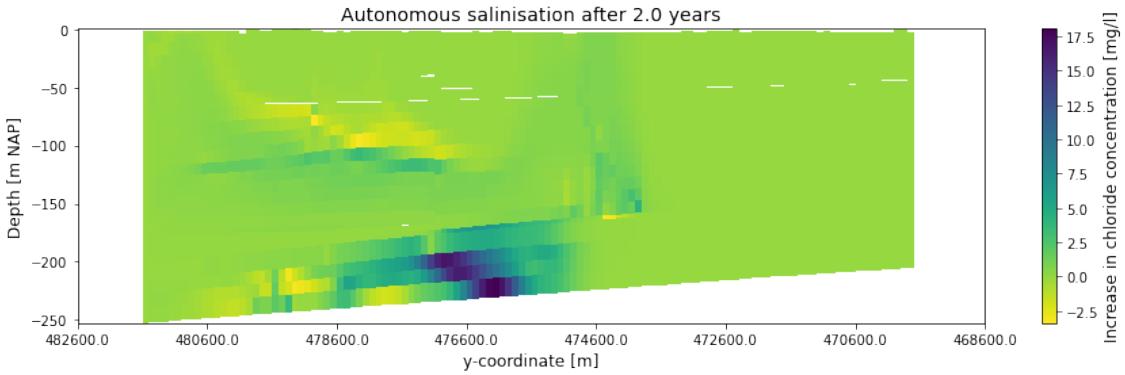

(d)

Figure 6.4: The effect of (a) the shallow well with a constant pumping rate of 55 m^3/h, (b) the deep well with the same pumping rate and (c) the combination of the shallow well and deep well with both a constant pumping rate of 50 m^3/h on the chloride concentration in the cone of the upconing compared to the situation before the well placement. In (d), the autonomous salinisation during the two years is visualised.

deep well. Moreover, the pumping of the shallow well results in the salinisation of the middle of the upconing. This effect is not present in the scenario in which the deep well is pumping (Figure 6.4b). In both cases, the most significant decrease takes place above the well screens. In the situation that both wells are operating (scenario 3), the reduction of the chloride concentration is high over a larger depth than in scenario 2 (Figure 6.4c). Although, just like in scenario 2, the most significant reduction takes place above the deeper well screen. In addition, the model simulates a reduction of the chloride concentration at the south of the cone. Hence, the cone becomes narrower due to the well.

Moreover, Figure 6.4d the simulated autonomous salinisation below the upper clay layer of the Maassluis Formation (>220 m NAP) just north of the Horstermeer Polder. After two years, the tip of the interface moved slightly further southwards, and hence the chloride concentration increases there. In the south of the polder, autonomous salinisation also occurs. This is counteracted by the extraction of brackish water by the wells.

6.2.3. Concentration of the Well Water

Based on Figure 6.4, it was expected that the concentration of the water that is pumped up by the wells is higher for the deeper well than for the shallow well. Figure 6.5 confirms this hypothesis. However, the concentration increases over time in the shallow well, whereas it decreases over time in the deeper well. The pumping rate appears to have an insignificant influence on the concentration of the water from the shallow well. However, with an active deep well, a higher pumping rate led to a lower average concentration. In scenario 3, where both wells are operating, the chloride concentration of the water pumped up by the shallow well is significantly lower over time compared

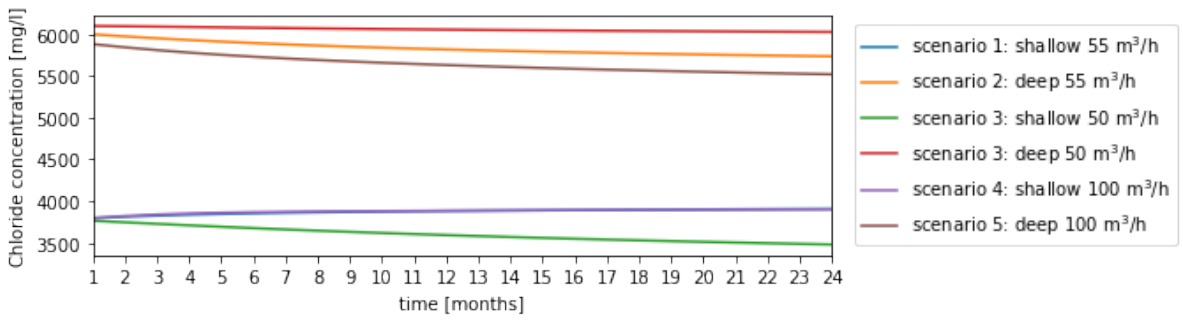

Figure 6.5: The concentration of the groundwater pumped up by the wells in the different scenarios over time.

to the scenarios in which only the shallow well is active. In contrast with the scenarios in which solely the shallow well pumps, the chloride concentration decreases over time. Contradictory, the deeper-well water has a higher chloride concentration if both wells are operating.

6.3. Flux out of the Horstermeer Polder

Since the well pumps up brackish groundwater, the flux and the salt load decreases, which is shown in Table 6.1. The most effective scenario is scenario 4, in which the shallow well pumps with a constant rate of 100 m^3/h. In this scenario, the flux and the salt load are decreased the most , however, also scenarios 3 and 5 are very effective. However, the reduction of the chloride load is considerably higher in scenario 3 compared to scenario 5.

Table 6.1: Overview of the model results and the reduction in flux, the chloride load and the chloride concentration of the water flowing out of the Horstermeer Polder compared to the situation without the pilot well (baseline).

Scenario	**$Flux_{out}$ [MCM*/y]**	**Reduction** [%]	**Cl-load** [**kt/y**]	**Reduction** [%]	**Cl-concentration** [**mg/l**]	**Reduction** [**%**]
Baseline	26.07	-	17.04	-	627	-
1	25.83	0.94	16.50	3.18	613	2.31
2	25.85	0.85	16.58	2.75	615	1.97
3	25.65	1.63	16.14	5.31	603	3.84
4	25.62	1.72	16.10	5.55	602	3.99
5	25.67	1.55	16.19	4.98	604	3.70

* MCM: Million Cubic Meters

7

Discussion

In this chapter, the results presented in the previous two chapters will be discussed. The regional variable-density groundwater model gave both insights into the flow regime and chloride distribution in the area, as well as new insights into the influence of the former Zuiderzee and the clay layers. Moreover, the effects of brackish water extraction will be evaluated. Lastly, the limitations of the used methodology will be discussed.

7.1. Regional Aquifer System

The results of the regional variable-density groundwater model show the draining nature of the Horstermeer Polder and the corresponding brackish flux. The simulated steep surface of the brackish upconing at the east side of the polder (Figure 5.8a) corresponds well with the findings of Delsman *et al.* [10]. Furthermore, especially the simulated chloride concentration of the seepage flux corresponds better with the field observations than the simulated chloride concentration in the studies of Fakhari [12] and Bos-Burgering *et al.* [17]. Furthermore, the results suggest the autonomous salinisation will increase the chloride concentration in the future. The increase of the chloride concentration over time is also visible in the chloride measurements just outside the polder at the main pumping station. Moreover, the run time is significantly lower than that of previous models, with an average run time of 32 minutes. Nonetheless, the model results still slightly deviate from field conditions, specifically around the Amsterdam-Rhine Canal (ARC) and at greater depth below the Horstermeer Polder. The underestimation of the point-water head between the Vecht and the Naardermeer is probably a result of an overestimation of the top layer's vertical hydraulic conductivity (K_v) at that location. On the other hand, the overestimation of the point-water head south of the city of Weesp is likely the result of the location of the western boundary and the subsequent underestimation of the freshening effect of the ARC. The deviation in the shape of the upconing at surface level in the Horstermeer Polder is most likely also due to the K_v of the top layer. A more thorough discussion of these individual factors will be presented in Section 7.3. Lastly, the outcomes gave new insights into the influence of the former Zuiderzee, the upper clay layer in the Maassluis Formation, and the clay layer in the Waalre Formation on the groundwater system. Therefore, these findings will be discussed below.

7.1.1. Influence Former Zuiderzee

Although the long history of marine influence north of the Horstermeer Polder stopped after the construction of the Afsluitdijk in 1932 AD [16], the results show that brackish water infiltrated before 1932 AD still influences the chloride distribution in the area, both in the deep and the shallow subsurface (> -50 m NAP). These results align with the chloride measurements of samples taken in the northern part of the area (Figure A.7). However, the former Zuiderzee influences not only the area north of the Horstermeer Polder, but also the chloride distribution within the polder. As shown in Figure 5.13b and based on Figure 5.7, the chloride originating from the former Zuiderzee will be transported to the Horstermeer Polder due to advection. Moreover, in contrast to the isohypse map

resulting from the Regional Groundwater Model of Waternet ($RGWM_{Waternet}$), the isohypse map of this study, given in Figure 5.7, indicates that groundwater flow does occur over the northern boundary. The model in the study of Fakhari [12] did not simulate the shallow brackish groundwater in the north and had an impermeable northern boundary and, therefore, the influence of the Zuiderzee had not been taken into account. The model presented in this study has an initial chloride distribution based on the NHI data set, which in its turn is based on all measurements before 2017 AD. Hence, the model simulates the shallow brackish water that probably originates from the former Zuiderzee.

7.1.2. Influence Clay Layer in the Waalre Formation

The clay layer in the Waalre Formation has an average thickness of 2.5 meters in the model area and is located at an average depth of -56 m NAP. However, Figure D.1 shows that the clay layer is not present everywhere or with a very small thickness. The largest difference of the freshwater heads above and below the layer is as high as 92 cm. In other words, the clay layer has a significant influence on the flow regime in the regional groundwater system. Moreover, the largest decrease in the freshwater head of 0.8 m over the clay layer is simulated below the southeast of the Horstermeer Polder (Figure D.5). These results indicate that the clay layer influences the upward seepage path significantly, particularly since the thickness differs below the Horstermeer Polder and the northwest part has vertical pass-through cells (Figure D.1). This raises the question of whether taking the clay layer into account at locations where its thickness is less than 1 meter, e.g. the northwest of the polder, would better represent the field conditions. However, measurements at the location of the pilot well indicate that the difference in point-water head over the clay layer is limited to 4 cm in the north of the polder [96]. Although the influence of the clay layer in the Waalre Formation has been recognized in studies at different locations in the Netherlands [17, 97], this study proves that it also influences the upconing below the Horstermeer Polder due to the usage of MODFLOW 6, in which pinch-out layers, like this clay layer, can be better represented.

7.1.3. Maassluis Formation

The main reason that the aquifer in the Maassluis Formation was included in the model was to research if, even with a (partly) freshwater aquifer, the chloride concentration of the seepage in the Horstermeer Polder can correspond well with field observations. The result in Table 5.4 confirms this hypothesis. Moreover, contrary to the studies by Fakhari [12] and Delsman *et al.* [10], the results of this model indicate that the upper clay layer in the Maassluis Formation almost completely disconnects the aquifers below and above it. The groundwater flow over the clay layer is minimal, as the model simulates a maximum upward vertical specific discharge of 0.11 mm/d (Figure D.8). Since advection is the primary transport process of salts, salt transport over the Maassluis Formation is limited. This very low vertical flux also occurs with a freshwater head difference of up to 80 cm over the upper clay layer (Figure D.6). However, from the measurements is known that the chloride concentration is slightly lower directly above the clay layer compared a bit higher up in the aquifer, suggesting that some upward transport might occur over the clay layer. Although the simulated heads directly above and below the Maassluis Formation do not correspond well with observations at the location of the deep drilling (Figure 5.11), the simulated point-water head difference between the depth of filter 4 (-151 m NAP) and 1 (-221 m NAP) of 82 cm is almost equal to the observed head difference of 79 cm. In other words, the effect of the clay layer on the head distribution corresponds well with field observations

Another reason to include this aquifer was the very local fresher area in the shallow subsurface in the middle of the upconing in the Horstermeer Polder (Figure 3.6) and the hypothesis that this local fresher area originates from the fresh aquifer below the upper clay layer of the Maassluis Formation [13]. However, a flow path of more than 150 meters without significant mixing is improbable, and the model results from this study contradict this theory, as no fresher zone could be indicated in the middle of the upconing (Figure 5.13). Therefore, the local fresher zone is probably the result of

a rainwater lens contained by dams in the specific ditch with lower chloride concentrations. However, chemical analyses are needed to confirm the age and origin of the water.

However, from the results could be concluded that correctly simulating the conditions below the clay layer might be hard. Head measurements in this aquifer are very scarce. There are only five measurement locations in this aquifer in the surroundings of the Horstermeer Polder, and none of them is in the potentially brackish part of the aquifer (Figure B.2). This makes it challenging to define correct head values at the boundaries. Moreover, validation of the simulated chloride distribution is hard, since the chloride measurement locations in the aquifer are scarce too. In this research, significant autonomous salinisation of the aquifer was simulated during both the first (Figure 5.2) and second stress period (Figure 6.4d). However, the subsequent chloride distribution at the end of the first stress period did not correspond to field observations in the deep drilling of the Horstermeer Polder. In other words, to correctly represent the aquifer in the Maassluis Formation, more deep drillings and measurements of both heads and chloride concentrations might be needed, which are very expensive. This model showed that the influence of the lower aquifer on the upper aquifer is minimal, and therefore, the upper clay layer of the Maassluis Formation could be used as the base layer of a future model. In NLMOD the base layer can easily be changed. This would simplify the model without the loss of important information. However, as shown in Figure 6.1, the pilot well has a minor influence on the head distribution in the lower aquifer in the Maassluis Formation. With the currently used operational settings, the influence is limited, yet if higher pumping rates in deep wells are wanted, it might be better to simulate its effect on the head distribution in the Maassluis Formation and the vertical specific discharge over the clay layer. Hence, in those cases, it might be preferred to include this aquifer in the model.

7.2. Brackish Water Extraction

The chloride concentration in the seepage water in the Horstermeer Polder, as shown in Figure 6.3d, is expected to only increase over time due to the seepage of more saline water. This corresponds with the findings of [8]. Therefore, the need for more sustainable mitigation measures will grow in the future. In this study, the mitigation measure of extracting brackish water was researched. The results shown in Table 6.1 indicate that in the best scenario, the pilot well, i.e. an active shallow well with a constant pumping rate of 100 m^3/h, can reduce the chloride load by 5.5% and the corresponding chloride concentration in the discharge of the Horstermeer Polder will be 24 mg/l lower that the original scenario of 627 mg/l. This result indicates that the effects of the pilot well are rather limited on the water quality of the discharge water. As a consequence, a total of 24 of these shallow wells with a constant pumping rate of 100 m^3/h might be needed to achieve the acceptable concentration of 250 mg Cl^-/l[1]. However, in the Netherlands, a maximum permissible concentration of 150 mg Cl^-/l is used for surface waters with drinking-water purposes, and to achieve a condition in which no harmful environmental effects are to be expected, a concentration of 94 mg Cl^-/l is needed. If one of these limits will be the project's aim, 37 and 49 shallow wells with a constant pumping rate of 100 m^3/h would be needed, respectively. In these calculations, it was assumed that all wells have the same effect as the pilot well, but the location of the well will probably influence its effect in practice. From Figures 5.13 and 5.14 can be concluded that the chloride concentration is considerably lower at the edges of the upconing than in the middle of the upconing. Hence, a well more towards the middle of the upconing could have a higher reducing effect on the chloride load than a well more towards the edge of the upconing, like the pilot well. Furthermore, De Louw *et al.* [5] determined that the majority of the brackish flux occurs via local boils. Thus, wells at those specific locations could have higher efficiency. Moreover, a well field could potentially enhance the effect of the individual wells, but so far, no research has been performed on that matter, and an estimation of the effect on the seepage flux without a model result is impossible.

[1] 250 mg/l is the target concentration of discharge out of polders with brackish seepage used in the COASTAR project in the Netherlands [17]

Based on these results, it is expected that an extensive well field will be needed to sufficiently lower the chloride concentration in the discharge water out of the Horstermeer Polder. However, a well also influences the hydraulic heads in its surroundings. The results showed that the active shallow well leads to a drawdown of up to 4 cm in the top layer of the Horstermeer Polder and even more in the layer below it. As this is the average drawdown in one cell of 100 x 100 m, the drawdown is higher close to the well in practice. The majority of the built-up area in the northeast of the polder is supported by wooden pile foundations [17, 98], making it susceptible to rot if the phreatic surface is lowered. Moreover, there is a legal limit of 5 cm drawdown, above which drought compensation needs to be paid to the inhabitants in the Netherlands [99]. Hence, the wells cannot be placed close to any buildings in the northeast of the polder. Figure 5.14 shows, however, that the highest chloride concentrations occur in the built-up area of the polder. Therefore, the locations of wells with most probably the highest efficiency rates are inapplicable. Moreover, it reduces the usable area in which wells could be placed considerably.

7.3. Limitations

Lastly, this research has some limitations. These limitations arose from the used methodology. The limitations influence the result and model performance. To be open about these uncertainties, the limitations will be discussed below.

7.3.1. Rainwater Lenses

As shown in Figure 5.14, the model simulates some large rainwater lenses in the Horstermeer Polder. Within the majority of these cells, the estimated Holocene layer is less than 1 meter, i.e. the first model layer is inactive in these cells. Moreover, all cells within the rainwater lenses are not present in the RIV nor the DRN data set based on surface water-groundwater interaction. In other words, in these specific cells, no surface water is present. In most of these cells, however, a DRN data set is active based on overland flow. However, whereas the surrounding cells have a simulated drainage level of -3.45 m NAP, the surface elevation acts as the drainage level in these cells. This drainage level is in some cells up to 80 cm higher than the drainage level of the surface waters. As a result, the seepage water will not flow towards these cells as the surrounding cells have a lower hydraulic head, and rainwater lenses are created. Moreover, the surface elevation data set of the AHN has a no-data value in many cells. Consequently, overland flow is not everywhere simulated. Moreover, at most locations of the rainwater lenses, buildings are present which would result in lower recharge values in practice. A decrease of the recharge locally could possibly inhibit the formation of these rainwater lenses at those locations.

Nonetheless, in practice, the drainage level in cells within the polder without surface waters would be below surface elevation. Especially in tile-drained agriculture fields, which are present in the area with rainwater lenses [100], the drainage level would be located below the surface elevation. Therefore, the height of these drains would have been a better representation of the drainage level compared to the surface elevation level. This is true for the Horstermeer Polder and other areas in which no infiltration was simulated in the current model (Figure 5.15). Both the area west of 's Gravelandsche Polder and the oval area north of 's Gravelandsche Polder currently have neither a simulation of infiltration nor of drainage in the model. However, both areas are tile-drained, and hence drainage occurs in practice [100]. Therefore, inclusion of those tile drains would better represent the field conditions than solely the simulation of overland flow. Since a rise of the hydraulic heads above surface level is improbable in the controlled environments of the polders, overland flow only occurs whenever the rainfall intensity exceeds the infiltration capacity. This, however, only occurs at periods of a few minutes, but not in the time frame of a year that is used as the time step in this research.

7.3.2. Calibration Procedure

The model was only calibrated by hand, and the only parameter that has been changed is the vertical hydraulic conductivity of the top layer using a trial-and-error method. The main focus output parameter was the average seepage/infiltration flux in the polders in the model area. This has been chosen over head measurements or chloride concentration because the former can highly fluctuate over time and is only informative if the chloride concentration is measured simultaneously [80] and the latter is measured too scarcely in time. However, the seepage/infiltration flux in the polders can not directly be compared with the fluxes at the pumping stations of the polder since the many inlets in the polders make it impossible to determine the inflow into the polder correctly. Moreover, seepage rates cannot be measured directly [101]. Hence, to calibrate on fluxes, water-balance calculations of the polders were needed that determine the net inflow or outflow into the polder. These water balance calculations entail many assumptions. The main assumptions are (1) the seepage flux, (2) the inlet of water into the polders through inlets controlled by farmers, and (3) the corresponding chloride concentrations of these fluxes. Therefore, the calibration of this model has only be done to a limited extent.

Better model performance is expected with a more thorough calibration procedure, even when the minimum value of the top layer's vertical hydraulic conductivity (K_v) is the only parameter that is calibrated. This is because the currently used K_v still results in a deviation from the field conditions. Predominantly, the shape of the 1000 mg Cl^-/l contour surface is determined by the used K_v of the top layer and can still be improved. Nevertheless, the achieved model performance with the used calibration is good enough to identify the effect of the pilot well on the flow regime and spatial distribution of chloride since the general outcome corresponds well with the field conditions.

7.3.3. Grid-Cell Size

The used grid-cell size is 100 x 100 m, which required upscaling of the hydraulic parameters [86]. However, detailed information on the input parameters is often not available for the whole model area. Therefore, model simplifications, assumptions, and approximations are needed [3]. This research uses many interpolated data sets made by experts, i.e. REGIS II, GEOTOP, and NHI fresh-saline, to approximate the spatial variability in the input parameters. However, little is known on the needed level of complexity or simplicity [3]. Especially variable-density groundwater models tend to be sensitive to the initial salinity distribution, heterogeneity of the subsurface, and preferential flow paths due to paleochannels and fractures [5, 102]. Although heterogeneity of the subsurface and chloride concentration were taken into account as much as possible, this was not the case for these paleochannels and fractures. The used grid-cell size is not able to simulate these local preferential flow paths. Moreover, very local differences in chloride concentrations could not be simulated (Figure 5.14). Although it appears that the model can simulate rainwater lenses, the observed rainwater lenses in between the small ditches within one cell cannot be identified. This is the result of the used grid-cell size. Nonetheless, the model is capable of simulating the general spatial distribution of hydraulic head, chloride concentration, and fluxes into and out of the subsurface, providing insightful output for this research.

However, the simulation of drawdown resulting from the pumping of the well are highly influenced by the grid-cell size. This is because the model can only calculate the hydraulic head per cell, and since each cell has an area of 0.01 km^2, the calculated hydraulic head is the average in that area. At the same time, the drawdown close to or even in the well is very high, whereas 50 meters further, the drawdown is already significantly less. Hence, the drawdown in the well calculated by the model is significantly less than the measured drawdown as a result of the used grid-cell size.

Lastly, transferring the small-scale experimental results to real-world simulations is difficult [3]. As mentioned before, one example is the dispersion coefficient, of which laboratory-derived values cannot explain the thicker observed mixing zones. Therefore, even with a smaller grid-cell, size approximations are needed to simulate real-world problems. Additionally, high-resolution modelling

requires higher computational power. This was experienced when the grid resolution of the model was reduced to 25 x 25 m. This smaller resolution model could not be run on a computer with 8 GB of RAM.

7.3.4. Steady-State Modelling

The model has no time-dependent input data. In other words, the surface water level in the polders, the groundwater recharge, the bottom resistance, and pumping rates are all constant in time and thus steady. In practice, however, the controlled surface water levels have a seasonal pattern in many polders, and also the groundwater recharge is time-dependent. During summer, the surface water level is often higher than in winter, although not every polder has seasonal-depending surface water levels. The variability in hydrological stresses does result in variability in the seepage rate and corresponding chloride concentration. Moreover, the time-variant bottom resistance of the ARC results in a fluctuating infiltration rate of the ARC, and hence the freshening effect of the ARC is time-variant [59]. The Horstermeer Polder has a fixed surface water level throughout the year, but precipitation and evaporation differences, changing surface water levels, and fluctuations of the fresh infiltration in the surrounding areas will likely affect the brackish upconing. The difference between the measurements of Van Wielink [11], which were executed in winter, and of Jain *et al.* [18], which were executed in summer, depicted in Figure 3.6, already show this influence. Therefore, the effect of the pilot wells simulated in this research can deviate from the observed effect over time. Nonetheless, the model gives a reasonable first estimate of the effect of the pilot well and therefore is a valuable first step.

7.3.5. Model Boundaries

The model has a head-controlled boundary condition at its boundaries, and the boundary cells have freshwater heads that are hydrostatic over the depth. As a result, whenever the equivalent freshwater head is high in the top layer, the heads over the whole depth are high. This leads to an overestimation of the flux in that specific cell (Figure 6.2). However, especially the upper clay layer of the Maassluis Formation but also the clay layer in the Waalre Formation separate aquifers. The hydraulic head can be significantly different above and below the clay layer. This is also visible in Figure 5.11 as the model overestimates the freshwater head equivalents above the Maassluis Formation and underestimates the freshwater head equivalents below the clay layer at the location of the deep drilling in the Horstermeer Polder. Hence, the model likely overestimates the flow towards the polder below the upper clay layer of the Maassluis Formation, resulting in the eastward movement of the fresh-brackish interface over time (Figure 5.2). The eventual location of the interface below the deep clay layer does, however, not correspond to the measurements since the measured chloride concentration below the upper clay layer of the Maassluis Formation at the deep drilling are fresh (Figure 3.4) and in the model outcome, the concentration is >1000 mg Cl^-/l. Likewise, the overestimation of the freshwater-head equivalents above this deep clay layer leads to a decreased flux towards the Horstermeer Polder and hence seepage flux (Table 5.3). Since the overestimation increases with the depth until the upper clay layer of the Maassluis Formation, the model boundaries likely cause this deviation. Hence, the hydrostatic heads at the boundaries do not correspond well with practice.

Second, the heads at the boundary are hydrostatic over the depth, but no attention was given to the heads in neighbouring cells. As a result, whenever the head in a neighbouring cell is significantly larger in the top layer due to, for example, the boundary of polders or the river Vecht, this deviation is kept over the depth. As a result, the groundwater will flow into the aquifer in one cell and partly flow out of the aquifer in the neighbouring cell with a lower hydraulic head value. This behaviour can be seen in Figure 5.7 whenever the groundwater flow is drawn perpendicular to the isohypses. Both in the north as well as in the west, curvatures at the boundaries are present. This behaviour is implausible in practice since the controlled surface water levels in the polder and the river Vecht will not influence the hydraulic heads to this extent at greater depths.

Third, it appeared that the model boundaries also influence the spatial distribution of chloride. Initially, the model was run with the model boundaries conform the model of Fakhari [12]. However, since the ARC acts as a water divide and the modified NHI fresh-saline underestimates the chloride concentration east of the ARC, the eventual chloride concentration in the Horstermeer Polder was highly underestimated. Thus, it was chosen to relocate the model boundary to the east edge of the ARC. It was not chosen to place it precisely on the ARC since the hydrostatic nature of the boundary would result in an overestimation of the fluxes into the aquifer system. Nonetheless, the exact location of the boundary appeared to be very influential on the model outcome. Hence, using a trial-and-error method, the best location for the current representation of the boundary was determined.

Lastly, since the best location of the boundary is just east of the ARC, the freshening effect of the ARC is not correctly simulated. This is because the hydrostatic nature of the boundary led to almost no infiltration of the surface water of the ARC. In practice, the hydraulic heads below the ARC will be lower than the surface water level of the canal, and hence significant infiltration will take place [59]. Due to an underestimation of the infiltration rate, the freshening effect of the ARC is also underestimated. However, Beemster and Ouboter [59] determined that the freshening effect of the ARC is considerable, especially in the last years. The reduced freshening effect in the model outcome is enhanced by fixed chloride concentrations, based on the modified NHI p50-model, on the boundaries. This is because whenever a chloride concentration, corresponding to brackish water, is estimated in the NHI model below the ARC, the chloride concentration on the boundary will lead to a brackish flux into the model. This is especially the case in the north of the model area south of the city of Weesp. Therefore, the model outcome has a smaller fresh lens below the whole ARC, as shown in all cross-sections in Appendix E, compared to the measured fresh lens in Figure 5.13b. At least in the Aestveldse Polder Oost, this led to an overestimation of the chloride concentration (Figure E.5).

8

Conclusion

The currently used mitigation measure of the brackish seepage in the Horstermeer Polder, located between the cities of Amsterdam and Hilversum in the Netherlands, is far from sustainable. Large quantities of freshwater are used for flushing out relatively small amounts of brackish water. Therefore, research on the brackish upconing in the polder as well as additional mitigation measures are needed. This research aimed to evaluate a new mitigation measure: the extraction of brackish groundwater by the newly installed pilot well. To achieve this main objective two underlying objectives were formulated. First, a better general understanding of the subsurface characteristics, and geohydrology surrounding and within the Horstermeer Polder was gained by analysing all available data on geology, hydraulic head, and chloride distribution. Second, the groundwater system in the area was modelled as closely as possible to field conditions by improving the existing model.

The analysis of the available data showed that the stratigraphic architecture in the area consists of a deep thick clay layer at approximately -150 m NAP, although it dips towards the north of the area, and another thinner clay layer at approximately -55 m NAP. In between the clay layers, a very thick aquifer of approximately 100 meters is present. Above the upper clay layer, the geology is more complex, and the sediment layers differ in space. An ice-pushed ridge is present in the east and north, whereas sand layers with different hydrogeological properties characterise the remaining part of the area. At approximately -25 to -35 m NAP, the sand is very coarse, and at some locations there is even gravel present, creating a so-called 'race layer' in which the specific discharge is considerably larger. Finally, the top layer differs significantly, both within the polder itself and from its surroundings. There is no Holocene layer in the east, and in all other areas, its thickness varies. The western half has mainly a clayey top layer due to the sedimentation of the river Vecht. The other areas are characterised either by peat or sand due to peat mining in the past. The influence of humankind goes beyond the top layer in the area. Land reclamation, sand and peat mining, and the creation of polders, influence the flow regime and thus the chloride distribution. Within the thick deep aquifer, the groundwater is brackish due to marine transgression during the beginning of the Holocene. Marine transgression took place both in the north and west of the study area; hence, the brackish groundwater is limited in the southeastern part of the area. In the north and west, surface water bodies influence the chloride distribution as infiltration of fresh surface water pushes the fresh-brackish interface downwards. However, the reclamation of the Horstermeer Lake caused a decrease of the phreatic surface, leading to the development of a brackish seepage flux originating from the north and west of the deep aquifer to the surface level. The surrounding fresh surface waters push the brackish seepage towards the middle of the northern half of the polder. Moreover, the fresh fluxes from the Hill Ridge in the east, the river Vecht, and the Amsterdam-Rhine Canal (ARC) in the west, are not capable of preventing the brackish seepage from entering the surface waters in the polder.

The created 3D model was built using MODFLOW 6 in a Python environment (FloPy) and simulates the aforementioned characteristics, using the stratigraphic architecture and water management sit-

uation as input data sets. Due to the usage of MODFLOW 6, pinch-out layers, like the upper clay layer, could be better represented, and hence the influence of the upper clay layer could be researched. From the results it can be concluded that its influence is significant, especially on the flow path of the deep brackish water to the surface. Moreover, the results showed that the deep clay layer almost completely disconnects the aquifers above and below it. Besides the influence of the clay layers, the model outcome also showed the influence of the Horstermeer Polder on the chloride distribution. Deep brackish groundwater, mostly originating from the northwest of the area, seeps out in the polder and creates a very steep fresh-brackish interface in the east of the polder. After a first calibration of the vertical hydraulic conductivity of the confining top layer, the model appeared to be in good correspondence with the field conditions. At 70% of the measurement locations, the simulated head deviated less than 30 cm from the measured average head of the period 2000 to 2020 AD, and the Root Mean Square Error (RMSE) has a value of 0.29 m. All simulated heads are in the range of 0.53 m NAP in the east to -3.43 m NAP in the Horstermeer Polder. However, the deviation of heads increases with depth below the Horstermeer Polder. This is caused by the model boundaries used, and results in an underestimation of 20% of the seepage flux in the polder. The corresponding simulated chloride load of the discharge out of the polder is only -5.45% off. Thus, it can be concluded that the representation of the brackish upconing is significantly better than in previous models. The modelled seepage flux and chloride load are 26.07 million m^3/y and 17.04 kt/y, respectively. However, the location of the interface of the brackish upconing is a few hundred meters more to the west than the measured 1000 mg Cl^-/l interface. Nonetheless, the deviation of the chloride concentration is less than 200 mg/l at 80% of the measurement locations. Hence, the simulated chloride distribution is in reasonable agreement with the observed distribution.

Using the calibrated model, five scenarios have been run with different operation settings of the pilot wells and one additional scenario acting as a baseline in which the wells are inactive. The scenarios 1 and 2 simulate the well with a pumping rate of 55 m^3/h through the shallow (-55 to -92 m NAP) and deep (-98 to -150 m NAP) well screen, respectively. In the third scenario, water is simultaneously pumped at a rate of 50 m^3/h through both screens. The scenarios 4 and 5 are similar to the first two scenarios, but a constant pumping rate of 100 m^3/h is used. The scenario results demonstrate that the pilot wells can reduce the brackish upconing below the Horstermeer Polder. The shallow well water has a lower chloride concentration than the deep well water. However, the concentration in the shallow well water increased over time, whereas the concentration of the deep well water decreased. Moreover, the shallow well led to a slightly higher reduction of the salt load and chloride concentration in the surface waters of the Horstermeer Polder when compared to the deep well. This is emphasised by the fact that the most considerable reduction in chloride concentration occurs just above the well screen since mixing will reduce the effect. In general, the pilot well decreased the chloride load discharged out of the Horstermeer Polder with ± 3% in scenarios 1 and 2 and with ± 5% in the other scenarios when compared to the baseline scenario. This reduction is beneficial as it indicates that with the help of a well field, the chloride load discharged by the polder can be reduced. Like the effect on the chloride concentration, the shallow well has a slightly higher reduction of the flux, although in all scenarios the reduction is limited between 0.8 and 1.7%. However, with the currently modelled effects, 24 shallow wells with a constant pumping rate of 100 m^3/h might be needed to achieve a chloride concentration of 250 mg/l in the discharged water. Moreover, the well causes considerable drawdown. In all scenarios, the simulated drawdown can reach up to 4 cm at surface level, which is considerable since (1) the wooden pile foundations in the Horstermeer polder are susceptible to rot and (2) a drawdown of 5 cm requires compensation due to drought damage in the Netherlands. The effect on the hydraulic head below the deep clay layer is negligible, and wells with the simulated operational settings will most likely not lead to flux over the clay layer.

All in all, this research showed the slight reducing effects on the brackish seepage below the Horstermeer Polder by extracting the brackish groundwater. However, more research on the effects of multiple wells with higher pumping rates is needed to determine whether the taming of the brackish seepage below the Horstermeer Polder is feasible.

9

Recommendations

Following this research, some recommendations can be made to improve the model performance. These recommendations are focused on the improvement of the model itself and on additional measurements that could improve the initial input data of the model, the model performance, or the estimation of the effects of a well field. This chapter will start with the latter, and end with the recommendations for the modelling process.

9.1. Measurements

The model's input can significantly be improved by establishing an initial chloride distribution based on airborne electromagnetic measurements. Moreover, the shape of the upconing is highly influenced by the vertical hydraulic conductivity (K_v) of the Holocene complex. In other words, the model performance will improve by classifying the top layer within the Horstermeer Polder to a higher degree. These recommendations will be elaborated upon below. Lastly, the simulated effect of the pilot wells should be tested in practice by measuring the drawdown and the movement of the fresh-brackish interface during pumping tests.

9.1.1. Airborne Electromagnetic Measurements

The spatial distribution of the chloride concentration in the model area, estimated by the NHI fresh-saline model, does not correspond with the measurements within the Horstermeer Polder [62]. Hence, the model needed to be run for 450 years to achieve a stable solution of the chloride distribution. Faneca Sànchez *et al.* [103] proved that with the help of airborne EM measurements, it is possible to establish a 3D chloride distribution. This estimated spatial distribution took only fifteen years to reach a stable solution. Hence, the model's run time can significantly be reduced by using a spatial distribution of the chloride concentration that corresponds with the current situation and measurements. In the study, helicopter FDEM (HEM) measurements were combined with helicopter TDEM (SkyTEM) measurements. The first is applicable in the shallow subsurface (about 1–100 m), whereas the latter can measure well between 10 to 400 m below the surface level [104]. Hence, whenever chloride is expected to be present in the shallow subsurface, HEM should be applied, whereas in all other cases, TDEM provides more information. Airborne measurements are preferred over regular TDEM and FDEM measurements because large areas can be measured quickly [30].

To reduce the model's run time and better represent the spatial distribution of the chloride concentration in the Horstermeer Polder and its surroundings, it is therefore recommended to perform HEM and SkyTEM measurements. Since these measurements are only useful whenever chloride is present in the subsurface, Figure 9.1 depicts where it is recommended to perform airborne EM measurement. It can be seen that the recommendation would be to measure in the northwestern part of the model area, of which the groundwater has been proven to be brackish. In a smaller area, it is moreover recommended to perform HEM measurements as the current model simulates the

interface to be in the shallow subsurface.

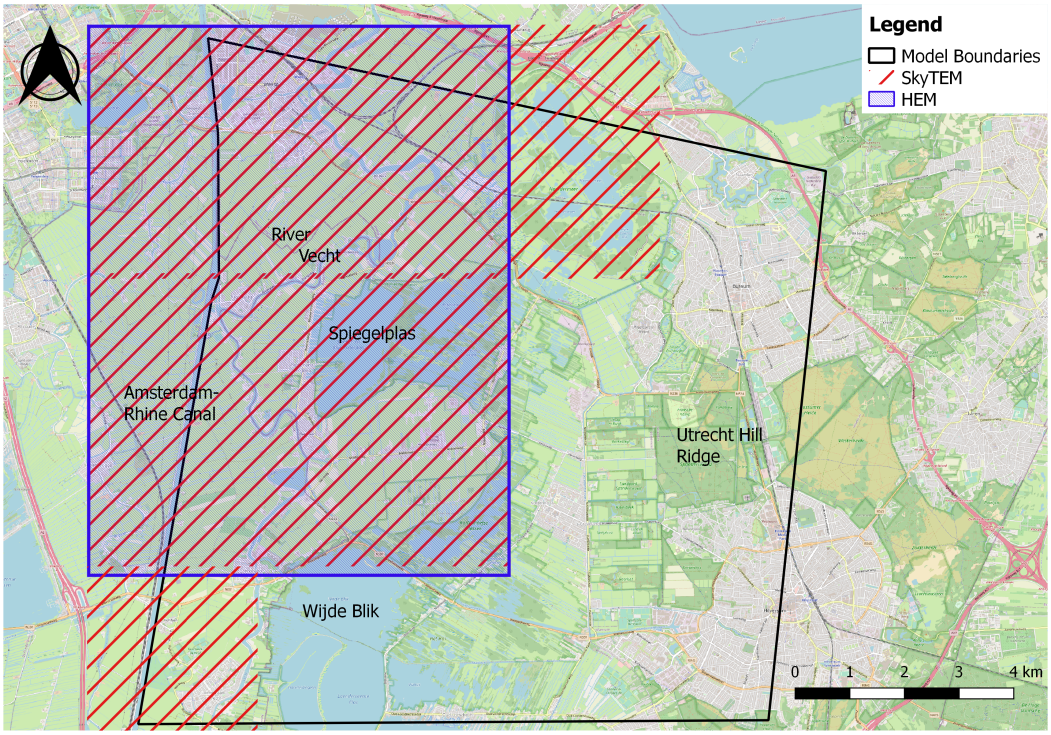

Figure 9.1: Indication of the areas in which it is recommended to perform HEM measurements (blue) and SkyTEM measurements (red).

Besides determining the spatial distribution of the chloride concentration, airborne electromagnetic measurements can be used to identify clay layers. This is because electrical conductivity also depends on clay content [104]. Since the clay layer of the Waalre Formation influences the flow path of the brackish groundwater to the shallow subsurface, it is helpful to check its representation within REGIS II with the field situation, especially below the Horstermeer Polder. Thus, these airborne measurements are very useful to improve the model.

9.1.2. Classification Top Layer

The vertical hydraulic conductivity (K_v) of the top layer appeared to be very influential on the model outcome. Not only does it influence the flow paths and the total seepage flux, but it also largely determines the shape of the upconing at the surface level. The vertical hydraulic conductivity was calibrated in this model based on the classification of the top layer. However, the degree of classification was lower compared to the original BRO Bodemkaart 2018. Moreover, the estimated K_v was not based on measurements. To improve the model outcome it is therefore recommended to increase the level of detail of the classification of the top layer. The BRO Bodemkaart 2018 is a result of interpolation of 340,000 drillings. Hence, it would be better to check the classification of the Bodemkaart. This is especially important in the north west of the polder, characterised by a very local clay area. It is hypothesised that this clayey area affects the fresh-brackish interface in the shallow subsurface of the polder and hence causes the notch in the measured interface.

Moreover, it would be beneficial to measure the K_v of the different top layer types to better estimate the K_v of these types. This can be done by taking sediment columns by applying the direct-push technique, which preserves the structures in the sediment. On those columns a permeameter test can be performed in the laboratory [105]. This method is less expensive than a pumping test [105] and hence recommended here.

9.1.3. Pumping Tests

Since models are only a simplified version of the field conditions, it is crucial to check whether the simulated effects also occur in practice. As said before, the used grid-cell size is too coarse to visualise the local drawdown close to the well. Therefore, it is recommended to perform pumping tests for both the shallow and the deep well. During a pumping test, the head is monitored at the well and in the observation well close by while the well pumps large quantities of water [19]. It is recommended to pump for longer periods at the time at a constant rate to test the long-term effects. This is especially important since the wells will be pumping at a constant rate to suppress the brackish seepage.

Furthermore, during these pumping tests, the hydraulic conductivity and the storage parameters of the aquifer can be determined, which can be used to improve the input data of the model [19, 105]. Especially, early-time drawdown data is needed to determine these storage parameters more precisely [106]. These storage parameters and the aquifer's transmissivity can not directly be calculated from the pumping test, but log-log curve matching can be used to determine these parameters[19]. However, since the determined data applies mostly to the proximity of the well and to a lesser degree to the region at the observation well [19], the direct-push techniques explained in the section above are still needed in the remainder of the polder.

Lastly, it is recommended to determine the effect of the pilot wells on the salinity distribution. Hence, the chloride concentration in the well water should be determined and the Electrical Conductivity (EC) of the groundwater in the near vicinity of the well should be measured during the pumping tests. Since it is essential to test the decrease of the chloride concentration in the shallow subsurface, the EC measurements are recommended till a depth of -10 m NAP. In other words, the chloride concentration should be measured in the first sand layer below the confining top layer. By doing so, rainwater will probably have an insignificant influence on the chloride concentration.

9.2. Modelling

Besides additional measurements, the model itself can be improved. The most important improvements in sequential order are the inclusion of tile drainage in the model, a better representation of the model boundaries, grid refinement within the Horstermeer Polder and sensitivity analysis, and a more thorough calibration procedure. The inclusion of tile drainage is the least time-consuming and is expected to improve the model outcome as it might prevent the formation of the rainwater lenses in the Horstermeer Polder and increases the drained area. A better representation of the model boundaries will, however, have the most significant impact on the model. It has been proven in this research that the used representation overestimates the heads below the polder and hence underestimates the flux towards the polder. Grid refinement is recommended if the objective of the follow-up research is to determine the drawdown and change in chloride concentration in more detail. Lastly, sensitivity analysis is an essential step as it determines the uncertainty of the model results, which is important for decision-makers, and a more thorough calibration procedure will improve the model performance. The improved model can then be used to determine the effects of multiple wells on the brackish seepage in the Horstermeer Polder.

9.2.1. Tile Drainage

At many locations within the model area, tile drainage is used [100]. This type of drainage is installed in the subsurface to remove excess water from the soil. In other words, the drainage level in these areas is the depth at which the tile-drainage system is installed in case the system is installed above the phreatic surface or the controlled surface water level in the polder. Hence, replacing the overland-flow drainage data set in the model with a tile-drainage data set is recommended. It would be best to check the data set with practice to ensure that the data set is correct. It is expected that this will increase the drainage flux in the Horstermeer Polder, but also the area west of 's Gravelandsche Polder and the oval area north of 's Gravelandsche Polder (area 4250 in Figure 5.15). The overland-

flow drainage data set is unrealistic since constant overland flow over a year is highly improbable.

9.2.2. Model Boundaries

The model boundaries in this research are based on the outcome of the Regional Groundwater Model of Waternet with a correction for the negligence of variable-density effect based on the head measurements in DINOloket. However, this estimate resulted in a circulation of groundwater that entered the model area at the bottom of the Peize-Waalre Formation and left the model area again a few meters higher. Therefore, hydrostatic boundary conditions were used. Hydrostatic heads are, however, not in good agreement with the field conditions. Thus, it is recommended to use different model boundaries.

The best way to create new model boundaries would be to create a low-resolution model with a model area considerably larger than the model area in this research. The North Sea could be the west boundary, and the IJsselmeer the north boundary to have easily definable model boundaries. The Utrecht Hill Ridge acts as a watershed delineation feature, and hence the highest locations of the ridge can be used as a boundary in the east. The southern boundary is less of interest as it appeared that almost no water is coming for the south towards the polder (Figure 5.7). The low-resolution model should simulate variable-density flow to have correct point-water head estimates, and the main features in the area should be taken into account. Moreover, he model must correspond relatively well with the chloride and head measurements. The results of this model can then be used as input for the model boundaries of the model in this research. The use of such a model will result in a better representation of the field conditions, and hence it is expected that the deviation of the flux towards the Horstermeer Polder will decrease.

9.2.3. Grid Refinement

The current grid resolution is not able to describe the very local effects of the pumping of the well. Since there is a legal limit at which drought damage compensation should be paid, which is only 1 cm higher than the currently calculated drawdown [99], it is recommended to use a higher resolution model to determine the drawdown at the surface level more accurately. However, since the computational cost of a high-resolution model is high, it is recommended to use local-grid refinement. Such an unstructured grid is supported in MODFLOW 6 but requires the replacement of the DIS-Package with a DISV-Package [89]. This package is also included in NLMOD, which simplifies the transition from the DIS towards the DISV-Package. However, the algorithm to determine the chloride concentration based on the modified NHI fresh-saline model has to be adapted.

9.2.4. Sensitivity Analysis and Calibration

Since this model was only calibrated on one parameter using a trial-and-error method, the calibration procedure can be improved by automated calibration based on hydraulic head measurements, chloride measurements and the water balance. However, these automated calibration methods are high in computational cost [80]. Therefore, before an automated calibration can be performed, sensitivity analyses should be performed to choose the parameters that should be changed in the process effectively. This is because the number of parameters in this model is high and because some parameters are space-dependent, e.g. hydraulic conductivity, bottom resistance, and depth of the surface waters. As a result, calibration is difficult and time-consuming [107].

Based on the experience gained from this research special, the main focus input data sets during calibration should be the vertical hydraulic conductivity of the top layer and the maximum occurring chloride concentration if the modified NHI data set is used. Since the model's run time is 32 minutes, a limited range of values should be used, which can be determined with the help of the measurements explained in Section 9.1.2. The best way to calibrate the model would be to include all head measurements in the model area, the measurements of the chloride concentration, and preferably the water balances of the polders. Automated calibration can be performed with the

help of PEST software. PEST software can calibrate the model and determine the uncertainty of the model parameters and predictions [107]. This is beneficial since a model will always be a simplified version of the field conditions and hence cannot simulate these perfectly. Therefore, the justification of using a model increases once the uncertainty of the predictions is known [107]. Since this model is used to simulate the effect of wells on the saline upconing and can be used to design a well field, the uncertainty of the model predictions is an critical characteristic for decision-makers.

References

[1] E. Parizi, S. M. Hosseini, B. Ataie-Ashtiani, and C. T. Simmons, *Vulnerability mapping of coastal aquifers to seawater intrusion: Review, development and application,* Journal of Hydrology **570**, 555 (2019).

[2] B. Neumann, A. T. Vafeidis, J. Zimmermann, and R. J. Nicholls, *Future Coastal Population Growth and Exposure to Sea-Level Rise and Coastal Flooding - A Global Assessment,* PLOS ONE **10**, e0118571 (2015), publisher: Public Library of Science.

[3] A. D. Werner, M. Bakker, V. E. A. Post, A. Vandenbohede, C. Lu, B. Ataie-Ashtiani, C. T. Simmons, and D. A. Barry, *Seawater intrusion processes, investigation and management: Recent advances and future challenges,* Advances in Water Resources 35th Year Anniversary Issue, **51**, 3 (2013).

[4] V. Post and E. Abarca, *Preface: Saltwater and freshwater interactions in coastal aquifers,* Hydrogeology Journal **18**, 1 (2010).

[5] P. G. B. De Louw, G. H. P. Oude Essink, P. J. Stuyfzand, and S. E. A. T. M. Van der Zee, *Upward groundwater flow in boils as the dominant mechanism of salinization in deep polders, The Netherlands,* Journal of Hydrology **394**, 494 (2010).

[6] M. Mirzavand, H. Ghasemieh, S. J. Sadatinejad, and R. Bagheri, *An overview on source, mechanism and investigation approaches in groundwater salinization studies,* International Journal of Environmental Science and Technology **17**, 2463 (2020).

[7] World Health Organization, *Guidelines for drinking-water quality*, 4th ed. (World Health Organization, Geneva, 2011) oCLC: ocn744951652.

[8] G. H. P. Oude Essink, E. S. Van Baaren, and P. G. B. De Louw, *Effects of climate change on coastal groundwater systems: A modeling study in the Netherlands,* Water Resources Research **46** (2010), 10.1029/2009WR008719, _eprint: https://agupubs.onlinelibrary.wiley.com/doi/pdf/10.1029/2009WR008719.

[9] P. G. B. De Louw, S. Eeman, B. Siemon, B. R. Voortman, J. Gunnink, E. S. Van Baaren, and G. H. P. Oude Essink, *Shallow rainwater lenses in deltaic areas with saline seepage,* Hydrology and Earth System Sciences **15**, 3659 (2011), publisher: Copernicus GmbH.

[10] J. R. Delsman, K. R. M. Hu-a ng, P. C. Vos, P. G. B. De Louw, G. H. P. Oude Essink, P. J. Stuyfzand, and M. F. P. Bierkens, *Paleo-modeling of coastal saltwater intrusion during the Holocene: an application to the Netherlands,* Hydrology and Earth System Sciences **18**, 3891 (2014).

[11] I. Van Wielink, *Karteren en Modelleren van het Zoet-Brak Grondwatersysteem in de Horstermeer*, Master's thesis, Vrije Universiteit Amsterdam, Amsterdam (2016).

[12] M. Fakhari, *Saline Water Upconing Modelling in the Horstermeer Polder Area*, Master's thesis, UNESCO-IHE, Delft (2018).

[13] F. Smits and L. Smulders, *Pilot Temmen van Brakke Kwel - eerste resultaten van de eerste boring [Presentation]* (Waternet, Amsterdam, 2019).

[14] S. Y. Philip, S. F. Kew, K. v. d. Wiel, N. Wanders, and G. J. v. Oldenborgh, *Regional differentiation in climate change induced drought trends in the Netherlands,* Environmental Research Letters **15**, 094081 (2020), publisher: IOP Publishing.

[15] P. A. C. Raats, *Salinity management in the coastal region of the Netherlands: A historical perspective,* Agricultural Water Management The Jim Oster Special Issue, **157**, 12 (2015).

[16] M. Bonte and J. J. G. Zwolsman, *Climate change induced salinisation of artificial lakes in the Netherlands and consequences for drinking water production,* Water Research **44**, 4411 (2010).

[17] L. Bos-Burgering, S. Buijs, I. America, J. Klooster, P. G. B. De Louw, S. Stofberg, K. Raat, R. Franssen, and J. Posma, *COASTAR Nationaal. Regionale en nationale opschaling COASTAR toepassingen,* , 132 (2021).

[18] A. Jain, H. Dannak, J. Montoya, N. Kwarkye, and F. Smits, *Delineation of fresh-brackish water interface in the Horstermeerpolder, the Netherlands*, Internship Report, IHE Delft Institute for Water Education, Amsterdam (2020).

[19] C. R. Fitts, *Groundwater Science* (Elsevier, 2002) google-Books-ID: Nr7gmSD4N4UC.

[20] V. Post, H. Kooi, and C. Simmons, *Using Hydraulic Head Measurements in Variable-Density Ground Water Flow Analyses,* Groundwater **45**, 664 (2007), _eprint: https://ngwa.onlinelibrary.wiley.com/doi/pdf/10.1111/j.1745-6584.2007.00339.x.

[21] D. A. Nield and A. Bejan, *Convection in Porous Media* (Springer New York, New York, NY, 2013).

[22] C. D. Langevin, S. Panday, and A. M. Provost, *Hydraulic-Head Formulation for Density-Dependent Flow and Transport,* Groundwater **58**, 349 (2020), _eprint: https://ngwa.onlinelibrary.wiley.com/doi/pdf/10.1111/gwat.12967.

[23] J. Jiao and V. Post, *Coastal Hydrogeology* (Cambridge University Press, 2019) google-Books-ID: 5oKWDwAAQBAJ.

[24] X. Mao, H. Prommer, D. A. Barry, C. D. Langevin, B. Panteleit, and L. Li, *Three-dimensional model for multi-component reactive transport with variable density groundwater flow,* Environmental Modelling & Software **21**, 615 (2006).

[25] L. F. Konikow, D. J. Goode, and G. Z. Hornberger, *A Three-dimensional Method-of-characteristics Solute- Transport Model (MOC3D)* (U.S. Department of the Interior, U.S. Geological Survey, 1996) google-Books-ID: BJZPAQAAMAAJ.

[26] V. Post, H. Van der Plicht, and H. Meijer, *The origin of brackish and saline groundwater in the coastal area of the Netherlands,* Netherlands Journal of Geosciences **82**, 133 (2003).

[27] J. C. Van Dam and J. J. Meulenkamp, *Some Results of the Geo-Electrical Resistivity Method in Ground Water Investigations in the Netherlands*,* Geophysical Prospecting **15**, 92 (1967), _eprint: https://onlinelibrary.wiley.com/doi/pdf/10.1111/j.1365-2478.1967.tb01775.x.

[28] M. Hayashi, *Temperature-Electrical Conductivity Relation of Water for Environmental Monitoring and Geophysical Data Inversion,* Environmental Monitoring and Assessment **96**, 119 (2004).

[29] J. G. Paine, *Determining salinization extent, identifying salinity sources, and estimating chloride mass using surface, borehole, and airborne electromagnetic induction methods,* Water Resources Research **39** (2003), https://doi.org/10.1029/2001WR000710, _eprint: https://agupubs.onlinelibrary.wiley.com/doi/pdf/10.1029/2001WR000710.

[30] K. I. Sørense and E. Auken, *SkyTEM? A new high-resolution helicopter transient electromagnetic system,* Exploration Geophysics **35**, 194 (2004), publisher: CSIRO PUBLISHING.

[31] S. Park, S. Shin, D. Lee, C. Kim, and J. Son, *Relationship between Electrical Resistivity and Physical Properties of Rocks,* (Barcelona, Spain, 2016).

[32] R. Wagner, R. Boulger, C. Oblinger, and B. Smith, *Guidelines and Standard Procedures for Continuous Water-Quality Monitors: Station Operation, Record Computation, and Data Reporting* (2006).

[33] USGS MODFLOW Team, *MODFLOW and Related Programs* (2020) https://www.usgs.gov/mission-areas/water-resources/science/modflow-and-related-programs?qt-science_center_objects=0#qt-science_center_objects, Accessed: 15-12-2020.

[34] M. Bakker, *A Dupuit formulation for modeling seawater intrusion in regional aquifer systems,* Water Resources Research **39** (2003), 10.1029/2002WR001710, _eprint: https://agupubs.onlinelibrary.wiley.com/doi/pdf/10.1029/2002WR001710.

[35] J. Beaujean, F. Nguyen, A. Kemna, A. Antonsson, and P. Engesgaard, *Calibration of seawater intrusion models: Inverse parameter estimation using surface electrical resistivity tomography and borehole data,* Water Resources Research **50**, 6828 (2014), _eprint: https://agupubs.onlinelibrary.wiley.com/doi/pdf/10.1002/2013WR014020.

[36] M. Bonte and A. Biesheuvel, *The application of the SEAWAT variable density code for the Lake Wieringen project, the Netherlands,* , 9 (2006).

[37] A. M. Dausman, C. Langevin, M. Bakker, and F. Schaars, *A comparison between SWI and SEAWAT – the importance of dispersion, inversion and vertical anisotropy,* , 4 (2010).

[38] T. Feseker, *Numerical studies on saltwater intrusion in a coastal aquifer in northwestern Germany,* Hydrogeology Journal **15**, 267 (2007).

[39] C. Llopis-Albert and D. Pulido-Velazquez, *Discussion about the validity of sharp-interface models to deal with seawater intrusion in coastal aquifers,* Hydrological Processes **28**, 3642 (2014), _eprint: https://onlinelibrary.wiley.com/doi/pdf/10.1002/hyp.9908.

[40] H. A. Michael, C. J. Russoniello, and L. A. Byron, *Global assessment of vulnerability to sea-level rise in topography-limited and recharge-limited coastal groundwater systems,* Water Resources Research **49**, 2228 (2013), _eprint: https://agupubs.onlinelibrary.wiley.com/doi/pdf/10.1002/wrcr.20213.

[41] H. Shishaye, *Groundwater Flow Modeling in Coastal Aquifers: The Influence of Submarine Groundwater Discharge on the Position of the Saltwater-Freshwater Interface,* Journal of Coastal Zone Management **19** (2016), 10.4172/2473-3350.1000419.

[42] A. Szymkiewicz, A. Gumuła-Kawęcka, J. Šimůnek, B. Leterme, S. Beegum, B. Jaworska-Szulc, M. Pruszkowska-Caceres, W. Gorczewska-Langner, R. Angulo-Jaramillo, and D. Jacques, *Simulations of freshwater lens recharge and salt/freshwater interfaces using the HYDRUS and SWI2 packages for MODFLOW,* Journal of Hydrology and Hydromechanics **66**, 246 (2018).

[43] T. Laattoe, A. D. Werner, and C. T. Simmons, *Seawater Intrusion Under Current Sea-Level Rise: Processes Accompanying Coastline Transgression,* in *Groundwater in the Coastal Zones of Asia-Pacific*, Coastal Research Library, edited by C. Wetzelhuetter (Springer Netherlands, Dordrecht, 2013) pp. 295–313.

[44] E. Luijendijk, T. Gleeson, and N. Moosdorf, *Fresh groundwater discharge insignificant for the world's oceans but important for coastal ecosystems,* Nature Communications **11**, 1260 (2020), number: 1 Publisher: Nature Publishing Group.

[45] L. K. Morgan, A. D. Werner, and C. T. Simmons, *On the interpretation of coastal aquifer water level trends and water balances: A precautionary note,* Journal of Hydrology **470-471**, 280 (2012).

[46] A. Vandenbohede, E. Van Houtte, and L. Lebbe, *Groundwater flow in the vicinity of two artificial recharge ponds in the Belgian coastal dunes,* Hydrogeology Journal **16**, 1669 (2008).

[47] T. A. Watson, A. D. Werner, and C. T. Simmons, *Transience of seawater intrusion in response to sea level rise,* Water Resources Research **46** (2010), 10.1029/2010WR009564, _eprint: https://agupubs.onlinelibrary.wiley.com/doi/pdf/10.1029/2010WR009564.

[48] M. D. Webb and K. W. F. Howard, *Modeling the Transient Response of Saline Intrusion to Rising Sea-Levels,* Groundwater **49**, 560 (2011), _eprint: https://ngwa.onlinelibrary.wiley.com/doi/pdf/10.1111/j.1745-6584.2010.00758.x.

[49] C. D. Langevin, J. D. Hughes, E. R. Banta, A. Provost, R. G. Niswonger, and S. Panday, *MODFLOW 6 Modular Hydrologic Model version 6.2.0: U.S. Geological Survey Software Release,*

[50] J. D. Hughes, C. D. Langevin, and E. R. Banta, *Documentation for the MODFLOW 6 Framework*, U.S. Geological Survey Techniques and Methods, Vol. A57 (2017).

[51] C. D. Langevin and D. Brakenhoff, *Github MODFLOW-USGS/modflow 6 Issues: Model with transport+density running on Linux but not on Windows,* GitHub (2021), https://github.com/MODFLOW-USGS/modflow6, Accessed: 08-03-2021.

[52] H.-E. Reineck and I. B. Singh, *Depositional Sedimentary Environments: With Reference to Terrigenous Clastics* (Springer Science & Business Media, 2012).

[53] H. Ortner, A. Kositz, E. Willingshofer, and D. Sokoutis, *Geometry of growth strata in a transpressive fold belt in field and analogue model: Gosau Group at Muttekopf, Northern Calcareous Alps, Austria,* Basin Research **28** (2015), 10.1111/bre.12129.

[54] C. D. Langevin, *Github: HUF package support · Issue #27 · modflowpy/flopy,* GitHub (2017), https://github.com/modflowpy/flopy/issues/27. Accessed: 7-4-2021.

[55] TNO Geologische Dienst Nederland, *DINOloket,* (2020), https://www.dinoloket.nl/. Accessed: 2020-11-12.

[56] F. J. Van der Linden and C. A. J. Appello, *Hydrochemie en Herkomst van Zout Kwelwater in de Horstermeerpolder,* H20 **22**, 71 (1988).

[57] L. v. Liere, R. M. M. Roijackers, and P. J. T. Verstraelen, eds., *Integraal waterbeheer in het Gooi/Utrechts stuwwallen- en plassengebied*, Rapporten en nota's No. 22 (Commissie voor Hydrologisch Onderzoek, 's-Gravenhage, 1989) oCLC: 46102315.

[58] A. B. Pomper, *De gevolgen van de uitvoering van de verbeteringswerken van het Amsterdam-Rijnkanaal in het kanaalgedeelte tussen Utrecht en Amsterdam op de hydrologie van de aangrenzende polders*, Nota 841 (Instituut voor Cultuurtechniek en Waterhuishouding, Wageningen, 1975).

[59] J. G. R. Beemster and M. Ouboter, *Geohydrologisch onderzoek wellen langs ARK [Concept]*, Tech. Rep. (Waternet, Amsterdam, 2021).

[60] Naturalis, TNO Bouw en Ondergrond, and Koninklijk Nederlands Aardrijkskundig Genootschap, *Geologie van Nederland* (2020) https://www.geologievannederland.nl/. Accessed: 2020-11-11.

[61] J. Hummelman, D. Maljers, A. Menkovic, R. Reindersma, R. Vernes, and J. Stafleu, *Totstandkomingsrapport Hydrogeologisch Model (REGIS II)*, TNO-rapport TNO 2019 R11654 (TNO, Utrecht, 2019).

[62] J. R. Delsman, G. H. P. Oude Essink, S. Huizer, H. Bootsma, T. Mulder, P. Zitman, R. Verastegui, and G. Janssen, *Actualisatie zout in het NHI- Toolbox NHI zoet-zout modellering en landelijk model*, Tech. Rep. 1205261-003-BGS-0001 (Deltares, Utrecht, 2020).

[63] H. Weerts, P. Cleveringa, and M. Gouw, *De Vecht/Angstel, een riviersysteem in het veen,* Grondboor & Hamer **3/4**, 6 (2002).

[64] C. De Bont, *Vergeten Land; ontginning, bewoning en waterbeheer in de West-Nederlandse veengebieden*, PhD, Wageningen University & Research, Wageningen (2008).

[65] S. Hooghoudt, *Rapport Betreffende de Verrichte Onderzoekingen in de Horstermeer Polder*, Tech. Rep. (Landbouw proefstation en bodemkundig Instituut, Groningen, 1947).

[66] J. Jansen, J. Baar, K. Scherpenhuijsen, G. Baar, and M. Stevens, *Themanummer: 40 jaar zandwinning in Nederhorst Den Berg,* Historische Kring Nederhorst Den Berg **3**, 43 (1991).

[67] B. F. Des Tombe, M. Bakker, F. Smits, F. Schaars, and K.-J. Van der Made, *Estimation of the Variation in Specific Discharge Over Large Depth Using Distributed Temperature Sensing (DTS) Measurements of the Heat Pulse Response,* Water Resources Research **55**, 811 (2019), _eprint: https://agupubs.onlinelibrary.wiley.com/doi/pdf/10.1029/2018WR024171.

[68] J. Hartmann and N. Moosdorf, *The new global lithological map database GLiM: A representation of rock properties at the Earth surface,* Geochemistry, Geophysics, Geosystems **13** (2012), 10.1029/2012GC004370, _eprint: https://agupubs.onlinelibrary.wiley.com/doi/pdf/10.1029/2012GC004370.

[69] J. Stafleu, D. Maljers, F. Busschers, J. Gunnink, J. Schokker, and J. Hummelman, *Totstandkomingsrapport GeoTOP*, TNO-rapport TNO 2019 R11655 (TNO, Utrecht, 2019) https://www.dinoloket.nl/sites/default/files/docs/geotop/R11655%20Totstandkomingsrapport%20GeoTOP.pdf.

[70] E. Custodio and G. A. Bruggeman, *Groundwater problems in coastal areas: a contribution to the International Hydrological Programme*, Studies and reports in hydrology No. 45 (Unesco, Paris, 1987).

[71] M. J. Wassen, A. Barendregt, P. P. Schot, and B. Beltman, *Dependency of local mesotrophic fens on a regional groundwater flow system in a poldered river plain in the Netherlands,* Landscape Ecology **5**, 21 (1990).

[72] F. Claessen, J. Van de Wijer, and E. Kasemier, *Evaluatie grondwatermeetnet van Oostelijk en Zuidelijk Flevoland en het aangrenzende oude land*, Nota 88.047 (Rijkswaterstaat, Lelystad, 1989).

[73] M. Bakker, *Lecture Notes CIE4420 Principles of Geohydrology* (Delft University of Technology, 2019).

[74] M. Bakker, V. E. A. Post, C. D. Langevin, J. D. Hughes, J. T. White, A. T. Leaf, S. R. Paulinski, J. D. Larsen, M. W. Toews, E. D. Morway, J. C. Bellino, J. J. Starn, and M. N. Fienen, *FloPy v3.3.4,* (2021),

[75] O. Ebbens and D. Brakenhoff, *NLMOD (under-development)*, Tech. Rep. v0.0.1b (Artesia Water, 2021) artesia Water. Version: April 2021.

[76] Nationaal Hydrologisch Instrumentarium - NHI, *Deelrapport Ondergrond*, Modelrapportage NHI\FASE_1+\2008\DR1\v1 (2008).

[77] J. G. R. Beemster, *Grondwatermodellering Horstermeerpolder en Meeruiterdijkse polder*, Tech. Rep. (Waternet, Amsterdam, 2012).

[78] G. Oude Essink, *Salinization of the Wieringermeerpolder, The Netherlands* (2002).

[79] D. Schnitzer, *Response of a fresh-brackish groundwater system to hydrological management in and around the Naardermeer wetland, the Netherlands*, Master's thesis (2010), accepted: 2010-10-28T17:00:33Z.

[80] J. Carrera, J. J. Hidalgo, L. J. Slooten, and E. Vázquez-Suñé, *Computational and conceptual issues in the calibration of seawater intrusion models,* Hydrogeology Journal **18**, 131 (2010).

[81] J. D. Hughes, C. D. Langevin, E. D. Morway, and M. W. Toews, *MODFLOW-USGS Modflow6-examples*, Tech. Rep. (U.S. Geological Survey, 2021) https://github.com/MODFLOW-USGS/modflow6-examples, Accessed: 13-04-2021.

[82] K. R. Rushton and L. M. Tomlinson, *Possible mechanisms for leakage between aquifers and rivers,* Journal of Hydrology **40**, 49 (1979).

[83] A. Black and H. Bootsma, *Github: Proposal: optional exfiltration conductance for RIV, GHB, LAK & SFR,* (2020), https://github.com/MODFLOW-USGS/modflow6/issues/419 Accessed: 22-04-2021.

[84] B. Wiese and G. Nützmann, *Transient Leakance and Infiltration Characteristics during Lake Bank Filtration,* Groundwater **47**, 57 (2009), _eprint: https://ngwa.onlinelibrary.wiley.com/doi/pdf/10.1111/j.1745-6584.2008.00510.x.

[85] J. R. Delsman, M. J. Waterloo, M. M. A. Groen, J. Groen, and P. J. Stuyfzand, *Investigating summer flow paths in a Dutch agricultural field using high frequency direct measurements,* Journal of Hydrology **519**, 3069 (2014).

[86] P. S. Pauw, S. E. A. T. M. Van der Zee, A. Leijnse, J. R. Delsman, P. G. B. De Louw, W. J. De Lange, and G. H. P. Oude Essink, *Low-Resolution Modeling of Dense Drainage Networks in Confining Layers,* Groundwater **53**, 771 (2015), _eprint: https://ngwa.onlinelibrary.wiley.com/doi/pdf/10.1111/gwat.12273.

[87] A. Di Ciacca, B. Leterme, E. Laloy, D. Jacques, and J. Vanderborght, *Scale-dependent parameterization of groundwater–surface water interactions in a regional hydrogeological model,* Journal of Hydrology **576**, 494 (2019).

[88] W. J. De Lange, *A Cauchy boundary condition for the lumped interaction between an arbitrary number of surface waters and a regional aquifer,* Journal of Hydrology **226**, 250 (1999).

[89] U.S. Department of the Interior and U.S. Geological Survey, eds., *MODFLOW 6 – Description of Input and Output*, Version mf6.2.0 (2020).

[90] S. A. Sakr, *Validity of a sharp-interface model in a confined coastal aquifer,* Hydrogeology Journal **7**, 155 (1999).

[91] D. Zijlema, *Lecture Notes CIE4340 Computational Modelling of Flow and Transport* (Delft University of Technology, Delft, 2020).

[92] J. W. Voort, *Waterbalansen Kortenhoef*, Tech. Rep. (Waternet, Amsterdam, 2017).

[93] J. Scibek, D. M. Allen, A. J. Cannon, and P. H. Whitfield, *Groundwater–surface water interaction under scenarios of climate change using a high-resolution transient groundwater model,* Journal of Hydrology **333**, 165 (2007).

[94] F. J. C. Smits, *Beschrijving van de werkzaamheden voor twee diepe boringen in de polder Horstermeer*, Tech. Rep. (Waternet, Amsterdam, 2020).

[95] J. G. R. Beemster, *Kwelkaart AGV - Regionaal Model* (Waternet, Amsterdam, 2010).

[96] F. J. C. Smits, *Dimensies winput pilot en indicatieve grondwaterstanden [E-mail],* (2021),

[97] M. A. J. Bakker and J. J. M. Van Der Meer, *Structure of a Pleistocene push moraine revealed by GPR: the eastern Veluwe Ridge, The Netherlands,* Geological Society, London, Special Publications **211**, 143 (2003).

[98] M. Swinkels and J. Hofstra, *Achtergrondrapport peilbesluit Horstermeerpolder en Meeruiterdijksepolder*, Tech. Rep. (Hoogheemraadschap Amstel, Gooi en Vecht, Amsterdam, 2014).

[99] AdviesCommissie Schade Grondwater, *Het invloedsgebied van grondwateronttrekkingen voor droogteschade*, Tech. Rep. (ACSG, Utrecht, 2019).

[100] H. Massop and C. Schuiling, *Buisdrainagekaart 2015 : update landelijke buisdrainagekaart op basis van de landbouwmeitellingen van 2012*, Tech. Rep. (Alterra, Wageningen, 2012).

[101] P. De Louw, Y. Van der Velde, and S. Van der Zee, *Quantifying water and salt fluxes in a lowland polder catchment dominated by boil seepage: A probabilistic end-member mixing approach,* Hydrology and Earth System Sciences Discussions **15** (2011), 10.5194/hess-15-2101-2011.

[102] V. E. A. Post, *Fresh and saline groundwater interaction in coastal aquifers: Is our technology ready for the problems ahead?* Hydrogeology Journal **13**, 120 (2005).

[103] M. Faneca Sànchez, J. L. Gunnink, E. S. Van Baaren, G. H. P. Oude Essink, B. Siemon, E. Auken, W. Elderhorst, and P. G. B. De Louw, *Modelling climate change effects on a Dutch coastal groundwater system using airborne electromagnetic measurements,* Hydrology and Earth System Sciences **16**, 4499 (2012).

[104] B. Siemon, A. V. Christiansen, and E. Auken, *A review of helicopter-borne electromagnetic methods for groundwater exploration,* Near Surface Geophysics **7**, 629 (2009), _eprint: https://onlinelibrary.wiley.com/doi/pdf/10.3997/1873-0604.2009043.

[105] C. Cheng and X. Chen, *Evaluation of methods for determination of hydraulic properties in an aquifer–aquitard system hydrologically connected to a river,* Hydrogeology Journal **15**, 669 (2007).

[106] X. Chen, J. Goeke, and S. Summerside, *Hydraulic Properties and Uncertainty Analysis for an Unconfined Alluvial Aquifer,* Groundwater **37**, 845 (1999), _eprint: https://ngwa.onlinelibrary.wiley.com/doi/pdf/10.1111/j.1745-6584.1999.tb01183.x.

[107] J. E. Doherty, R. J. Hunt, and M. J. Tonkin, *Approaches to highly parameterized inversion: A guide to using PEST for model-parameter and predictive-uncertainty analysis*, USGS Numbered Series 2010-5211 (U.S. Geological Survey, Reston, VA, 2010).

Appendices

A

Additional cross-sections within the Study Area Including the Chloride Measurements and Geology

This appendix contains the cross-sections over the depth in the whole research area. The chloride concentration measurements are retrieved from DINOloket [55], whereas the geology is based on REGIS II [61]. The names in the legend of the figure are equal to the names used in Table 3.1.

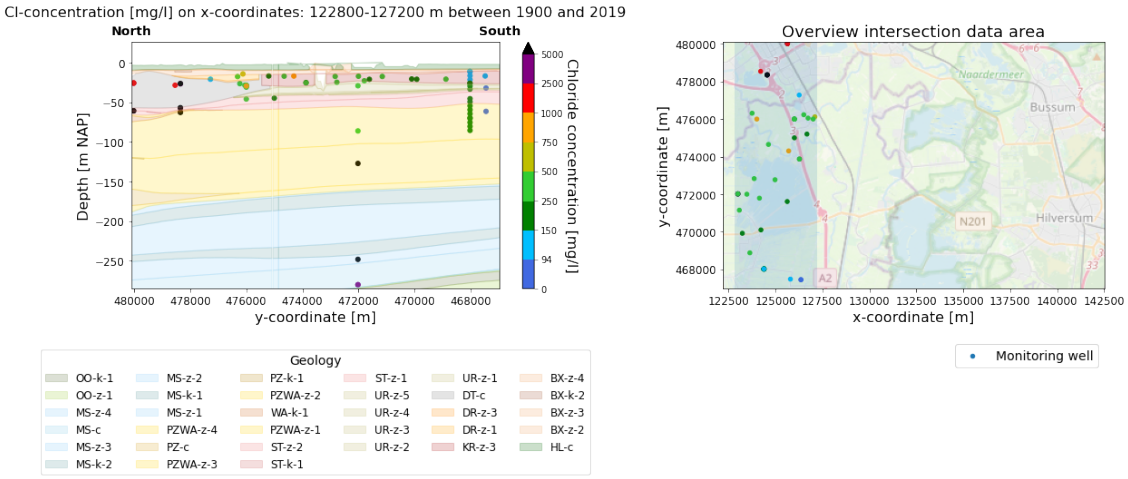

Figure A.1: Chloride concentration distribution over the depth from south to the north in the far west of the research area.

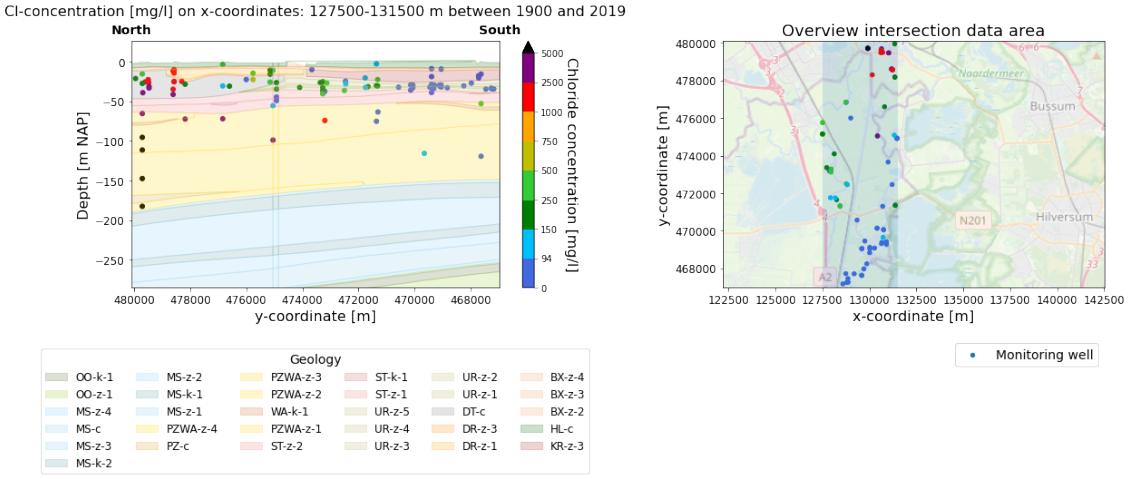

Figure A.2: Chloride concentration distribution over the depth from the south to the north in between Vinkeveense Plassen and the Horstermeer Polder.

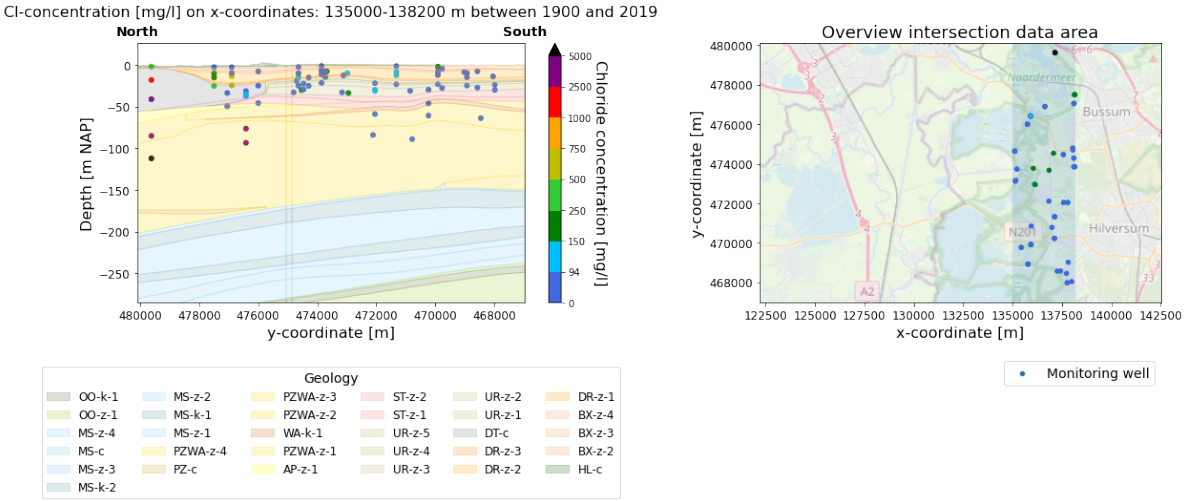

Figure A.3: Chloride concentration distribution over the depth from the south to the north directly east of the Horstermeer Polder.

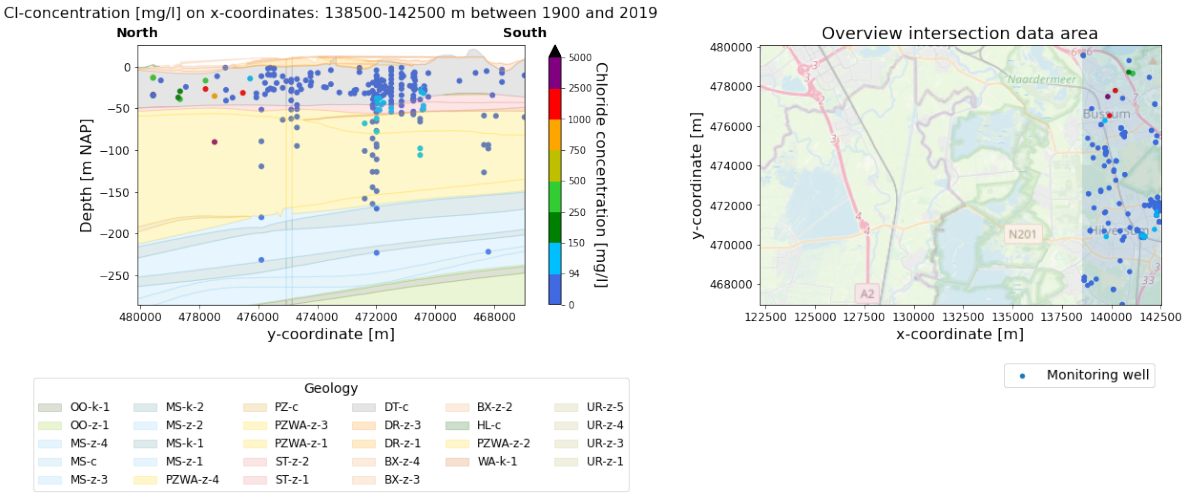

Figure A.4: Chloride concentration distribution over the depth from the south to the north in the far east of the research area.

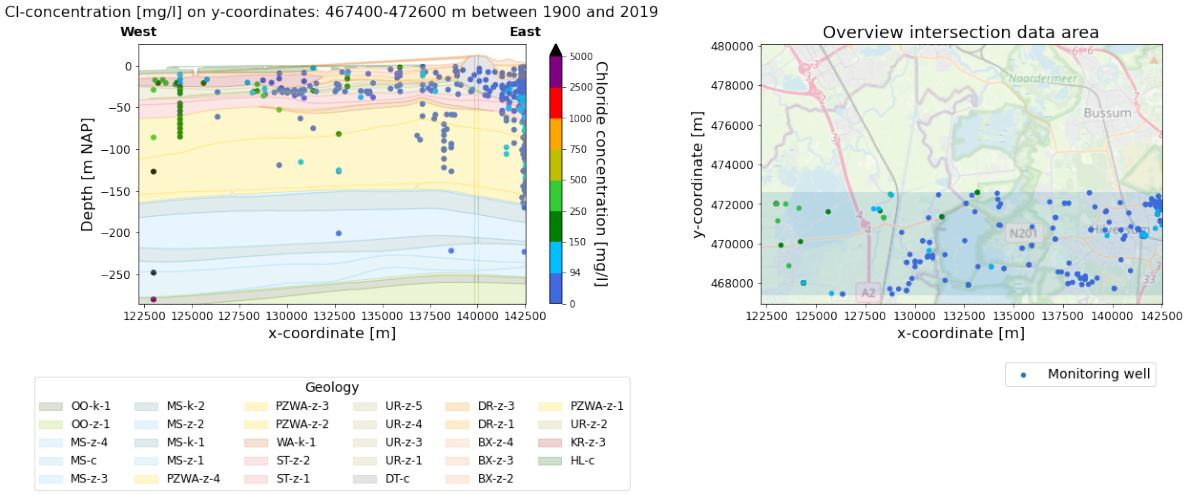

Figure A.5: Chloride concentration distribution over the depth from the west to the east in the south of the research area.

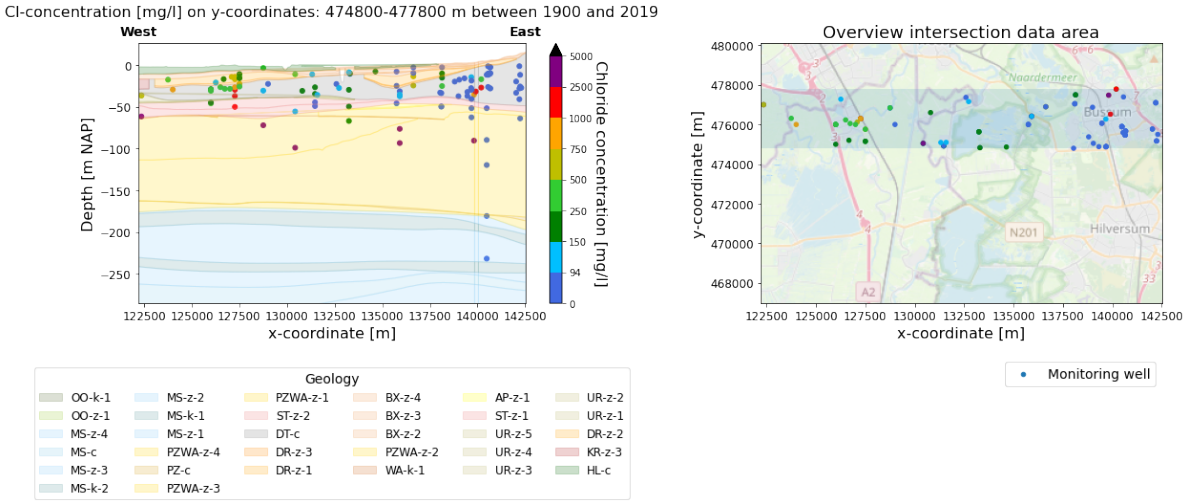

Figure A.6: Chloride concentration distribution over the depth from the west to the east directly north of the Horstermeer Polder.

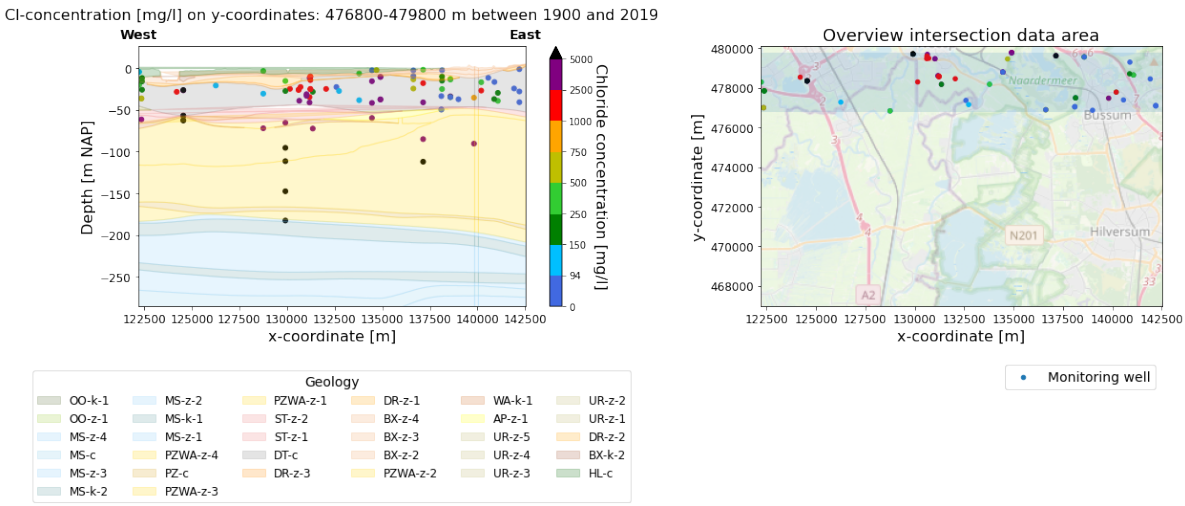

Figure A.7: Chloride concentration distribution over the depth from the west to the east in the far north of the research area.

B

Point-Water Head Distribution

In this appendix, an overview is given of all available point-water head measurements in DINOloket. Only a point-water head is given whenever at least in half of the years in the period 2000 to 2020 AD measurements were performed. Moreover, the Interquartile Range (IQR) is given for every measurement location.

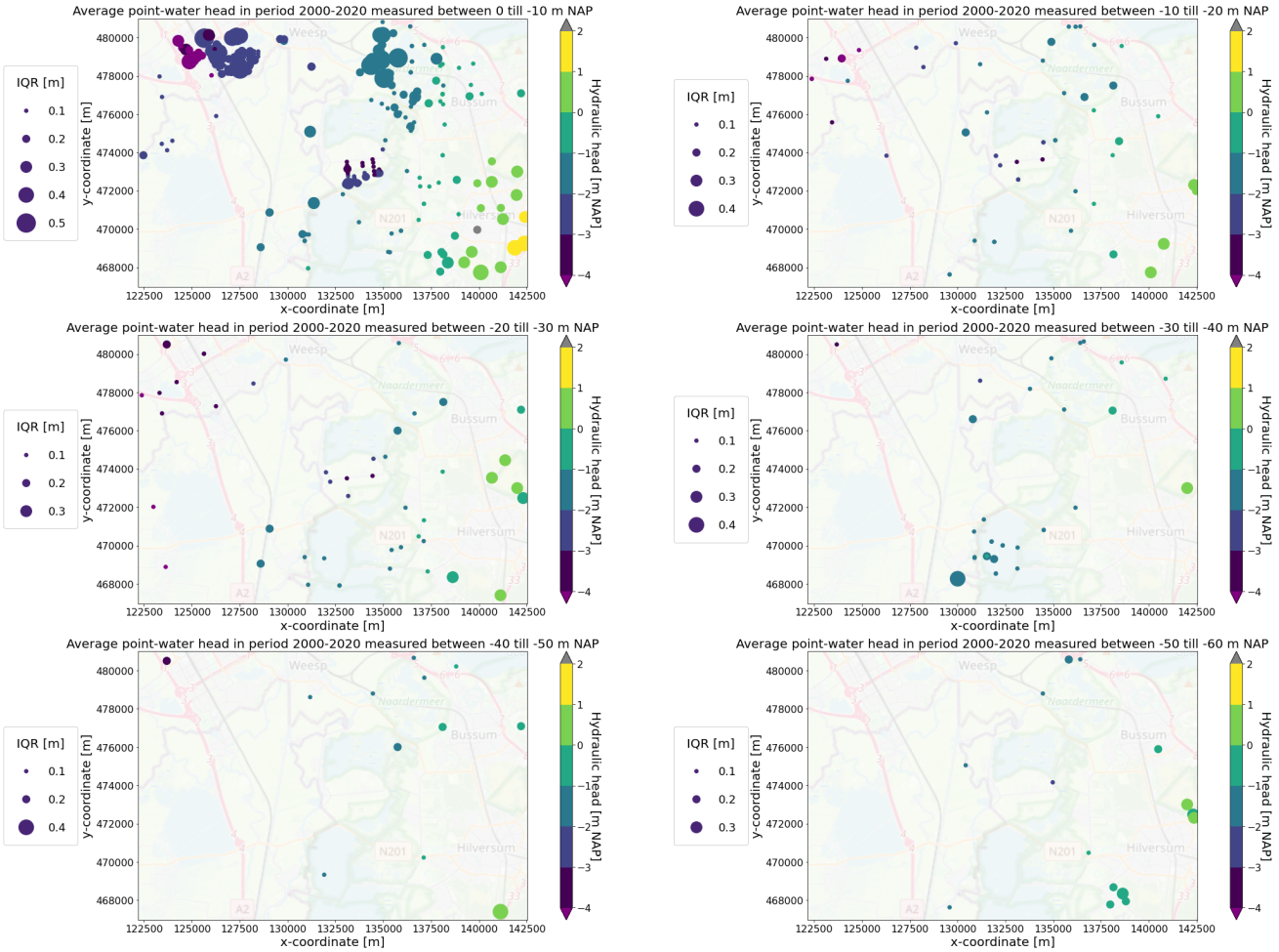

Figure B.1: Part 1 of an overview of the average point-water head distribution in the period 2000 to 2020 AD. The figure also includes the IQR.

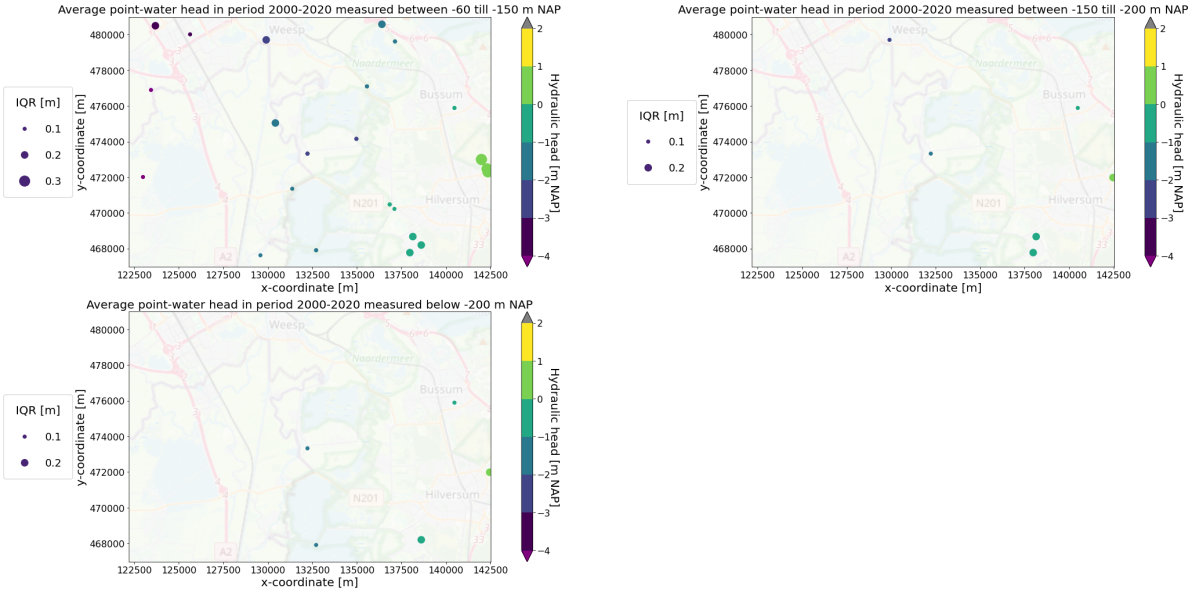

Figure B.2: Part 2 of an overview of the average point-water head distribution in the period 2000 to 2020 AD. The figure also includes the IQR.

C

Hydrostatic Boundary Conditions

To prevent vertical flow to occur at the boundary, a hydrostatic boundary condition was proposed on all boundaries. This hydrostatic boundary condition was determined in four steps:

1. The modified point-water head based on the regional model is determined in every cell that is the first in the column to have an IDOMAIN value > 0 (first active layer);
2. The head value is checked with the surface water levels in the polders;
3. The weight of every cell is calculated in every column;
4. The hydrostatic boundary is established.

C.1. First Active Layer

For every column in the model area, it was determined which layer is the first in the column to have an IDOMAIN value > 0. An IDOMAIN value above 0 means the cell is active and hence part of the calculation. The code to determine this is based on NLMOD, but minor changes were made in order for it to work on a non-rectangle model area. The first active layer in every cell is visualised in Figure C.1.

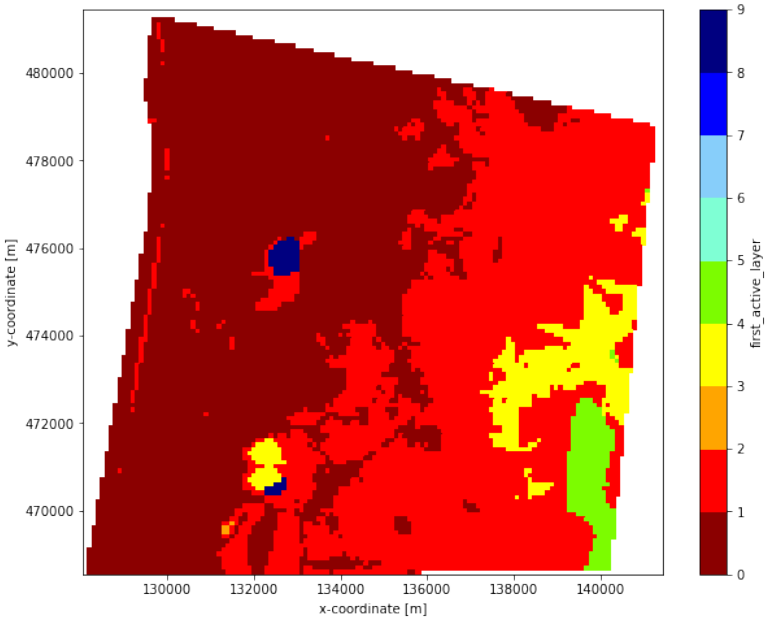

Figure C.1: An overview of the first active MODFLOW layer in every cell of the model area.

C.2. Surface-Water Level Polders

Within the model area, there are many polders, which have a man-controlled surface-water level. Therefore, it was checked whether the modified point-water heads do not exceed those man-controlled surface-water levels. If this was the case, the man-controlled surface-water level was taken as the head. Moreover, all cells below the first active layer were also filled with the same modified point-water head or man-controlled surface-water level as the first-active layer cell. This made the calculation for the weight in every cell easier later on.

C.3. Weight Above the Centre of the Cell

After steps 1 and 2, the water level in every column was determined, and hence the hydrostatic pressure could be calculated in every cell. The hydrostatic pressure (P) is defined in Equation C.1. Often the hydrostatic pressure is taken relative to the atmospheric pressure (P_0). Therefore, P_0 was set to 0.

$$P = P_0 + \rho g d \tag{C.1}$$

where P $\left[ML^{-1}T^{-2}\right]$ is the hydrostatic pressure, P_0 $\left[ML^{-1}T^{-2}\right]$ is the atmospheric pressure, ρ $\left[ML^{-3}\right]$ is the density of the water at a specific location , g $\left[LT^{-2}\right]$ is the gravitational constant, and d $[L]$ is the height of water above the specific location.

However, $\rho_i d$ is another notation for weight/m^2 and the g can be crossed-out when Equation C.1 is combined with Equation 2.1 to determine the hydrostatic head. This combination is shown in Equation C.2

$$h_{hydrostatic} = \frac{P}{\rho_f g} + z = \frac{\rho * d}{\rho_f} + z \tag{C.2}$$

Therefore, the weight above every cell centre was calculated. To be more precise, for every cell, the weight of half the cell above and half the cell itself was calculated and then the cumulative sum was taken. This was done by calculating the saturated thickness of every cell. The saturated thickness is equal to the thickness of the cell if the cell is completely saturated. If the water level is below the top of the cell, the saturated thickness is the height from the water level to the bottom of the cell. In total, there are five situations visualised in Figure C.2. Note that situations 2, 3 and 4 can only occur in the first active layer cell, whereas scenario 5 can occur in multiple cells below the first active layer cell if the water level is far below the surface level and scenario 1 occurs in all other cells.

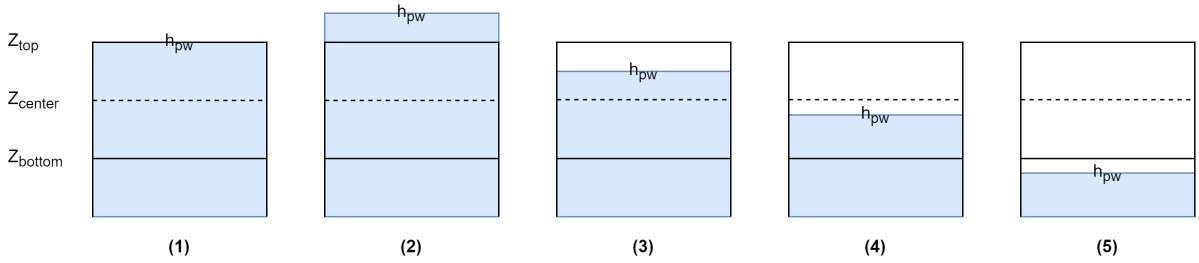

Figure C.2: Diagram of five possible situations of the water level (h_{pw}) with respect to the centre (Z_{centre}) of the first MODFLOW 6 cell: 1) completely saturated, 2) completely saturated and water above the surface level (due to surface water) 3) partly saturated; water level above the centre of the cell, 4) partly saturated; water level below the centre of the cell and 5) dry.

Due to the complexity resulting from these five situations, the calculation process of ρd was split into two parts: 1) determining the ρd in cell[i] due to its own weight above the cell centre, and 2) determining the $\rho d_{remaining}$ in the cell below (cell[i+1]) due to the weight below the cell centre of cell[i]. All methods are based on first calculating the weight of the complete cell, which increases the complexity of the calculation, but since most cells in the domain are equal to scenario 1, and hence are completely saturated, it was the most efficient way to perform this calculation. Below the

calculation of P and $P_{remaining}$ for the four scenarios are given. After combining P_i and $P_{remaining}$ for every cell and taking the cumulative sum the weight above every cell centre was calculated.

Scenario 1

$$\rho d_i = 0.5 * weight_i \tag{C.3}$$

$$\rho d_{remaining,i+1} = 0.5 * weight_i \tag{C.4}$$

Scenario 2

$$\rho d_i = 0.5 * weight_i + (h_{pw,i} - z_{top,i}) * \rho_i \tag{C.5}$$

$$\rho d_{remaining,i+1} = 0.5 * weight_i \tag{C.6}$$

Scenario 3

$$\rho d_i = (h_{pw,i} - z_{centre,i}) * \rho_i \tag{C.7}$$

$$\rho d_{remaining,i+1} = (z_{centre,i} - z_{bottom,i}) * \rho_i \tag{C.8}$$

Scenario 4

$$\rho d_i = 0 \tag{C.9}$$

$$\rho d_{remaining,i+1} = (h_{pw,i} - z_{bottom,i}) * \rho_i \tag{C.10}$$

Scenario 5

$$\rho d_i = 0 \tag{C.11}$$

$$\rho d_{remaining,i+1} = 0 \tag{C.12}$$

C.4. Hydrostatic Head

The last step of calculating the hydrostatic head values in every boundary cell was applying Equation C.2. However, in case of scenario 4 the dry cells would not get a hydrostatic head value and since these cells are active and can become part of the calculation MODFLOW requires a boundary value in these cells if these cells should be open for flow and transport. Therefore, it was decided to allocate the modified point-water head value to those cells.

D

Influence Clay Layers on the Flow Regime

The two clay layers in the subsurface of the model area influence the modelled hydraulic head distribution, i.e. both the point-water head and freshwater head distribution. Moreover, they determine the connectivity between the aquifers below and above them. This can be visualised with the help of specific vertical discharge maps. Before the maps of the difference of the hydraulic head over the clay layer and the specific vertical discharge in the clay layers are given, the thickness of the layers in the model area is visualised.

D.1. Clay Layer Thickness

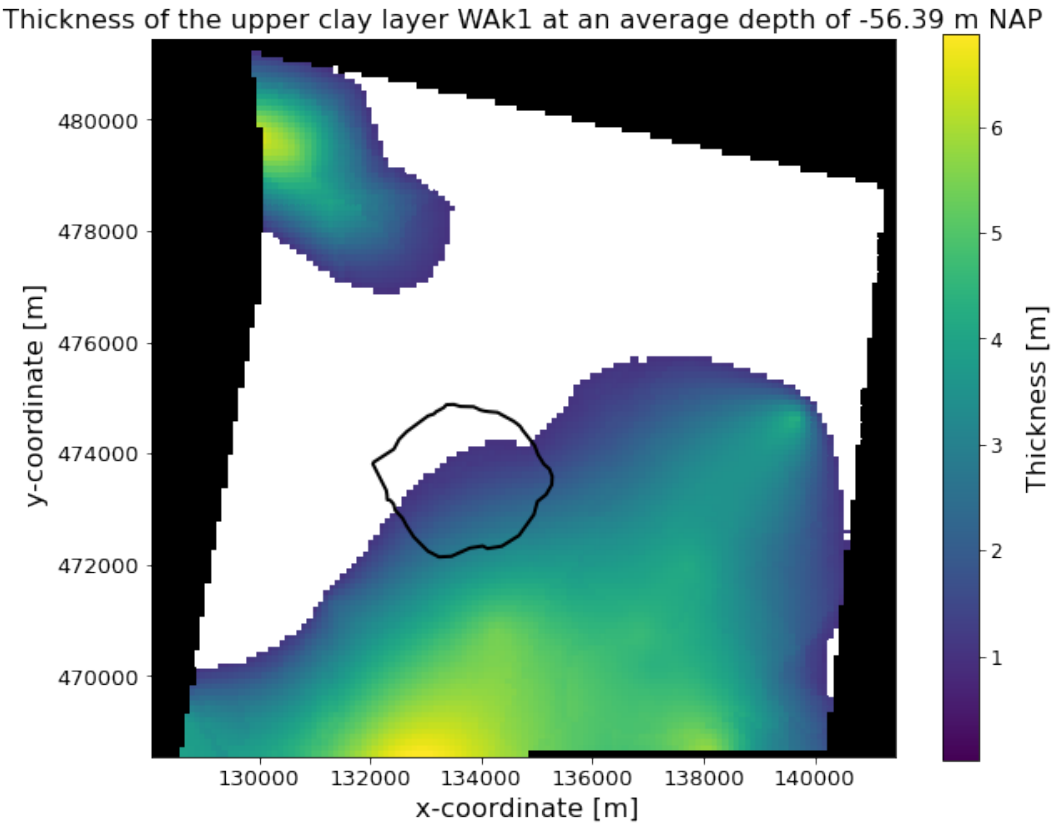

Figure D.1: The thickness of the clay layer in the Waalre Formation (WAk1).

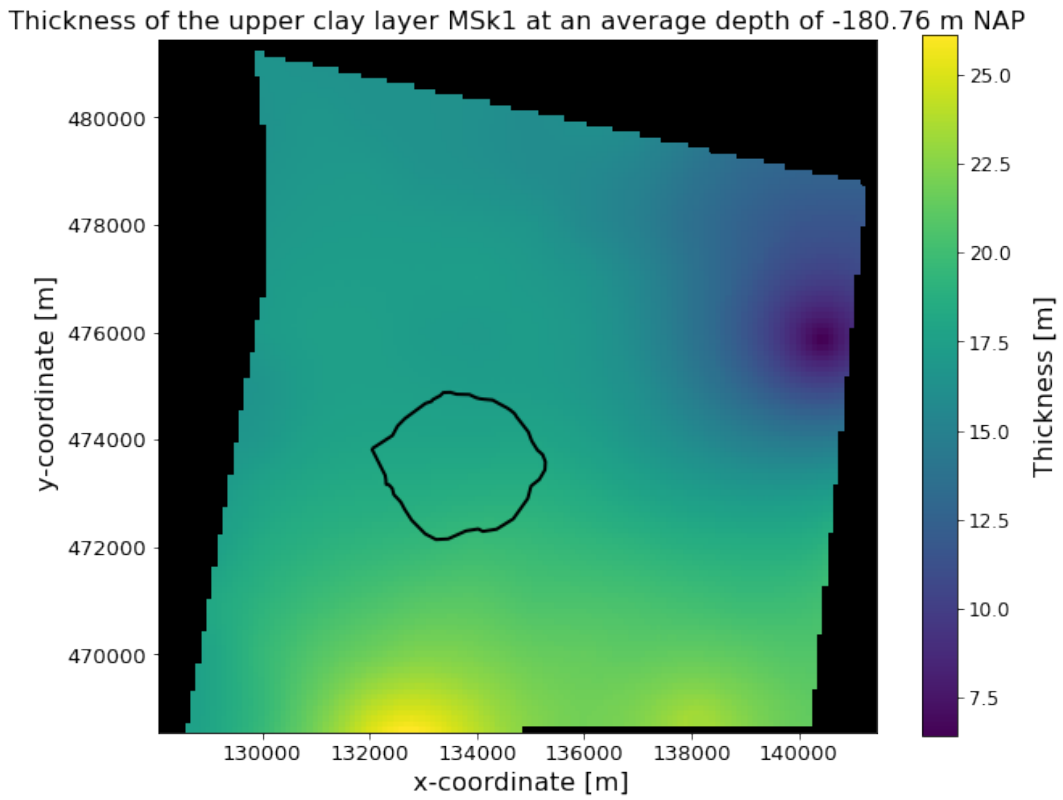

Figure D.2: The thickness of the upper clay layer in the Maassluis Formation (MSk1).

D.2. Point-Water Head Difference

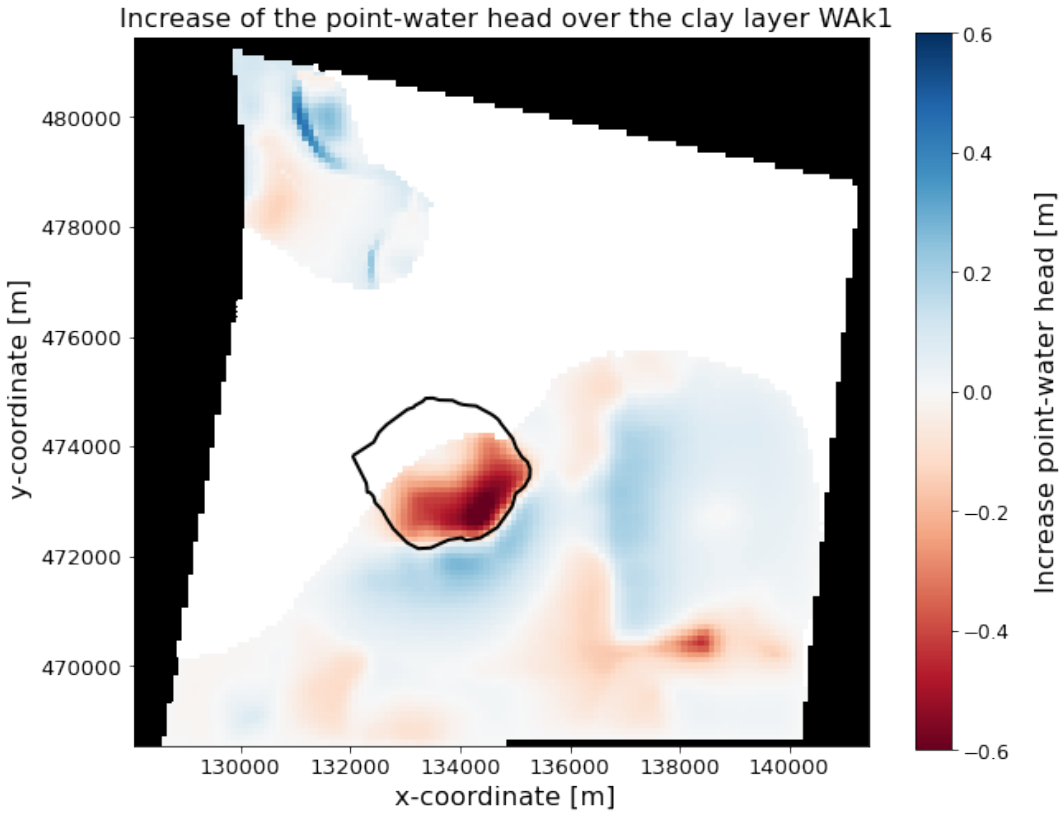

Figure D.3: The point-water head difference over the clay layer in the Waalre Formation (WAk1). The white cells indicate vertical pass-through cells.

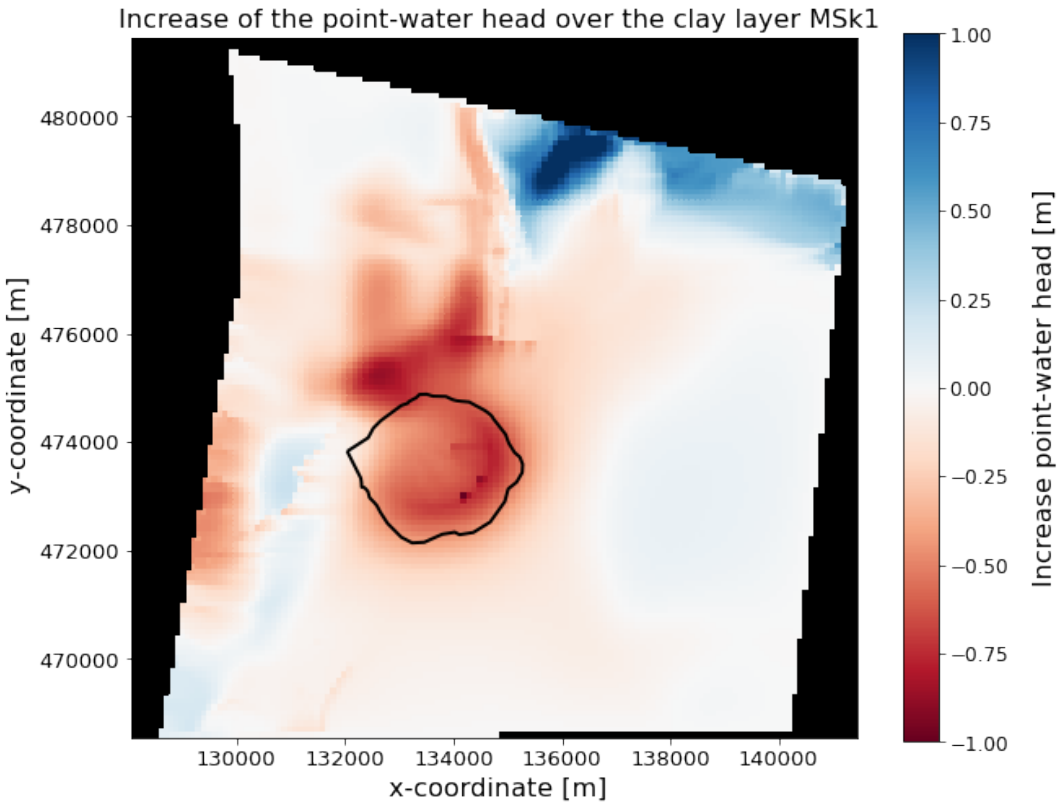

Figure D.4: The point-water head difference over the upper clay layer in the Maassluis Formation (MSk1).

D.3. Freshwater Head Difference

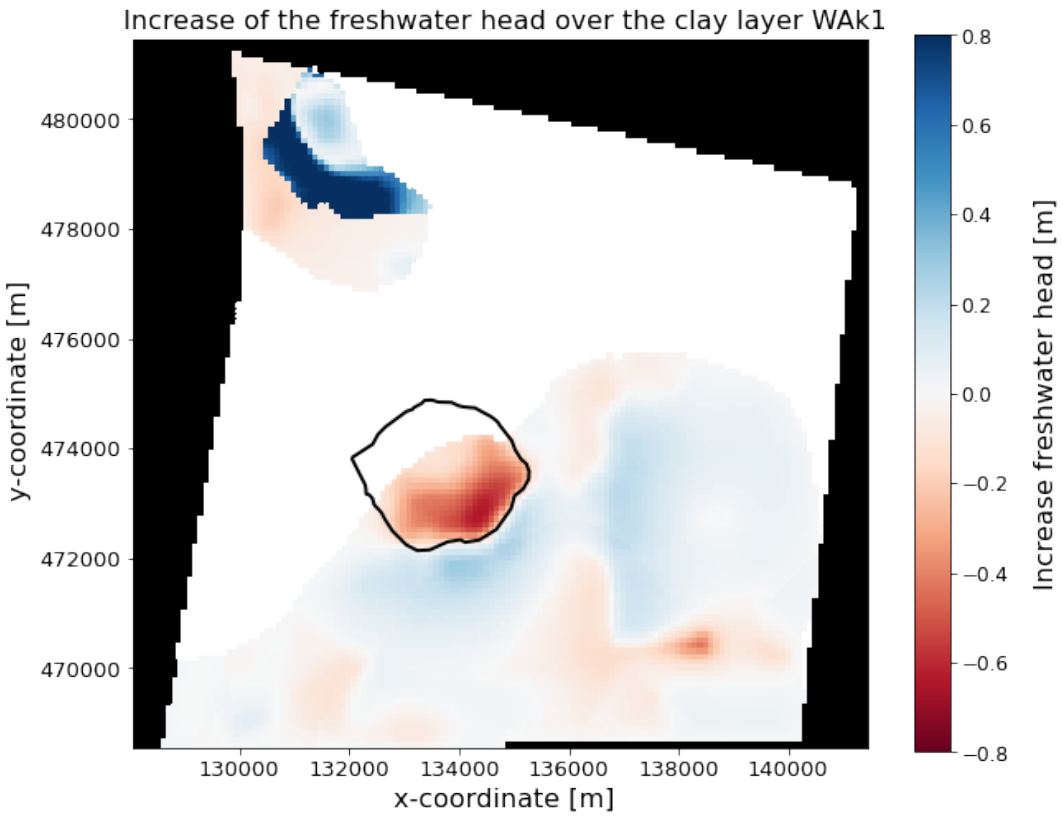

Figure D.5: The freshwater head difference over the clay layer in the Waalre Formation (WAk1).The white cells indicate vertical pass-through cells.

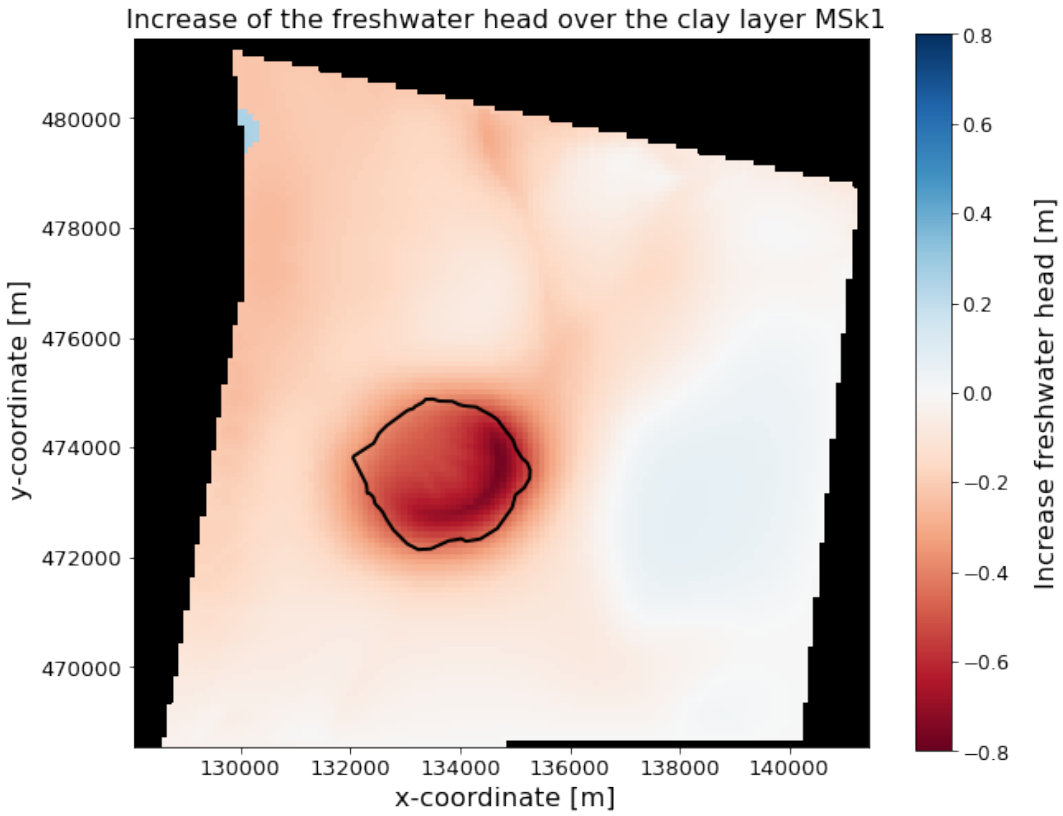

Figure D.6: The freshwater head difference over the upper clay layer in the Maassluis Formation (MSk1)

D.4. Vertical Specific Discharge

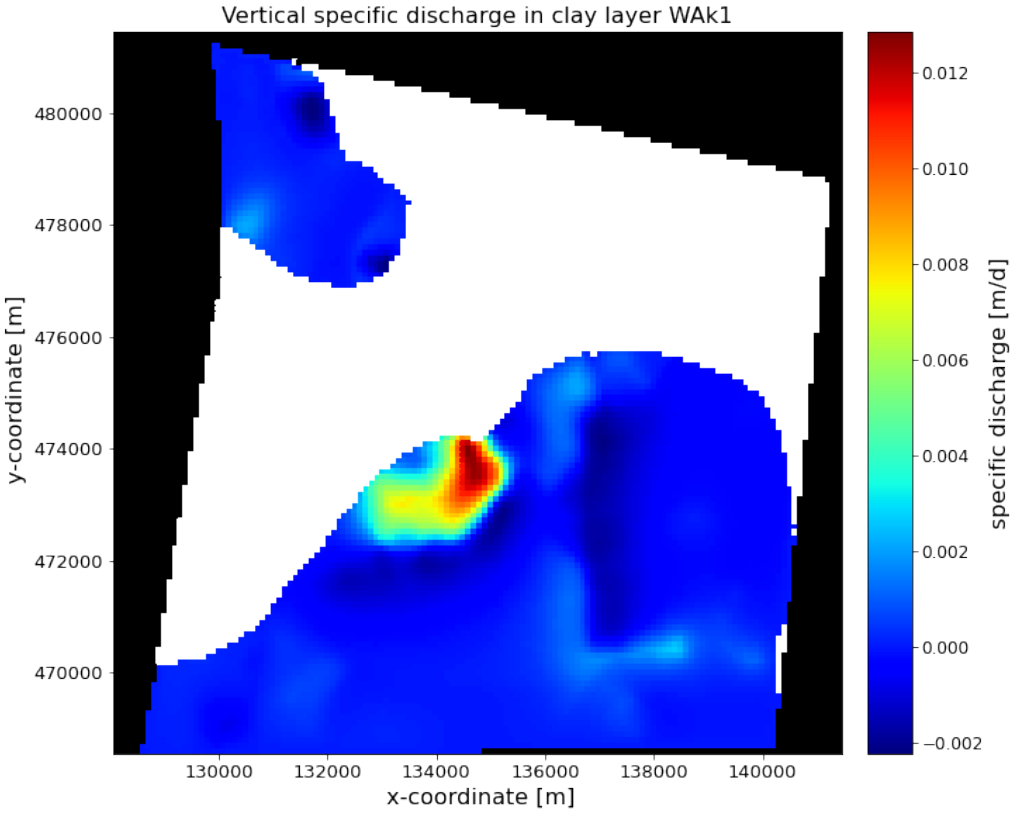

Figure D.7: The vertical specific discharge in the clay layer in the Waalre Formation (WAk1). The white cells indicate vertical pass-through cells.

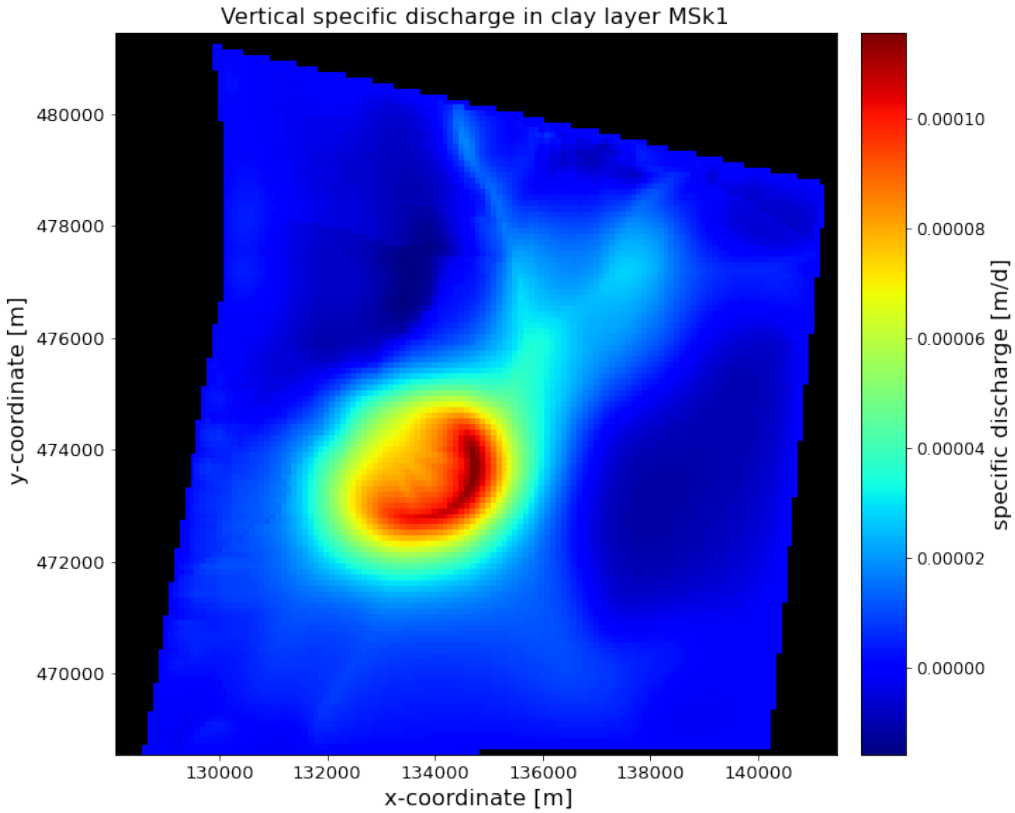

Figure D.8: The vertical specific discharge the upper clay layer in the Maassluis Formation (MSk1)

E

Additional Cross-Sections of the 3D Regional Model Chloride Concentration Output and the Measured Concentrations

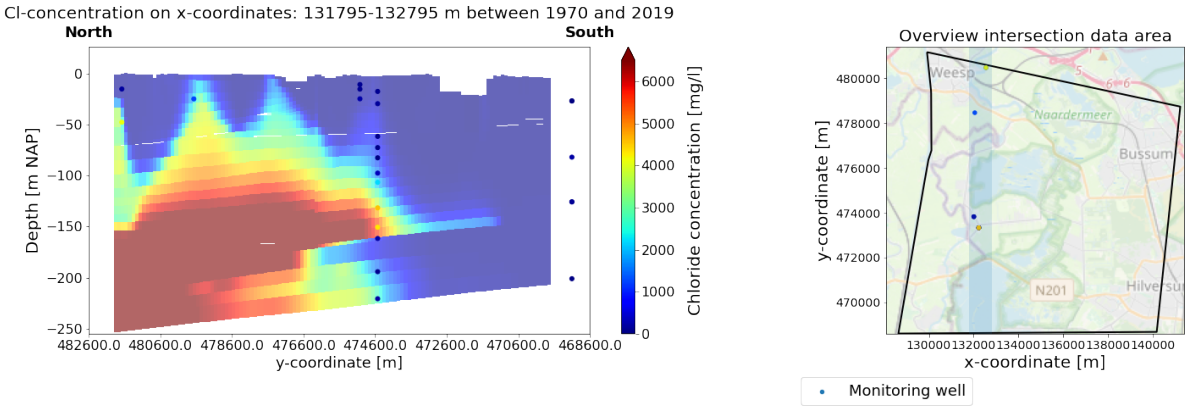

Figure E.1: Chloride concentration distribution over the depth from north to the south in the west of the Horstermeer Polder.

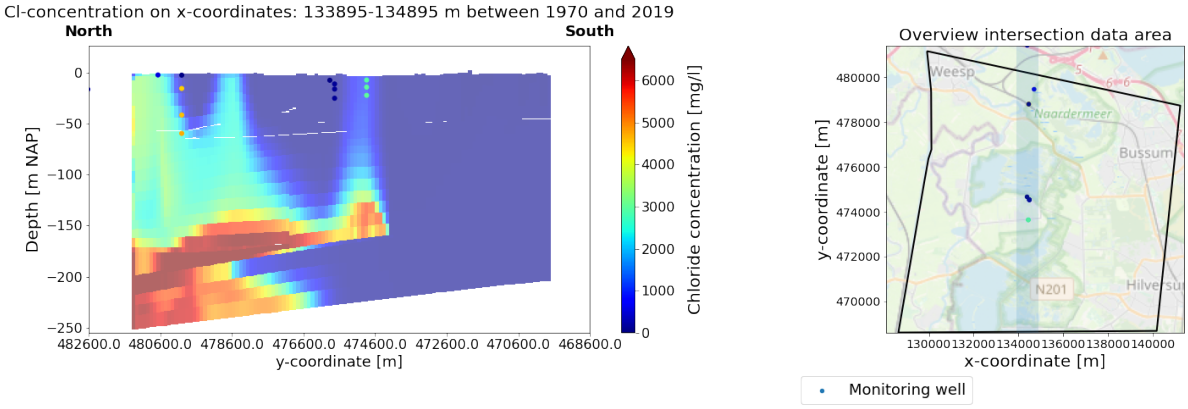

Figure E.2: Chloride concentration distribution over the depth from north to the south in the east of the Horstermeer Polder.

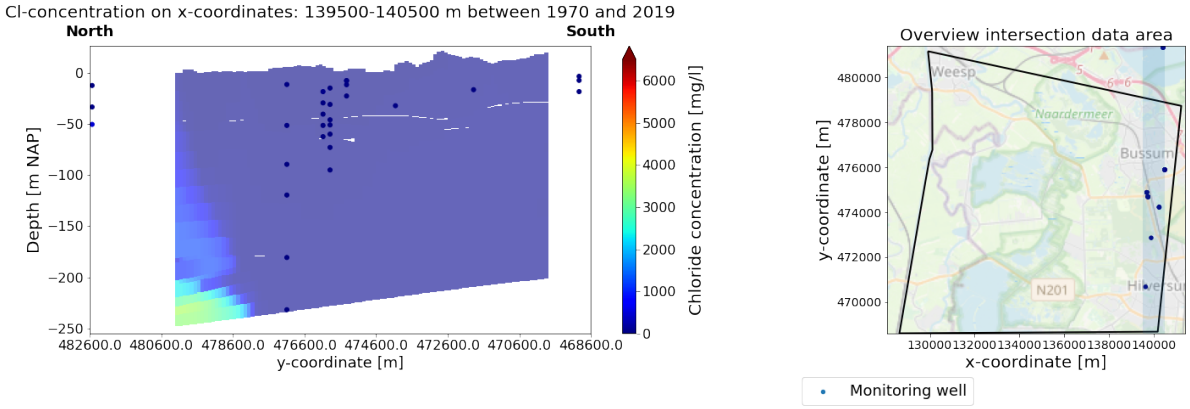

Figure E.3: Chloride concentration distribution over the depth from north to the south in the far east of the model area.

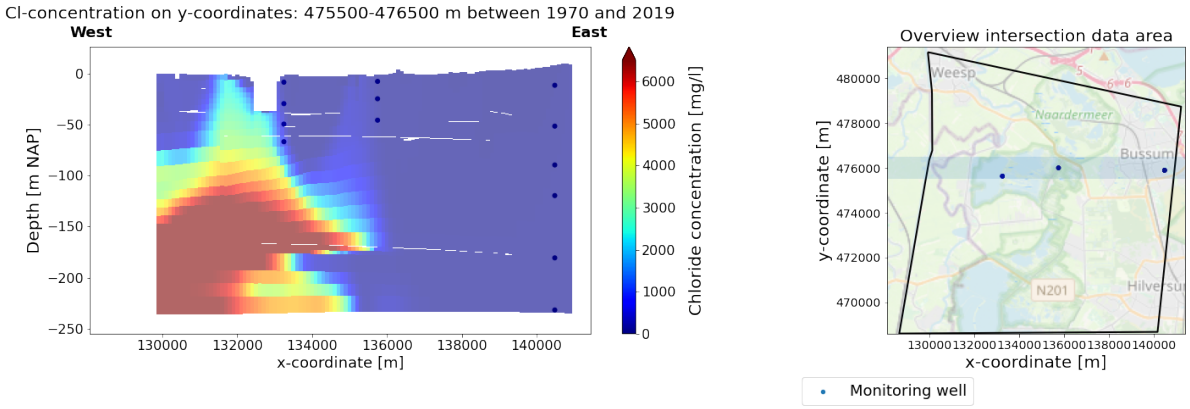

Figure E.4: Chloride concentration distribution over the depth from the west to the east just north of the Horstermeer Polder.

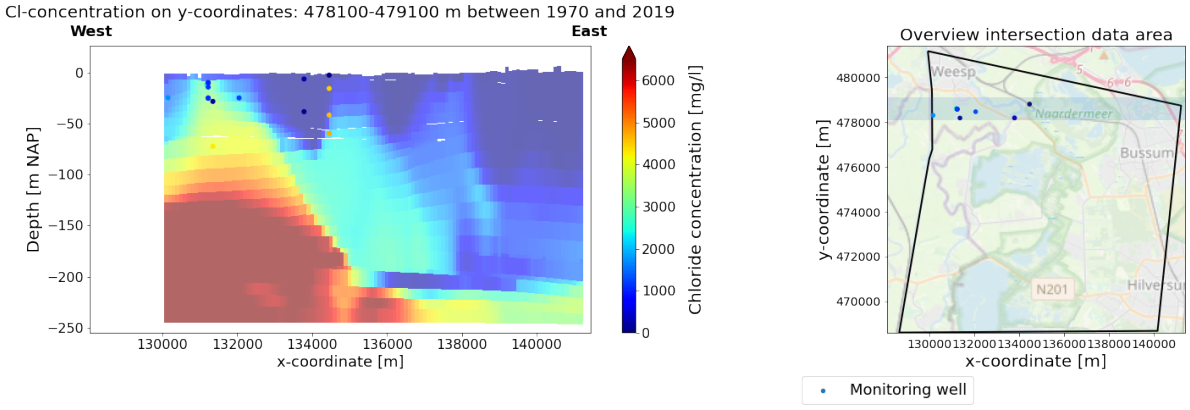

Figure E.5: Chloride concentration distribution over the depth from the west to the east just south of the city of Weesp.

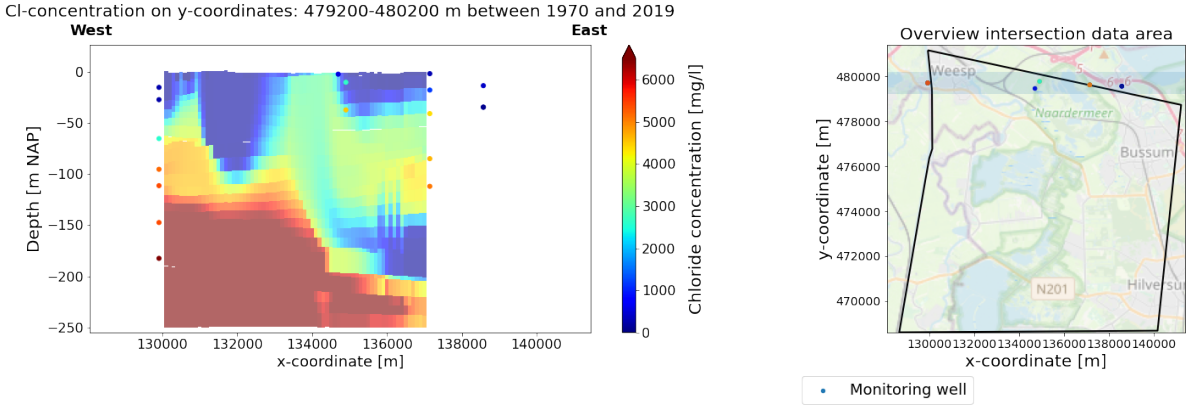

Figure E.6: Chloride concentration distribution over the depth from the west to the east in the far north of the model area.

F

Additional Results Effects of the Pilot Wells

In this appendix, the additional results of the effect of the pilot wells is given. Either the results of scenarios 1 and 2 are shown for one result or the results of scenarios 4 and 5. The structure of this chapter is equal to the structure used in Chapter 6.

F.1. Flow Regime

F.1.1. Drawdown

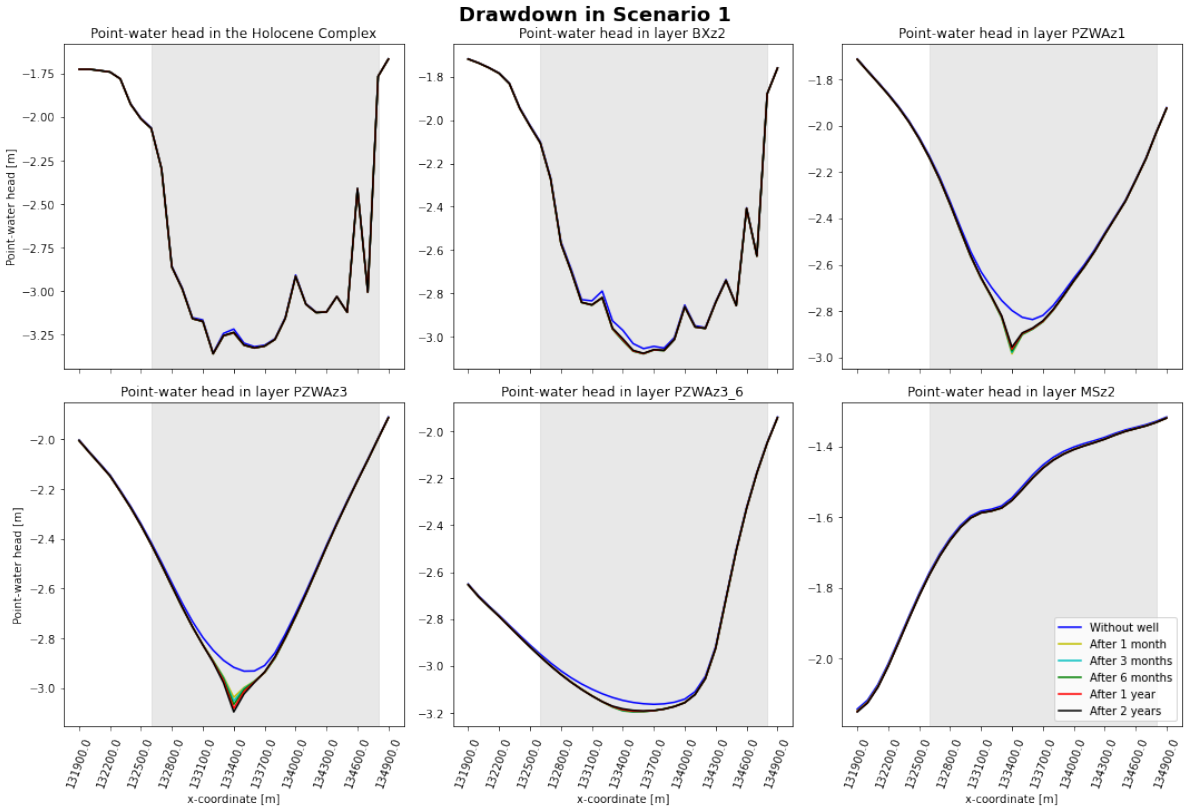

(a)

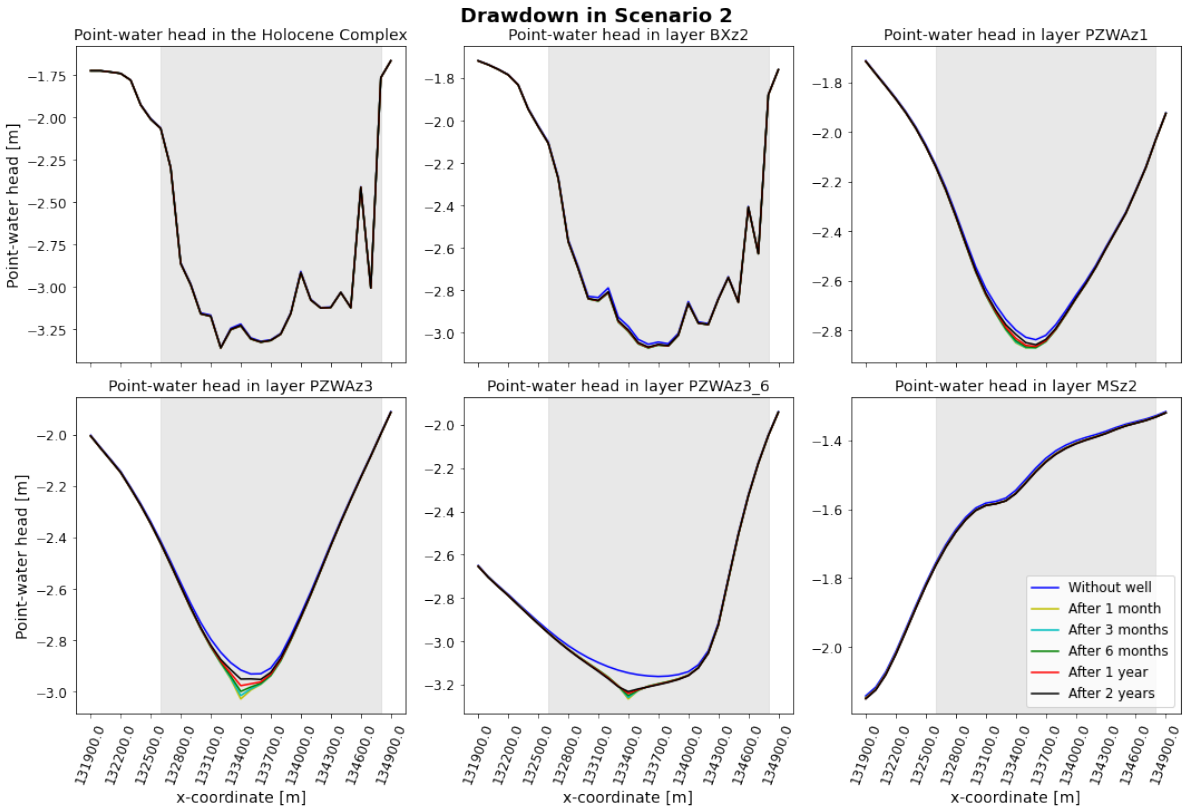

(b)

Figure F.1: The drawdown in terms of point-water heads in different layers in a cross-section of 3.0 km going through the well (x,y = 133400,474400 m). In (a) the simulated drawdown in scenario 1, i.e. pumping from the shallow well screen with a rate of 55 m^3/h, is given and in (b) the simulated drawdown in scenario 2, i.e. pumping from the deep well screen with a rate of 55 m^3/h, is given. In gray the delineation of the Horstermeer Polder is given. Within PZWAz1 the top of the shallow well screen is located, in PZWAz3 both the bottom of the shallow well screen as well as the top of the deep well screen is located and in PZWA3_6 the bottom of the deep well screen is located.

F.1.2. Flow Paths

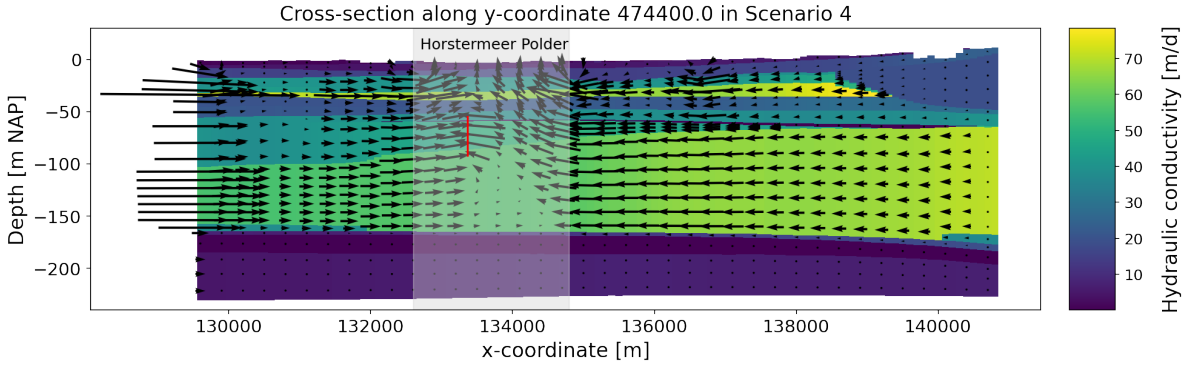

(a)

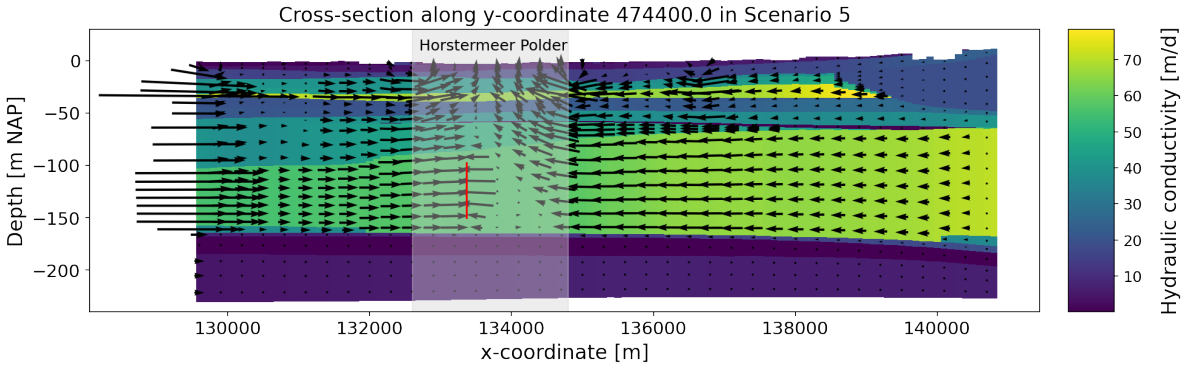

(b)

Figure F.2: The new flow paths as a result of the wells in the cross-section through the well location. In (a) the shallow well pumps with a pumping rate of 100 m^3/h (scenario 1) and in (b) the deep well has a pumping rate of 100 m^3/h. In red the location of the active well screen is depicted and in light gray the Horstermeer polder is indicated.

F.2. Chloride Distribution

F.2.1. Top Layer

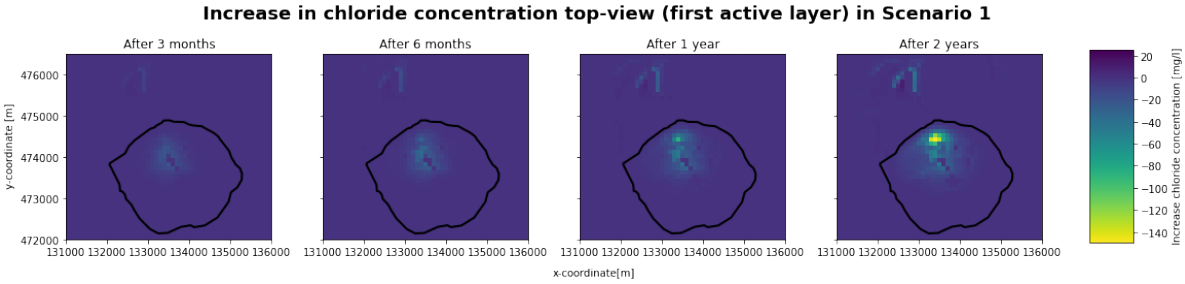

(a)

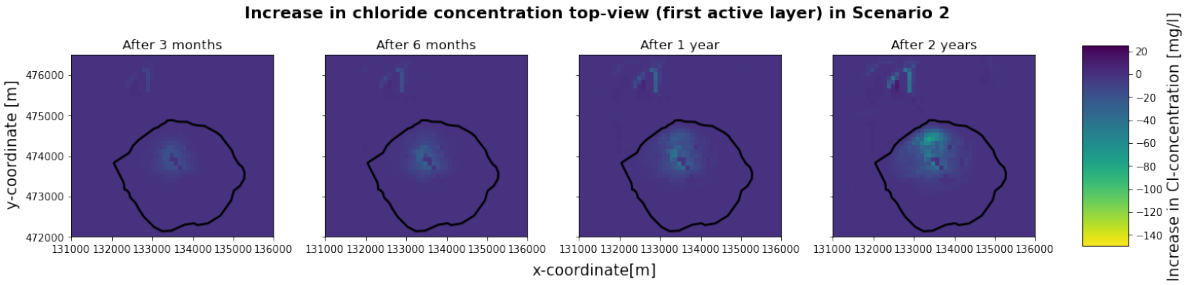

(b)

Figure F.3: The change in chloride concentration over time compared to before the placement of the well. In (a) the shallow well pumps with a constant rate of 55 m^3/h and in (b) the deep well pumps constantly with the same rate. In black the delineation of the Horstermeer Polder is visualised.

F.2.2. Brackish Upconing

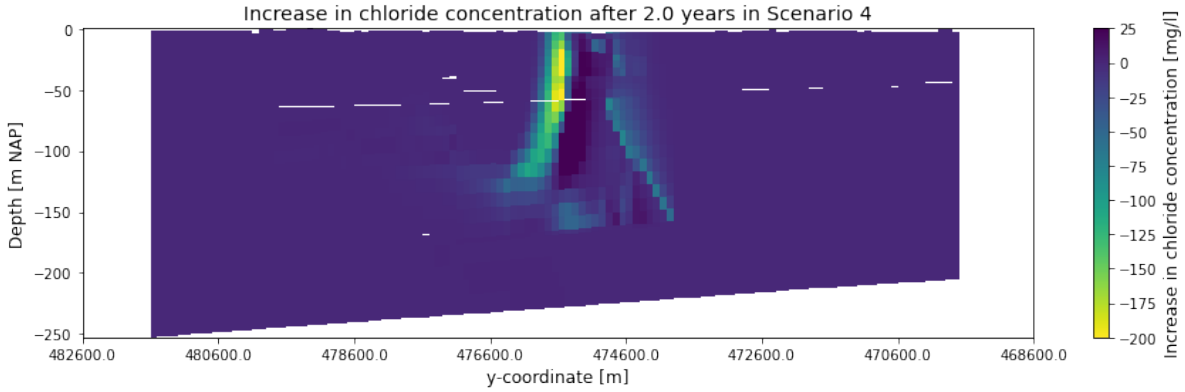

(a)

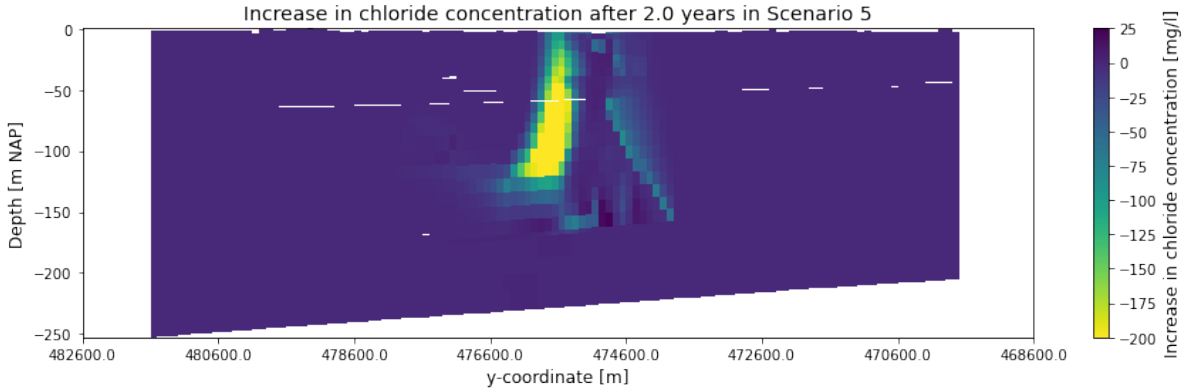

(b)

Figure F.4: The effect of (a) the shallow well with a constant pumping rate of 100 m^3/h and (b) the deep well with the same pumping rate and